

DISSERTATION

NOVEL MICROFLUIDIC DEVICES FOR AEROSOL ANALYSIS

Submitted by

Mallory M. Mentele

Department of Chemistry

In partial fulfillment of the requirements

For the Degree of Doctor of Philosophy

Colorado State University

Fort Collins, Colorado

Spring 2012

Doctoral Committee:

Advisor: Charles Henry

George Barisas
Melissa Reynolds
Branka Ladanyi
Sonia Kreidenweis

ABSTRACT

NOVEL MICROFLUIDIC DEVICES FOR AEROSOL ANALYSIS

Widespread interest in microfluidic technology over the past 20 years has led to the development of microfluidic devices that are as varied in their complexity and capabilities as they are in the applications they are used for. This dissertation describes the development of two microfluidic devices, each designed for measurement of specific aerosol components.

A microchip incorporating an interface between a continuous hydrodynamic sample flow and capillary electrophoresis separation was developed for analysis of atmospheric aerosols. The ability to separate and detect analytes from a continuous sample flow allows the microchip to be coupled to a particle-into-liquid aerosol sampler, providing a method for near real-time analysis of ionic aerosol components. Theoretical modeling of hydrodynamic and electroosmotic flows was used to predict flow behavior in the microchip and to optimize geometry. Separation and conductivity detection of common ionic aerosol components were carried out to observe device performance, and detection of nitrate and sulfate in Fort Collins air was accomplished with the coupled system. The simple design introduced here is the first example of a continuous flow microfluidic capillary electrophoresis device that incorporates conductivity detection, and is the first microfluidic device to be coupled to a continuous flow aerosol collector.

A paper-based microfluidic device was also designed for the purpose of assessing occupational exposure to particulate metals. Assays were developed for colorimetric detection of metals on paper and these were employed in detection reservoirs of the

device. A novel method was also developed for rapid digestion of particulate metals directly on a filter. Metal concentrations were quantified from color intensity images using a scanner in conjunction with image processing software. Finally, a standard incineration ash sample was aerosolized, collected on filters, and analyzed for the three metals of interest. This is the first paper-based device capable of multiplexed metal detection from a real, aerosolized sample.

ACKNOWLEDGEMENTS

I would like to thank the members of the Henry group for their assistance over the past four years; especially Jana Jokerst, who's presence makes life inside the lab and out more enjoyable.

I would like to thank Josephine Cunningham for all her work and ideas regarding the paper-based microfluidics project. The lab work and brainstorming she contributed to this project far exceeded the expected abilities of an undergraduate student. I know she continue to exceed all expectations as a graduate student as well. I can't imagine the last year without her.

I would also like to thank my husband, Emek Blair, for his help as a chemist and a friend; and my family for their constant encouragement.

I owe a great deal of thanks to Dr. Charles Henry for his guidance, assistance, and support. I can't imagine a better person to work for.

TABLE OF CONTENTS

ABSTRACT.....	ii
ACKNOWLEDGEMENTS.....	iv
LIST OF SYMBOLS AND ABBREVIATIONS.....	vii
CHAPTER 1: INTRODUCTION.....	1
1.1 Atmospheric Aerosols.....	1
1.2 Aerosols in Occupational Environments: Particulate Metal Exposure.....	7
1.3 Microfluidic Devices.....	10
1.5 References.....	13
CHAPTER 2: CAPILLARY ELECTROPHORESIS-BASED MICROFLUIDICS.....	18
2.1 Capillary Electrophoresis Theory.....	18
2.2 Microfluidic Capillary Electrophoresis.....	22
2.3 Aerosol Analysis with MCE.....	25
2.4 Continuous Sampling MCE Devices.....	26
2.5 References.....	28
CHAPTER 3: SIMPLIFIED INTERFACE BETWEEN MICROCHIP ELECTROPHORESIS AND CONTINUOUS FLOW SAMPLERS FOR AEROSOL ANALYSIS.....	30
3.1 Introduction.....	30
3.2 Experimental.....	34
Materials.....	34
Instrumentation and data acquisition.....	35
Device fabrication.....	36
Device operation.....	38
3.3 Results and Discussion.....	40
Hydrodynamic flow modeling.....	40
Evaluation of separation performance.....	43
Interfacing device to an aerosol sampler.....	48
3.4 Conclusion.....	49
3.5 References.....	51
CHAPTER 4: PAPER-BASED MICROFLUIDICS.....	54
4.1 What is paper-based microfluidics?.....	54
4.2 References.....	56
CHAPTER 5: COLORIMETRIC DETECTION OF METALS ON PAPER.....	57
5.1 Introduction.....	57
5.2 General Assay Procedures.....	60
Detection of Cadmium.....	60
Detection of Lead.....	61
Detection of Manganese.....	61
Detection of Iron.....	62
Detection of Nickel.....	62
Detection of Copper.....	62

5.3 Results and Discussion	64
Detection of Cadmium	64
Detection of Lead	67
Detection of Manganese	70
Detection of Iron.....	74
Detection of Nickel.....	75
Detection of Copper	79
5.8 Conclusion	83
5.8 References.....	85
CHAPTER 6: ADVANCING PAPER-BASED DEVICES - NOVEL METHODS OF CONTROLLING CHEMISTRY ON PAPER.....	88
6.1 Introduction.....	88
6.2 Controlling mobility of compounds on paper.....	91
6.3 Reducing hydrophobicity in a zone	95
6.4 Controlling pH in different zones of a device.....	96
6.5 Conclusion	99
6.6 References.....	100
CHAPTER 7: MICROFLUIDIC PAPER-BASED ANALYTICAL DEVICE FOR DETECTION OF PARTICULATE METALS.....	101
7.1 Introduction.....	101
7.2 Experimental	104
Fabrication and Design of μ PAD	104
Colorimetric Detection of Metals	105
Particulate metal collection and digestion	106
Quantitative Image Processing	107
7.3 Results and Discussion	109
Device design	109
Colorimetric Assays	112
7.4 Conclusion	119
7.5 References.....	120
CHAPTER 8: CONCLUSION AND FUTURE DIRECTIONS	123
8.1 Conclusions.....	123
8.2 Future Directions	124
APPENDIX 1: ORIGINAL PROPOSAL.....	127

LIST OF SYMBOLS AND ABBREVIATIONS

PDMS	Poly(dimethylsiloxane)
PM	Particulate matter
d_{ae}	Aerodynamic diameter
IC	Ion chromatography
CE	Capillary electrophoresis
AMS	Aerosol mass spectrometry
PILS	Particle-into-liquid sampler
MCE	Microchip capillary electrophoresis
WCPC	Water condensation particle collector
AAS	Atomic absorption spectroscopy
ICP-AES	Inductively-coupled plasma atomic emission spectroscopy
ICP-MS	Inductively-coupled plasma mass spectrometry
CZE	Capillary zone electrophoresis
μ_{ep}	Electrophoretic mobility
q	Charge
f	Frictional coefficient
r	Hydrodynamic radius
η	Viscosity
EOF	Electroosmotic flow

V_E	Electrophoretic velocity
μ_{EOF}	Mobility due to electroosmotic flow
E	Electric field
FITC	Fluorescein isothiocyanate
U	Hydrodynamic flow velocity
Φ	Volumetric flow rate
NIOSH	National Institute for Occupational Safety and Health
OSHA	Occupational Safety and Health Association
TMB	3,3',5,5'-tetramethylbenzidine
phen	1,10-phenanthroline
dmgH ₂	Dimethylglyoxime
bc	Bathocuproine
PEG	Polyethylene glycol

CHAPTER 1: INTRODUCTION

The work presented in this dissertation describes the development of two very different microfluidic devices, each designed to measure specific components of aerosol samples. Chapter 2 presents a microchip capillary electrophoresis device designed for near real-time analysis of ionic species in atmospheric aerosols. Chapters 3 and 4 describe a method for colorimetric detection of particulate metals on a microfluidic paper-based device designed for assessing occupational exposure to aerosols. Concluding this work, Chapter 5 will briefly discuss the merits and shortcomings of microfluidics in their current state, and what may be expected of this field in the future. This chapter serves to familiarize the reader with the themes encountered in the subsequent chapters, beginning with an introduction to the topics of aerosols found in the environment and generated in occupational settings. Following this, general capillary electrophoresis theory will be explained and the field of microfluidics will be introduced.

1.1 Atmospheric Aerosols

There has been great interest in the study of atmospheric aerosols over the past decade motivated by their impact on the environment and human health.¹⁻⁴ Aerosols, also referred to as atmospheric particulate matter (PM), are solid or liquid particles suspended in the air with aerodynamic diameters (d_{ae}) in the range of 1 nm – 100 μm .² They are generally comprised of a complex mixture of water, ionic salts, metal oxides, glasses, and carbonaceous material; however, their composition, size, and shape vary considerably

depending on the source and the interactions they undergo in the atmosphere.^{5,6} They can be classified as either primary or secondary, with primary aerosols being those that are directly emitted into the atmosphere, while secondary aerosols are formed in the atmosphere through physical or chemical transformations. Both aerosol types can undergo a variety of aging processes, in which various physical and chemical interactions and transformations lead to changes in particle size, structure, and composition.^{2,7-9}

Aerosol sources are divided into two categories: natural or anthropogenic. Biogenic natural sources often originate from constituents or secretions of plants and animals while geogenic natural sources include volcanic ash, mineral dust, and sea spray. Examples of anthropogenic sources are biomass burning, incomplete combustion of fossil fuels, and resuspension of industrial dust and soil from activities such as construction, farming, and mining.^{2,5,8} On a global scale, aerosols mainly originate from the natural sources sea salt and dust; however, anthropogenic aerosols, arising primarily from combustion sources, can dominate in and downwind of highly populated and industrialized regions.⁵

Aerosols are further categorized according to their size as coarse, fine, or ultrafine PM, and it has been shown that the sources, composition, optical properties, and secondary transformation mechanisms are generally very different for each of these classes of aerosols.⁸ Particulate matter with $d_{ae} > 2.5 \mu\text{m}$ are considered coarse particles. They are most likely comprised of resuspended dust, coal and oil fly ash, crustal element oxides, sea salts, and plant and animal debris. Due to their larger size, their atmospheric lifetimes last from minutes to days, and the furthest they travel is tens of kilometers. Fine particles are defined as having $d_{ae} \leq 2.5 \mu\text{m}$ and can contain sulfate, nitrate, ammonium,

H⁺, elemental carbon, organic compounds, water, and metals. Finally, ultrafine particles, with $d_{ae} \leq 100$ nm are believed to have the most aggressive health implications because they are small enough to be deposited into the lungs where they have the ability to penetrate tissue and be absorbed into the bloodstream.¹⁰ Particles in the fine and ultrafine size range persist in the atmosphere for days to weeks and can travel hundreds to thousands of kilometers.⁸ These long atmospheric lifetimes and travel distances make fine and ultrafine PM a more important component in the study of aerosols.

While it is known that both natural and anthropogenic aerosols have a strong impact on climate and human health, the mechanisms underlying these effects are not yet fully understood. The study of aerosols is challenged by the complex and varied composition of aerosols, as well as the aging processes they undergo in the atmosphere. It has been shown that atmospheric aerosols play significant roles in shaping conditions at the surface of the earth and in the lower atmosphere. They effect climate directly by scattering and absorbing radiation which alters the intensity of sunlight scattered into space, absorbed in the atmosphere, and arriving at the earth's surface. More specifically, scattering and reflection of solar radiation by aerosols results in a cooling of the Earth's surface (negative forcing); while absorption of solar radiation by greenhouse gases and clouds tend to warm it (positive forcing). Indirect climate effects result from aerosols' influence on clouds and precipitation. Aerosol particles modify the extent and properties of clouds as well as precipitation patterns by 1) acting as cloud condensation nuclei (CCN) on which water vapor can condense and form cloud droplets, and 2) absorbing solar radiation, thus changing the environment in which clouds are formed.^{2,5,11} These direct and indirect effects are dependent on aerosol particle size, structure, and chemical

composition, which, as previously mentioned, are often difficult to determine. Thus, there remains a limited understanding of both the interactions between aerosols, clouds, and precipitation and the effects these interactions have on climate change.⁸

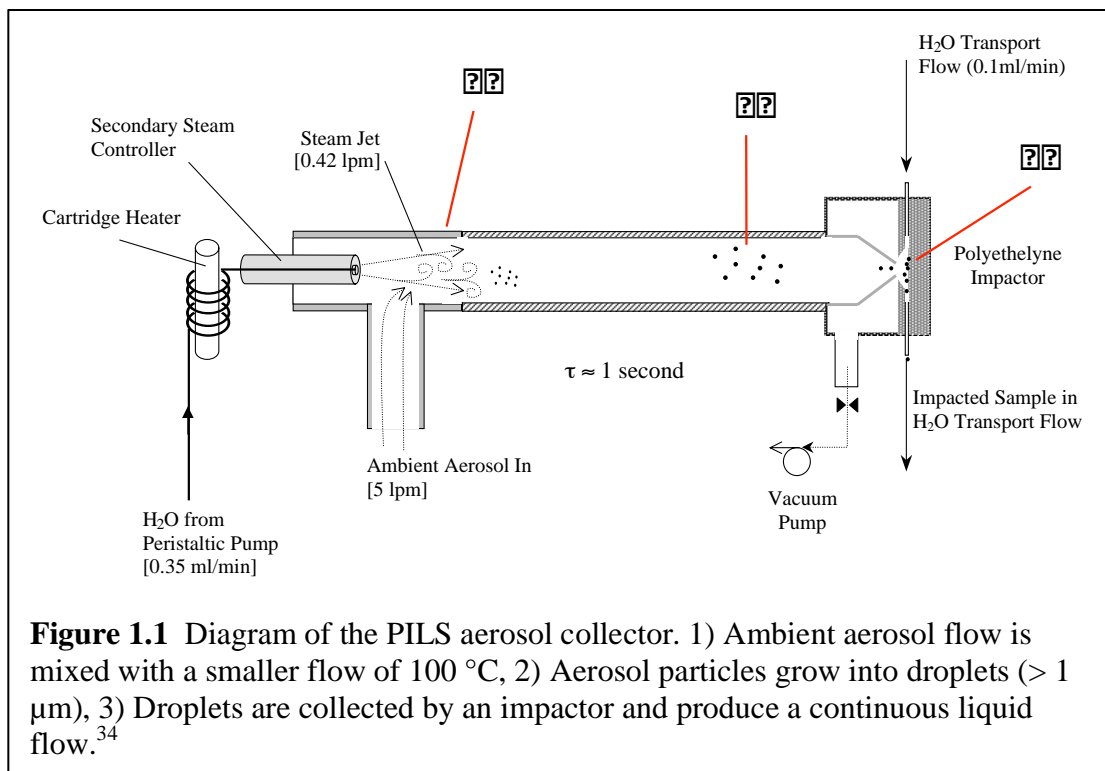
Epidemiological studies have shown that persistent, high levels of fine atmospheric particulates are strongly associated with adverse human health effects, including increased mortality from cardiopulmonary disease and lung cancer, as well as higher incidences of cardiovascular, respiratory, and allergic diseases.^{1,12-14} Toxicological studies have also demonstrated that particulate matter affects the cardiovascular and respiratory system, primarily due to ultrafine particles, as they deposit with high efficiency in the lungs and are not easily removed.¹⁵ The exact mechanisms and molecular processes by which aerosols cause adverse health effects remain unclear but possibilities include particulate or ozone-induced pulmonary inflammation, free radical and oxidative stress generation by transition metals and organic compounds, covalent modification of intracellular proteins, and suppression of normal defense mechanisms.¹ Similar to the ambiguous role aerosols play in climate, a clearer understanding of the ways in which they affect human health can only be gained with more complete knowledge of the composition, sources, and atmospheric transformations of aerosol pollutants.

Undoubtedly, improved chemical analysis of aerosols is necessary to shed some light on aerosol sources and the impact they have on the environment and human health; however, the variability of their composition and size over time and space make chemical analysis a daunting challenge. Over the past several decades, great strides have been made in the development of instrumentation for collection and chemical analysis of

aerosols. The following discussion of chemical analysis techniques focuses primarily on those best suited for analysis of anionic and cationic aerosol species, as these will be examined in later chapters. Ionic species often comprise the bulk, by mass, of secondary aerosols, and ionic content is used to estimate aerosol contributions of a known source.¹⁶⁻
²⁰ The traditional collection approach has been via filter methods, in which the transfer of aerosols from a dispersed state in the air to a compact sample on a filter facilitates the storage, transport, and pre-treatment required for offline analysis. Infrared spectroscopy and x-ray fluorescence can be used to measure a few species directly on the collection filter; however, the majority of all offline analysis techniques employed require that aerosols be extracted into solution. Ion selective electrodes and UV/Vis absorbance spectroscopy have been used for detection of various ionic aerosol components, but ion chromatography (IC) has become the standard method for determining dissolved anion and cation aerosol species.^{21,22} Capillary electrophoresis (CE) has more recently been introduced as a promising technique in aerosol analysis due to ease of operation, low running costs, and its proven ability to efficiently separate complex mixtures of ionic species.²³⁻²⁷ While not used as commonly as IC, many organizations and institutions are evaluating CE as a standard method.²⁷

While off-line measurements can provide useful information on a longer time scale, the chemical complexity and labile nature of atmospheric aerosols strongly favors real-time analysis techniques that do not require collection, storage, and transportation of samples.¹² Aerosol mass spectrometry (AMS) is a technique that provides real-time monitoring of aerosol size and composition.²⁸⁻³² These instruments continuously sample aerosol particles and pass them through an aerodynamic lens, forming a narrow particle

beam that is transmitted into a detection chamber. Here, particles are vaporized and chemically analyzed through various ionization techniques and mass spectrometry.¹² Another common approach to online aerosol collection and analysis is to couple traditional instrumentation to an aerosol collector that continuously samples ambient aerosols and dissolves particles into an aqueous stream. The most prevalent of these collectors is the particle-into-liquid sampler (PILS) developed by Weber *et. al* in 2001.^{33,34} A diagram of the PILS is shown in Figure 1.1. It operates by collecting aerosol particles from the atmosphere and then mixing this sample flow with a turbulent flow of steam. The supersaturated environment inside the PILS causes the aerosol particles to grow into droplets, which can then be collected by an impactor to produce a continuous liquid flow for online analysis of the collected aerosols.³⁴



The PILS is most often interfaced with ion chromatography, providing a semi-continuous method for analysis of cations and anions. The growing use of CE in environmental analysis suggests that coupling the PILS with CE would provide another viable method for semi-real-time analysis. Besides the advantages of CE mentioned previously, another benefit is its amenability to miniaturization. Microchip capillary electrophoresis (MCE) interfaced with the PILS would give semi-real-time analysis with all the benefits of CE, plus faster analysis times, greater portability, low cost, and minimal sample and reagent requirements. Noblitt *et al.* reported on-line coupling between MCE and a water condensation particle collector (WCPC), marking the first on-line coupling of this promising technique for aerosol analysis.³⁵ While the WCPC directly deposits aerosols into the microchip, it does not generate a continuous flow of sample; therefore, real-time analysis is more closely achieved using the PILS. Chapter 2 describes the development of a novel microchip CE device capable of being interfaced to a continuous flow, thus setting the stage for a PILS-MCE system.

1.2 Aerosols in Occupational Environments: Particulate Metal Exposure

Aerosols are generated in a number of basic industries that include petroleum refineries, metallurgical operations, power plants, mining, construction/demolition, manufacturing, and transportation.^{36,37} Even if prevented from polluting the surrounding areas, the aerosols generated in such industries may be harmful to workers employed in these types of fields. The occupational environment can be a source of significant risk to health due to a variety of potentially harmful agents that come in contact with workers. One important class of hazardous agents existing in many work sectors is airborne

particulate metals. In fact, the highest and most specific metal exposures have occurred and still occur in occupational settings or in the immediate environment of industrial sources.³⁷ Several studies involving particulate matter have indicated that metal components of aerosols may be responsible for many adverse health effects.^{38,39} In particular, it has been suggested that particulate metals in aerosols are the causative agents associated with mutagenesis, carcinogenesis, airway inflammation, and pulmonary toxicity.⁴⁰⁻⁴⁴ Studies have also shown that trace metals distributed widely throughout the lung can induce tissue damage by catalyzing the formation of oxidants.^{42,45}

Inhalation is the main route of human exposure to most aerosols.³⁶ As workers inhale particulate matter while performing various tasks, this exposure leads to a dose that accumulates in the human body. Exposure assessment is the process of evaluating the degree and specific sources of this exposure.³⁶ In industry, exposure assessment is carried out for several reasons: 1) to prove regulatory compliance, 2) to determine if a risk to worker health exists, 3) to identify highly hazardous job or specific work tasks so that corrective actions may be taken, 4) to evaluate effectiveness of controls (ventilation systems, protective equipment, specific work practices), and 5) to gather valid measurements for use in epidemiological studies.^{36,46}

Sampling of aerosols for occupational exposure assessment cannot be accomplished through the same techniques used to collect atmospheric aerosols. Two important factors create a distinction between measuring particulate matter concentrations and measuring worker exposure to particulate matter. First, each work task creates its own microenvironment that may have particulate matter concentrations that differ from the average workplace concentrations. Second, the concentration of

particulate matter that a worker inhales may be different from the average concentration existing in these microenvironments because not all airborne matter can be inhaled.³⁶ The inhalable aerosol fraction describes the fraction of total airborne particles that enters the body through the nose and/or mouth during breathing, and corresponds to particles with aerodynamic diameters (d_{ae}) $\leq 100 \mu\text{m}$.⁴⁷ Within the inhalable fraction are two subsets that describe the deposition site of particles. The thoracic fraction ($d_{ae} < 30 \mu\text{m}$) refers to particles that can penetrate into the lung and are responsible for causing asthma, bronchitis, and lung cancer. The respirable fraction ($d_{ae} < 10 \mu\text{m}$) includes only those particles that can deposit down to the alveolar region, and these can lead to the development of such chronic diseases as pneumoconiosis (black lung) and emphysema.^{47,48}

In order to obtain aerosol measurements that are meaningful to occupational exposure assessment, the sampling technique used must reflect actual worker exposure. The most reliable means of sampling in occupational settings is considered to be through the use of personal samplers which measure the individual exposure of a worker chosen to wear it.^{38,39,48} This worker, in turn, would be considered representative of a group of similarly exposed workers. Personal samplers and their pumps are designed to both mimic the average human breathing rate, and to sample only particulate matter that belongs to the health-relevant, inhalable fraction. Also, because personal samplers move with workers throughout their shift, the collection accounts for time spent in various microenvironments of the workplace. When a personal sampler is worn, air in the breathing zone of a worker is drawn into the sampling inlet, and particulate matter of health-relevant size is collected onto a filter. Filter samples are then analyzed using a

technique appropriate for the aerosol components of interest. For measurement of particulate metals, the early history of exposure assessment was revolutionized in the 1950s by the introduction of atomic absorption spectrometry (AAS).⁴⁸ This technique has largely been replaced as the method of choice for metal analysis by inductively-coupled plasma atomic emission spectrometry (ICP-AES) and inductively-coupled plasma mass spectrometry (ICP-MS), as both of these techniques provide multi-element measurements and lower detection limits than AAS. A major disadvantage to this method of exposure assessment is that collection filters must be sent out for chemical analysis, meaning that approximately two weeks time passes before exposure results are reported. Chapters 5-7 will discuss development of a method for detection of particulate metals on a paper-based device that could be performed on-site and would allow for almost immediate reporting of unsafe particulate metal levels.

1.3 Microfluidic Devices

Microfluidics is the science and technology of systems that process or manipulate small volumes of fluids within dimensions of tens to hundreds of micrometers.⁴⁹ This technology has been exploited in various fields that include medical analysis, environmental and food safety monitoring, biochemical analysis, and microchemistry.⁵⁰ The interest generated in microfluidic devices since the early 1990s is due to the number of useful capabilities they have to offer. These include the ability to use small quantities of samples and reagents, and to carry out separations and detection with high resolution and sensitivity. Additionally, microfluidic devices are low in cost relative to conventional instrumentation, afford short analysis times, and have small footprints making them

portable.⁵¹

The earliest microfluidic devices, produced in the 1980's – 1990's, were made with silicon wafers or glass, largely because fabrication techniques for these materials had already been developed.⁴⁹ Fabrication of silicon and glass devices was expensive and difficult, however, and their rigidity made incorporation of moving parts challenging. By the mid to late 1990s softer, plastic materials, such as poly(dimethylsiloxane) (PDMS), became popular device materials as they made fabrication easier, were much less expensive than silicon or glass, and could support useful components such as valves and pumps.⁴⁹ Plastics and glass are still commonly used as device materials today.

In the last few years there has been a renewed interest in using paper as a substrate for microfluidic devices. Paper has been routinely used for diagnostic devices since the early 20th century, primarily in the simple form of “test strips.”⁵² Common examples include pH litmus paper, urinalysis dipsticks, and glucose test strips. The more recent interest in paper arose due to work done by Whitesides *et al.*, demonstrating that patterned paper can serve as a microfluidic platform capable of multiplexed analysis and, along with imaging devices and software, can be used for quantitative analysis.⁵³⁻⁵⁵ Paper functions as a microfluidic substrate because its cellulose fiber network act as capillaries, wicking aqueous fluid without the need for active pumping. It has now become an attractive substrate because it is available everywhere, inexpensive, disposable, and easy to modify chemically.

The work presented in the subsequent chapters demonstrates the vastly diverse forms that microfluidic devices can take. Chapter 3 will introduce a PDMS MCE device that incorporates conductivity detection and is capable of sampling from a continuous

flow. This device was designed for analysis of ionic aerosol components, and provides the first example of an interface between microfluidics and a particle-into-liquid sampler (PILS). Chapter 7 will then demonstrate a paper-based microfluidic device that employs colorimetric detection for measurement of particulate metals. This is the first paper-based device shown to be capable of multiplexed metal detection from a real, aerosolized sample. The techniques developed for paper-based devices here have also laid the groundwork for several of the current projects in the Henry lab, including development of novel paper-based devices and the use of filters as a sample system for both paper- and PDMS- based devices.

1.5 References

- (1) Bernstein, J. A.; Neil, A.; Barnes, C.; Bernstein, I. L.; Bernstein, J. A.; Nel, A.; Peden, D.; Diaz-Sanchez, D.; Tarlo, S. M.; Williams, P. B., Health effects of air pollution. *The Journal of allergy and clinical immunology* **2004**, *114* (5), 1116-1123.
- (2) Pöschl, U., Atmospheric Aerosols: Composition, Transformation, Climate and Health Effects. *Angewandte Chemie International Edition* **2005**, *44* (46), 7520-7540.
- (3) Kanakidou, M.; Seinfeld, J. H.; Pandis, S. N.; Barnes, I.; Dentener, F. J.; Facchini, M. C.; Van Dingenen, R.; Ervens, B.; Nenes, A.; Nielsen, C. J.; Swietlicki, E.; Putaud, J. P.; Balkanski, Y.; Fuzzi, S.; Horth, J.; Moortgat, G. K.; Winterhalter, R.; Myhre, C. E. L.; Tsigaridis, K.; Vignati, E.; Stephanou, E. G.; Wilson, J., Organic aerosol and global climate modelling: a review. *Atmos. Chem. Phys.* **2005**, *5* (4), 1053-1123.
- (4) Lohmann, U.; Feichter, J., Global indirect aerosol effects: a review. *Atmos. Chem. Phys.* **2005**, *5* (3), 715-737.
- (5) Kahn, R. A.; Yu, H.; Schwartz, S. E.; Chin, M.; Feingold, G.; Remer, L. A.; Rind, D.; Halthore, R.; Decola, A. *Atmospheric Aerosol Properties and Climate Impacts, A Report by the U. S. Climate Change Science Program and the Subcommittee on Global Change Research*; National Aeronautics and Space Administration: Washington, D. C., **2009**.
- (6) Simon, P. K.; Dasgupta, P. K., Continuous Automated Measurement of the Soluble Fraction of Atmospheric Particulate Matter. *Analytical Chemistry* **1995**, *67* (1), 71-78.
- (7) Finlayson-Pitts, B. J.; Pitts, J. N., Jr., Tropospheric Air Pollution: Ozone, Airborne Toxics, Polycyclic Aromatic Hydrocarbons, and Particles. *Science* **1997**, *276* (5315), 1045-1051.
- (8) Pandis, S. N.; Wexler, A. S.; Seinfeld, J. H., Dynamics of Tropospheric Aerosols. *The Journal of Physical Chemistry* **1995**, *99* (24), 9646-9659.
- (9) Raes, F.; Dingenen, R. V.; Vignati, E.; Wilson, J.; Putaud, J.-P.; Seinfeld, J. H.; Adams, P., Formation and cycling of aerosols in the global troposphere. *Atmospheric Environment* **2000**, *34* (25), 4215-4240.
- (10) Oberdorster, G.; Oberdorster, E.; Oberdorster, J., Nanotoxicology: An Emerging Discipline Evolving from Studies of Ultrafine Particles. *Environ Health Perspect* **2005**, *113* (7).
- (11) Program, N. A. P. A. *1990 Integrated Assessment Report*; The U.S. National Acid Precipitation Assessment Program, Office of the Director: Washington, D. C. , **1991**.
- (12) Canagaratna, M. R.; Jayne, J. T.; Jimenez, J. L.; Allan, J. D.; Alfarra, M. R.; Zhang, Q.; Onasch, T. B.; Drewnick, F.; Coe, H.; Middlebrook, A.; Delia, A.; Williams, L. R.; Trimborn, A. M.; Northway, M. J.; DeCarlo, P. F.; Kolb, C. E.; Davidovits, P.; Worsnop, D. R., Chemical and microphysical characterization of ambient aerosols with the aerodyne aerosol mass spectrometer. *Mass Spectrometry Reviews* **2007**, *26* (2), 185-222.

- (13) Gauderman, W. J.; Avol, E.; Gilliland, F.; Vora, H.; Thomas, D.; Berhane, K.; McConnell, R.; Kuenzli, N.; Lurmann, F.; Rappaport, E.; Margolis, H.; Bates, D.; Peters, J., The Effect of Air Pollution on Lung Development from 10 to 18 Years of Age. *New England Journal of Medicine* **2004**, *351* (11), 1057-1067.
- (14) Katsouyanni, K.; Touloumi, G.; Samoli, E.; Gryparis, A.; Tertre, A. L.; Monopoli, Y.; Rossi, G.; Zmirou, D.; Ballester, F.; Boumghar, A.; Anderson, H. R.; Wojtyniak, B.; Paldy, A.; Braunstein, R.; Pekkanen, J.; Schindler, C.; Schwartz, J., Confounding and Effect Modification in the Short-Term Effects of Ambient Particles on Total Mortality: Results from 29 European Cities within the APHEA2 Project. *Epidemiology* **2001**, *12* (5), 521-531.
- (15) Stanek, L. W.; Brown, J. S.; Stanek, J.; Gift, J.; Costa, D. L., Air Pollution Toxicology, A Brief Review of the Role of the Science in Shaping the Current Understanding of Air Pollution Health Risks. *Toxicological Sciences* **2011**, *120* (suppl 1), S8-S27.
- (16) Tolocka, M. P.; Solomon, P. A.; Mitchell, W.; Norris, G. A.; Gemmill, D. B.; Wiener, R. W.; Vanderpool, R. W.; Homolya, J. B.; Rice, J., East versus West in the US: Chemical Characteristics of PM_{2.5} during the Winter of 1999. *Aerosol Science and Technology* **2001**, *34* (1), 88-96.
- (17) Solomon, P. A.; Larson, S. M.; Fall, T.; Cass, G. R., Basinwide nitric acid and related species concentrations observed during the Claremont nitrogen species comparison study. *Atmospheric Environment (1967)* **1988**, *22* (8), 1587-1594.
- (18) Chow, J. C.; Watson, D. H.; Lowenthal, P. A.; Solomon, P. A.; Magliano, K. L.; Ziman, S. D.; Richards, L. W., PM₁₀ source apportionment in California's San Joaquin Valley. *Atmospheric Environment* **1992**, *26A*, 3335-3354.
- (19) Magliano, K. L.; Hughes, V. M.; Chinkin, L. R.; Coe, D. L.; Haste, T. L.; Kumar, N.; Lurmann, F. W., Spatial and temporal variations in PM₁₀ and PM_{2.5} source contributions and comparison to emissions during the 1995 integrated monitoring study. *Atmospheric Environment* **1999**, *33* (29), 4757-4773.
- (20) EPA, U. S. *Air quality criteria for particulate matter*; Office of Research and Development, National Center for Environmental Assessment: Research Triangle Park, NC, **2001**.
- (21) Solomon, P. A.; Norris, G.; Landis, M.; Tolocka, M., Chemical Analysis Methods for Atmospheric Aerosol Components. In *Aerosol measurement principles, techniques, and applications*, Baron, P. A.; Willeke, K., Eds. Wiley: New York, **2001**; pp 261-293.
- (22) Haddad, P. R.; Jackson, P. E., *Ion Chromatography: Principles and Applications* Elsevier: Amsterdam, **1990**.
- (23) Blanco-Heras, G. A.; Turnes-Carou, M. I.; López-Mahía, P.; Muniategui-Lorenzo, S.; Prada-Rodríguez, D.; Fernández-Fernández, E., Determination of organic anions in atmospheric aerosol samples by capillary electrophoresis after reversed pre-electrophoresis. *ELECTROPHORESIS* **2008**, *29* (6), 1347-1354.
- (24) Dabek-Zlotorzynska, E.; Dlouhy, J. F., Application of capillary electrophoresis in atmospheric aerosols analysis: Determination of inorganic and organic anions. *Journal of Chromatography A* **1994**, *671* (1-2), 389-395.

- (25) Dabek-Zlotorzynska, E.; Dlouhy, J. F., Application of capillary electrophoresis in atmospheric aerosol analysis: determination of cations. *Journal of Chromatography A* **1995**, *706* (1-2), 527-534.
- (26) Fukushi, K.; Takeda, S.; Chayama, K.; Wakida, S.-I., Application of capillary electrophoresis to the analysis of inorganic ions in environmental samples. *Journal of Chromatography A* **1999**, *834* (1-2), 349-362.
- (27) Timerbaev, A. R.; Dabek-Zlotorzynska, E.; A. G. T. van den Hoop, M., Inorganic environmental analysis by capillary electrophoresis. *Analyst* **1999**, *124* (6), 811-826.
- (28) Allan, J. D.; Jimenez, J. L.; Williams, P. I.; Alfarra, M. R.; Bower, K. N.; Jayne, J. T.; Coe, H.; Worsnop, D. R., *Geophys. Res.* **2003**, 108.
- (29) DeCarlo, P. F.; Kimmel, J. R.; Trimborn, A.; Northway, M. J.; Jayne, J. T.; Aiken, A. C.; Gonin, M.; Fuhrer, K.; Horvath, T.; Docherty, K. S.; Worsnop, D. R.; Jimenez, J. L., Field-Deployable, High-Resolution, Time-of-Flight Aerosol Mass Spectrometer. *Analytical Chemistry* **2006**, *78* (24), 8281-8289.
- (30) Jimenez, J. L.; Jayne, J. T.; Shi, Q.; Kolb, C. E.; Worsnop, D. R.; Yourshaw, I.; Seinfeld, J. H.; Flagan, R. C.; Zhang, X.; Smith, K. A.; Morris, J. W.; Davidovits, P., Ambient aerosol sampling using the Aerodyne Aerosol Mass Spectrometer. *J. Geophys. Res.* **2003**, 108.
- (31) Nash, D. G.; Baer, T.; Johnston, M. V., Aerosol mass spectrometry: An introductory review. *International Journal of Mass Spectrometry* **2006**, *258* (1-3), 2-12.
- (32) Prather, K. A.; Hatch, C. D.; Grassian, V. H., *Annu. Rev. Anal. Chem.* **2008**, *1*, 485-514.
- (33) Weber, R. J.; Orsini, D.; Daun, Y.; Lee, Y. N.; Klotz, P. J.; Brechtel, F., A Particle-into-Liquid Collector for Rapid Measurement of Aerosol Bulk Chemical Composition. *Aerosol Science and Technology* **2001**, *35*, 718-727.
- (34) Orsini, D. A.; Sullivan, A.; Sierau, B.; Baumann, K.; Weber, R., Refinements to the particle-into-liquid sampler (PILS) for ground and airborne measurements of water soluble aerosol composition. *Atmospheric Environment* **2003**, *37*, 1243-1259.
- (35) Noblitt, S. D.; Lewis, G. S.; Liu, Y.; Hering, S. V.; Collett, J. L.; Henry, C. S., Interfacing Microchip Electrophoresis to a Growth Tube Particle Collector for Semicontinuous Monitoring of Aerosol Composition. *Analytical Chemistry* **2009**, *81* (24), 10029-10037.
- (36) Ramachandran, G., *Occupational Exposure Assessment for Air Contaminants*. Taylor & Francis Group: Boca Raton, FL, **2005**.
- (37) Wild, P.; Bourgkard, E.; Paris, C., Lung cancer and exposure to metals: the epidemiological evidence. *Methods in Molecular Biology* **2009**, *472*, 139-167.
- (38) Spengler, J. D.; Treitman, R. D.; Tosteson, T. D.; Mage, D. T.; Soczek, M. L., Personal exposures to respirable particulates and implications for air pollution epidemiology. *Environmental Science & Technology* **1985**, *19* (8), 700-707.
- (39) Wallace, L., A Decade of Studies of Human Exposure: What Have We Learned? *Risk Analysis* **1993**, *13* (2), 135-139.

- (40) Gioda, A.; Jimenez-Velez, B. D., Assessment of Heavy Metals in Fine Particulate Matter from a Workplace Environment in Puerto Rico. *Proceedings: Indoor Air* **2005**, 1526-1530.
- (41) Costa, D. L.; Dreher, K. L., Bioavailable Transition Metals in Particulate Matter Mediate Cardiopulmonary Injury in Healthy and Compromised Animal Models. *Environmental Health Perspectives* **1997**, *105*, 1053-1060.
- (42) Dreher, K. L.; Jaskot, R. H.; Lehmann, J. R.; Richards, J. H.; McGee, J. K.; Ghio, A. J.; Costa, D. L., Soluble Transition Metals in Particulate Matter Mediate Residual Oil Fly Ash Induced Acute Lung Injury. *Journal of Toxicological and Environmental Health* **1997**, *8*, 479-494.
- (43) Schaumann, F.; Borm, P. J.; Herbrich, A.; Knoch, J., Metal-rich Ambient Particles Cause Airway Inflammation. *American Journal of Respiratory and Critical Care Medicine* **2004**, *170*, 898-892.
- (44) Kodavanti, U. P.; Hauser, R.; Christiani, D. C.; Meng, Z. H.; McGee, J. K.; Ledbetter, A.; Richards, J. H.; Costa, D. L., Pulmonary responses to oil fly ash particles in the rat differ by virtue of their specific soluble metals. *Toxicological Sciences* **1998**, *43* (2), 204-212.
- (45) Ghio, A. J.; Stonehuerner, J.; Pritchard, R. J.; Piantadosi, C. A.; Quigley, D. R.; Dreher, K. L.; Costa, D. L., Humic-Like Substances in Air Pollution Particulates Correlate with Concentrations of Transition Metals and Oxidant Generation. *Inhalation Toxicology* **1996**, *8* (5), 479-494.
- (46) Abdel-Salam, M., Aerosol Sampling Methods in Workplace and Ambient Environments. *Journal of Aerosol Medicine* **2006**, *19* (4), 434.
- (47) Nieboer, E.; Thomassen, Y.; Chashchin, V.; Odland, J. O., Occupational exposure assessment of metals. *Journal of Environmental Monitoring* **2005**, *7* (5), 411-415.
- (48) Vincent, J. H.; Ramachandran, G.; Thomassen, Y.; Keeler, G. J., Application of recent advances in aerosol sampling science towards the development of improved sampling devices: the way ahead. *Journal of Environmental Monitoring* **1999**, *1*, 285-292.
- (49) Whitesides, G. M., The origins and the future of microfluidics. *Nature* **2006**, *442*, 368-373.
- (50) Bruin, G. J. M., Recent developments in electrokinetically driven analysis on microfabricated devices. *Electrophoresis* **2000**, *21* (18), 3931-3951.
- (51) Manz, A.; Harrison, D. J.; Verpoorte, E. M. J.; Fettingner, J. C.; Paulus, A.; Widmer, H. M., Planar chips technology for miniaturization and integration of separation techniques into monitoring systems: Capillary electrophoresis on a chip. *Journal of Chromatography A* **1992**, *593*, 253-258.
- (52) Zhao, W.; van den Berg, A., Lab on paper. *Lab on a Chip* **2008**, *8* (12), 1988-1991.
- (53) Bruzewicz, D. A.; Reches, M.; Whitesides, G. M., Low-Cost Printing of Poly(dimethylsiloxane) Barriers To Define Microchannels in Paper. *Analytical Chemistry* **2008**, *80* (9), 3387-3392.
- (54) Martinez, A. W.; Phillips, S. T.; Butte, M. J.; Whitesides, G. M., Patterned Paper as a Platform for Inexpensive, Low-Volume, Portable Bioassays. *Angewandte Chemie International Edition* **2007**, *46* (8), 1318-1320.

- (55) Martinez, A. W. P., S. T.; Whitesides, G. M., Three-dimensional microfluidic devices fabricated in layered paper and tape. *PNAS* **2008**, *105* (50), 19606-19611.

CHAPTER 2: CAPILLARY ELECTROPHORESIS-BASED MICROFLUIDICS

2.1 Capillary Electrophoresis Theory

An introduction to general CE theory is presented here to allow for better understanding of the separation technique and microfluidic flow modeling discussed in Chapter 2. Capillary electrophoresis is a separation technique based on the migration of chemical species subjected to an electric field. The use of capillaries for electrophoresis offers many advantages over the standard solid supports used during the evolution of electrophoresis, such as polyacrylamide and agarose gels.¹ Silica capillaries with internal diameters ranging from 20-100 μm are used almost exclusively for the majority of CE applications. The high surface-to-volume ratio of capillaries with these dimensions allows for efficient dissipation of Joule heat generated by the electric field. This dissipation of Joule heat is what permits electrophoretic separations to be performed at up to 30,000 V, which affords rapid separation times. Also, the microliter volumes of these capillaries require only milliliter quantities of buffer, and sample volumes as low as 5 μL , even for repetitive runs.¹

The simplest and most commonly used form of CE is capillary zone electrophoresis (CZE). This CE mode is applied in the work presented in Chapter 3 and will be the focus of this discussion. To perform a CZE separation, an electric field is applied across a buffer-filled capillary, and sample is introduced at the inlet. The applied

electric field dictates movement of analytes in the capillary through a combination of two phenomena: electrophoretic mobility and electroosmotic flow. Electrophoretic mobility occurs because charged species are attracted to the oppositely charged electrode at the end of the capillary. In the normal polarity mode of CE the anode (+) is at the inlet and the cathode (-) is at the detection end, causing positively charged particles to move toward the detection end. If polarity is reversed, negatively charged species will then move to the detection end, towards the anode (+). The electrophoretic mobility (μ_{ep}) of a charged species can be approximated with the equation

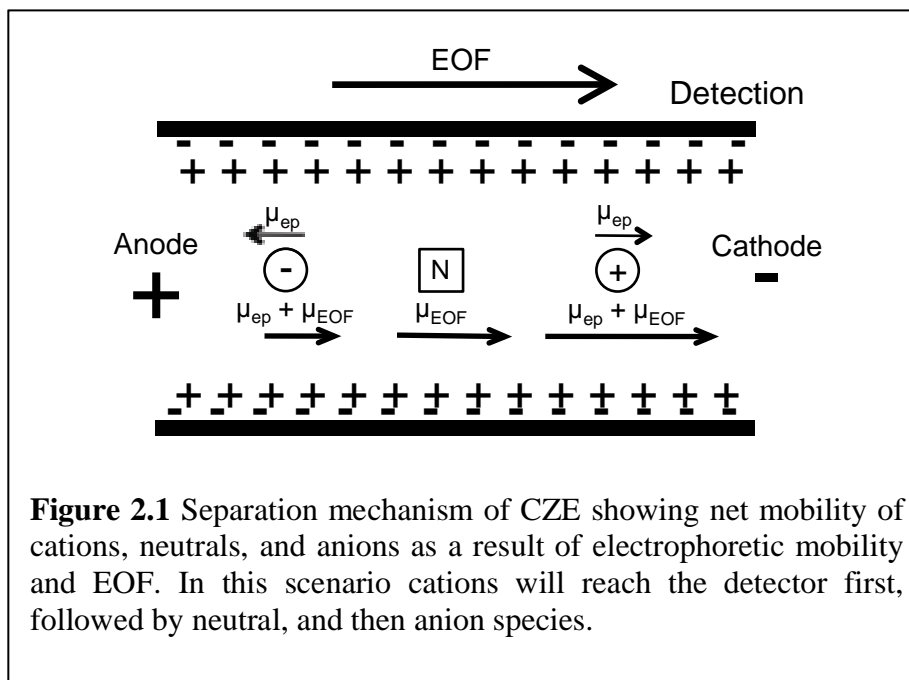
$$\mu_{ep} = \frac{q}{f} \quad (2.1)$$

where q is the charge of the species and f is the frictional coefficient for a spherical particle having a hydrodynamic radius, r , in a solution of viscosity, η , described by the Stokes equation (2.2).

$$f = 6\pi\eta r \quad (2.2)$$

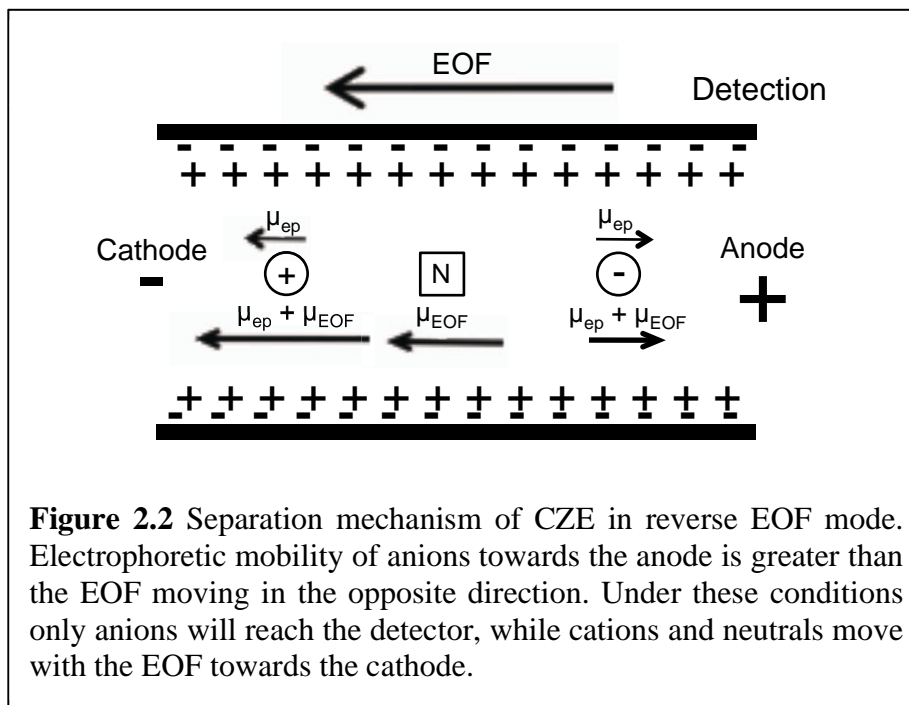
If electrophoretic mobility was the only mechanism dictating movement of analytes, then positive, negative, and neutral species could never all reach the detection end in a single CE run. This is not the case, however, due to the occurrence of electroosmotic flow (EOF) that results from formation of a charged double layer on the capillary wall. Deprotonated silanol groups at the surface of the capillary wall attract cationic species from the buffer, forming a positively charged double layer with a charge density that decreases with increasing distance from the wall. This is referred to as a double layer because cations closest to the wall form a static layer, while the more diffuse cations further from the wall form a dynamic layer. Upon application of an electric field, cations in the diffuse layer move towards the cathode (-), dragging waters of hydration

with them. Due to the hydrogen bonding between waters of hydration and free water molecules in solution, this ultimately results in a bulk flow of buffer that acts as a pumping mechanism to force all analytes, including neutral and anionic species, towards the cathode (-) end. The CZE separation mechanism is shown in Figure 2.1, which demonstrates the net movement of species due to both electrophoretic mobility and EOF.



Anionic species will only move towards the cathode if the velocity of EOF is greater than the anion's electrophoretic mobility. For analysis of anions with high mobility, a reverse EOF mode is often used and accomplished by reversing the electric field polarity. This also reverses the direction of electrophoretic mobilities so that anions move towards the detection end, while cations and neutrals cannot. Separation in reverse EOF mode is demonstrated in Figure 2.2. The strength of the EOF can also be modified by adjusting the buffer pH, as this dictates the degree to which silanol groups are

deprotonated. Higher pH yields greater charge density on the surface of the capillary wall, resulting in a stronger EOF. Below about pH 2, silanol groups are all protonated and EOF will cease to exist.



The electrophoretic velocity (V_E) of an analyte can be determined from electrophoretic mobility (μ_{ep}), the mobility due to EOF (μ_{EOF}), and the applied electric field (E) with Equation 2.3.

$$V_E = (\mu_{ep} + \mu_{EOF})E$$

Separation is achieved through differences in electrophoretic velocities of each analyte, which results in different migration times. Analytes are detected by measuring an associated physical property such as absorbance, fluorescence, or conductivity either on-capillary or at the immediate exit of the capillary.

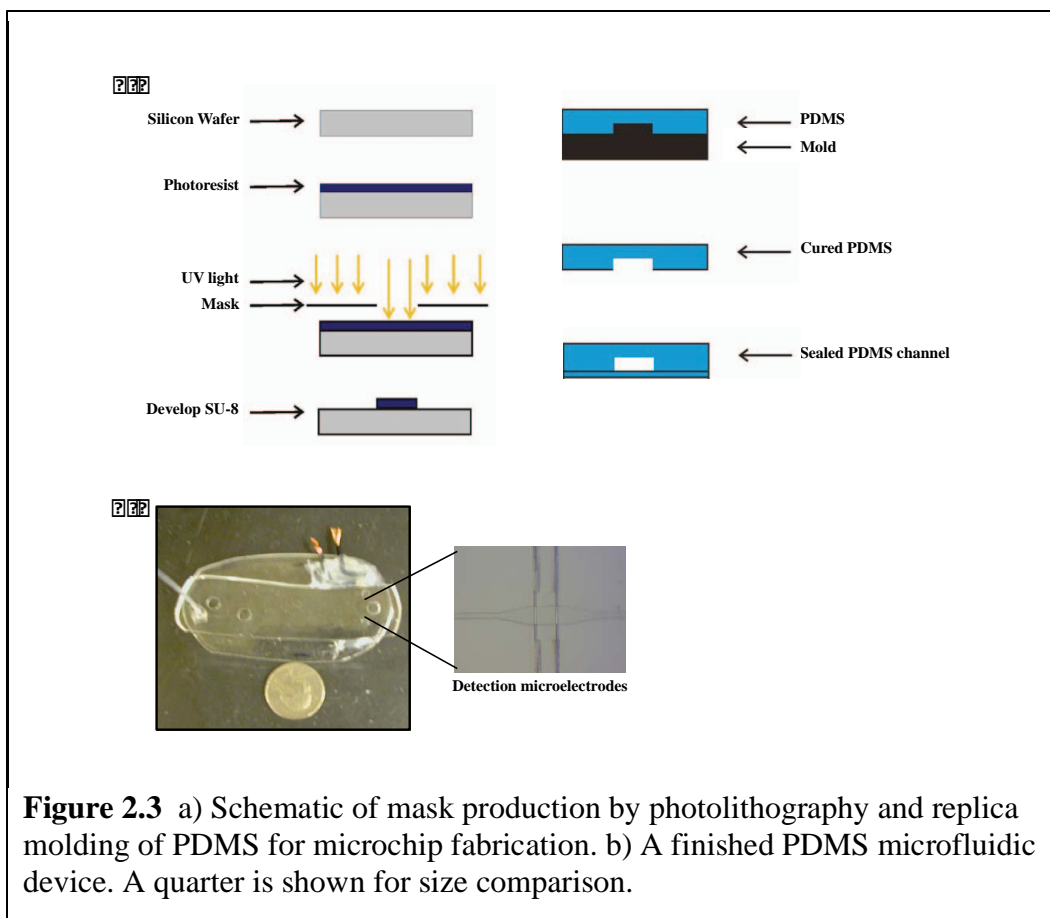
The efficiency of CE separations is typically much higher than that of other separation techniques, such as HPLC.² Because there is no packing material or stationary phase associated with this technique, there is no band broadening due to mass transfer between phases or due to multiple flow paths provided by packing material. In addition, the flow profile in EOF driven systems is flat, rather than the rounded parabolic flow profile characteristic of pressure-driven flow systems.³ Since a flat flow profile limits analyte dispersion relative to parabolic flow, EOF does not significantly contribute to band broadening.^{2,4} Theoretically, resolution in CE should only be limited by molecular diffusion; however, in practice it is possible for Joule heating and analyte-wall interactions to perturb the EOF, leading to band broadening effects.⁴

2.2 Microfluidic Capillary Electrophoresis

The CE theory described above also applies to microchip capillary electrophoresis (MCE), in which microfluidic channels incorporated into a device perform the function of capillaries. The same phenomena that occur inside the silica capillary tubing used in traditional CE are reproduced in microfluidic channels by fabricating devices with materials that have surface chemistry similar to that of silica capillary walls. The two most common examples of materials used for CE microfluidic devices are glass and poly(dimethylsiloxane) (PDMS). Micro-channels created with these materials contain silanol groups that provide the channel surface chemistry necessary to induce EOF, thus allowing for CE separation. Glass has been an attractive substrate material used for fabrication of capillary channels; however, the etching techniques used to produce glass devices are relatively difficult, expensive, and require access to specialized cleanroom

facilities.^{5,6} PDMS is one of the mostly widely used polymers for microfluidics, and the soft lithography techniques employed when using PDMS reduce the time, complexity, and cost of device fabrication when compared to the etching process used for glass.^{7,8}

The MCE device introduced in Chapter 3 was fabricated from PDMS using the soft lithography technique of replica molding.^{7,9} This process, shown by the schematic in Figure 2.3a, begins by creating a mold on a silicon wafer using photolithography. The wafer is coated with a photoresist material, the thickness of which will determine microchannel depth. After a short baking time, a mask of the device design is placed over the photoresist, which is then exposed to UV light. After development with a solvent, only features allowed exposure to UV light remain, resulting in a mold that is used to produce PDMS replicas. Replica molding is accomplished by first mixing the PDMS base with a curing agent, typically at a ratio of 10:1 (base:curing agent), and pouring this viscous liquid over the silicon mold. The PDMS pre-polymer conforms to the shape of the mold and cures as silicon hydride groups present in the curing agent react with vinyl groups of the base and form a cross-linked, elastomeric solid. The cured PDMS piece is peeled off the mold and its surface is oxidized briefly (< 1 min) with exposure to an air plasma. Surface-oxidized PDMS can then be sealed to a blank PDMS piece, or other materials such as glass or silicon, provided that they also have been plasma treated.¹⁰ When conductivity detection is employed, microelectrodes are placed across the separation channel, just before the waste reservoir, prior to sealing the two PDMS pieces. Electrodes controlled by an external power supply are placed in fluid reservoirs to generate the electric field needed to induce EOF. A completed PDMS microfluidic device with wires incorporated for conductivity detection is shown in Figure 2.3b.



MCE has several advantages over traditional CE, such as the ability to analyze smaller sample volumes, lower reagent and power consumption, and more portable, less expensive instrumentation. There are drawbacks to MCE, however, which include poor reproducibility due to capillary surface chemistry that is not completely understood, the need to frequently refill background electrolyte reservoirs, and the potential for increased joule heating due to low thermal conductivity and heat transfer coefficients of plastics like PDMS.¹¹

2.3 Aerosol Analysis with MCE

There are several examples of environmental monitoring using MCE technology, though the majority of these describe analysis of water samples (river water, ground water, tap water, etc.).¹²⁻¹⁴ Aerosol analysis with MCE has not been as common. Garcia *et al.* were the first to report aerosol composition analysis with MCE.¹⁵ They developed a method for using MCE with pulsed amperometric detection to measure levoglucosan and other carbohydrates that result from biomass burning. Liu *et al.* reported detection of sulfate and nitrate in aerosols using conductivity detection in MCE.¹⁶ Significant improvements to aerosol analysis methods using MCE with conductivity detection were made by Noblitt *et al.* through optimization of PDMS device dimensions, use of internal standards, and development of a selective separation for sulfate, nitrate, chloride, and oxalate.¹⁷ As mentioned in the previous chapter, Noblitt *et al.* also reported on the first on-line coupling of MCE with an aerosol sampler.¹⁸ They demonstrated an interface between a water condensation particle collector (WCPC) and MCE for detection of anionic aerosol components. Sampled particles are enlarged in the WCPC through water condensation and are then accumulated over time into a microfluidic device sample reservoir. This method allows for low limits of detection, as samples are concentrated in the reservoir before CE separation and detection; however, real-time analysis cannot be achieved through coupling MCE to an accumulation mode sampler. Real-time analysis is closer to being achieved using the Particle into Liquid Sampler (PILS) described in the previous chapter; however, coupling MCE to a PILS requires a device capable of sampling from a continuous flow.

2.4 Continuous Sampling MCE Devices

Several groups have developed continuous flow microfluidic devices. Chen *et al.* developed a microchip for protein analysis that uses a voltage-gated injection, requiring an optimized voltage that varies with sample pump speed.¹⁹ Li *et al.* incorporated PDMS pneumatic valves into a microchip, and these along with an applied potential, control injection of sample from a continuous hydrodynamic flow.²⁰ They later incorporated electrochemical detection in this device and used it for microdialysis sampling.^{20,21} A microchip designed by Attiya *et al.*, capable of on chip mixing, reactions, and separation, relied on a large difference in flow resistance between the sample flow channel and the rest of the device to keep continuous flow from perturbing liquids within the device.²² A sample channel containing pressure driven flow that was 300 μm deep and 1 mm wide was connected to a network of electrokinetic flow channels with depths in the range of 10-13 μm and widths of 36-275 μm . Sample flow rates of up to 1 mL/min were used successfully. Razunguzwa *et al.* used a similar concept to this and, with laser micromachining, incorporated a hydrodynamic flow restrictor into a CE-mass spectrometry interface.²³ The flow restrictor, which consisted of 6 parallel 10 μm wide channels, served to provide continuous introduction of a make-up solution and to negate the hydrodynamic backpressure in the CE channel. Fang *et al.* developed continuous sample introduction into a microchip by implementing a 20 μL sample reservoir that could be continuously filled with sample.²⁴ The fluid level of the reservoir was kept constant through the use of a guided-overflow trough leading to a waste reservoir. At certain stages of operation, electroosmotic flow (EOF) was induced in the other channels of the microchip to prevent sample leakage. Sample could either be introduced

continuously at a fixed rate; or introduction of discrete samples could be achieved by turning on and off the pump, and rinsing with water in between samples. This microchip accommodated flow rates in the range of 0.48-0.6 mL/min. Finally, a microchip was developed by Büttgenbach and Wilke in which a passive valve in the device isolates the sample and the hydrodynamic pressure from the separation channel.²⁵ An active valve at the outlet of the sample channel controls injection. When the active valve is open, sample is able to flow out of the chip and hydrodynamic pressure is reduced. Upon closing it, hydrodynamic pressure pushes sample through the passive valve and into the rest of the device.

While these devices worked well for their respective applications, their incorporation of valves and pumps require additional power supplies and difficult fabrication methods, and operation of devices is more complicated relative to more traditional microchips. An ideal MCE device for real-time aerosol analysis should be capable of interfacing to existing aerosol samplers, such as the PILS, and have a simple design that does not require use of additional equipment and allows for easy operation in the field. The continuous sampling device introduced in Chapter 3 was designed to fit these criteria, and allowed for development of a PILS-MCE system for analysis of inorganic cation and anion components of atmospheric aerosols.

2.5 References

- (1) Landers, J. P., *Handbook of capillary and microchip electrophoresis and associated microtechniques*. CRC Press: Boca Raton, **2008**.
- (2) Skoog, D. A., *Principles of instrumental analysis*. Saunders College Pub Harcourt Brace College Publishers: Philadelphia, **1998**.
- (3) O'Grady, J. F. K. Y. N., Patrick McDonnell, Aaron J. Mancuso, Kimberley A. Frederick, Detecting deviations from pure EOF during CE separations. *Electrophoresis* **2007**, 28 (14), 2385-2390.
- (4) Ghosal, S., Fluid mechanics of electroosmotic flow and its effect on band broadening in capillary electrophoresis. *Electrophoresis* **2004**, 25, 214-228.
- (5) Harrison, D. J.; Fluri, K.; Seiler, K.; Fan, Z.; Effenhauser, C. S.; Manz, A., Micromachining a Miniaturized Capillary Electrophoresis-Based Chemical Analysis System on a Chip. *Science* **1993**, 261 (5123), 895-897.
- (6) Manz, A.; Harrison, D. J.; Verpoorte, E. M. J.; Fettingner, J. C.; Paulus, A.; Widmer, H. M., Planar chips technology for miniaturization and integration of separation techniques into monitoring systems: Capillary electrophoresis on a chip. *Journal of Chromatography A* **1992**, 593, 253-258.
- (7) McDonald, J. C.; Duffy, D. C.; Anderson, J. R.; Chiu, D. T.; Wu, H.; Schueller, O. J. A.; Whitesides, G. M., Fabrication of microfluidic systems in poly(dimethylsiloxane). *Electrophoresis* **2000**, 21 (1), 27-40.
- (8) Madou, M. J., *Fundamentals of microfabrication the science of miniaturization*. CRC Press: Boca Raton, **2002**.
- (9) Duffy, D. C.; McDonald, J. C.; Schueller, O. J.; Whitesides, G. M., Prototyping of microfluidic systems in poly(dimethylsiloxane). *Analytical Chemistry* **1998**, 70, 4974-4984.
- (10) McDonald, J. C.; Whitesides, G. M., Poly(dimethylsiloxane) as a Material for Fabricating Microfluidic Devices. *Accounts of Chemical Research* **2002**, 35 (7), 491-499.
- (11) Revermann, T.; Gotz, S.; Kunnemeyer, J.; Karst, U., Quantitative analysis by microchip capillary electrophoresis - current limitations and problem-solving strategies. *Analyst* **2008**, 133 (2), 167-174.
- (12) Jokerst, J. C.; Emory, J. M.; Henry, C. S., Advances in microfluidics for environmental analysis. *Analyst* **2012**, 137 (1).
- (13) Crevillen, A. G.; Hervas, M.; Lopez, M. A.; Gonzalez, M. C.; Escarpa, A., Real sample analysis on microfluidic devices. *Talanta* **2007**, 74 (3), 342-357.
- (14) Li, H.-F.; Lin, J.-M., Applications of microfluidic systems in environmental analysis. *Analytical and Bioanalytical Chemistry* **2009**, 393 (2), 555-567.
- (15) Garcia, C. D.; Engling, G.; Herckes, P.; Collett, J. L.; Henry, C. S., Determination of levoglucosan from smoke samples using microchip capillary electrophoresis with pulsed amperometric detection. *Environ. Sci. Technol.* **2005**, 39 (2), 618-623.
- (16) Liu, Y. M., D. A.; Yu, X. Y.; Hering, S. V.; Collett, J. L.; Henry, C. S., Analysis of anions in ambient aerosols by microchip capillary electrophoresis. *Analyst* **2006**, 131, 1226-1231.

- (17) Noblitt, S. D.; Schwandner, F. M.; Hering, S. V.; Collett Jr, J. L.; Henry, C. S., High-sensitivity microchip electrophoresis determination of inorganic anions and oxalate in atmospheric aerosols with adjustable selectivity and conductivity detection. *Journal of Chromatography A* **2009**, *1216* (9), 1503-1510.
- (18) Noblitt, S. D.; Lewis, G. S.; Liu, Y.; Hering, S. V.; Collett, J. L.; Henry, C. S., Interfacing Microchip Electrophoresis to a Growth Tube Particle Collector for Semicontinuous Monitoring of Aerosol Composition. *Analytical Chemistry* **2009**, *81* (24), 10029-10037.
- (19) Chen, S.-H.; Lin, Y.-H.; Wang, L.-Y.; Lin, C.-C.; Lee, G.-B., Flow-Through Sampling for Electrophoresis-Based Microchips and Their Applications for Protein Analysis. *Analytical Chemistry* **2002**, *74* (19), 5146-5153.
- (20) Li, M. W.; Martin, R. S., Integration of continuous-flow sampling with microchip electrophoresis using poly(dimethylsiloxane)-based valves in a reversibly sealed device. *Electrophoresis* **2007**, *28* (14), 2478-2488.
- (21) Mecker, L. C.; Martin, R. S., Integration of Microdialysis Sampling and Microchip Electrophoresis with Electrochemical Detection. *Analytical Chemistry* **2008**, *80* (23), 9257-9264.
- (22) Attiya, S.; Jemere, A. B.; Tang, T.; Fitzpatrick, B.; Seiler, K.; Chiem, N.; Harrison, D. J., Design of an interface to allow microfluidic electrophoresis chips to drink from the fire hose of the external environment. *Electrophoresis* **2001**, *22* (2), 318-327.
- (23) Razunguzwa, T. T.; Lenke, J.; Timperman, A. T., An electrokinetic/hydrodynamic flow microfluidic CE-ESI-MS interface utilizing a hydrodynamic flow restrictor for delivery of samples under low EOF conditions. *Lab on a Chip* **2005**, *5* (8), 851-855.
- (24) Fang, Q.; Xu, G.-M.; Fang, Z.-L., A High-Throughput Continuous Sample Introduction Interface for Microfluidic Chip-based Capillary Electrophoresis Systems. *Analytical Chemistry* **2002**, *74* (6), 1223-1231.
- (25) Büttgenbach, S.; Wilke, R., A capillary electrophoresis chip with hydrodynamic sample injection for measurements from a continuous sample flow. *Analytical and Bioanalytical Chemistry* **2005**, *383* (5), 733-737.

CHAPTER 3: SIMPLIFIED INTERFACE BETWEEN MICROCHIP ELECTROPHORESIS AND CONTINUOUS FLOW SAMPLERS FOR AEROSOL ANALYSIS

The previous two chapters explained the benefits of using MCE for aerosol composition measurement, and made clear the need for real-time atmospheric aerosol analysis. Most aerosol collectors that allow for online measurement generate a hydrodynamic sample flow that is difficult to couple to an MCE device. This chapter introduces a simple interface between the PILS aerosol collector and MCE. It is the first example of a continuous flow MCE device that incorporates contact conductivity detection, and is the first microfluidic device to be coupled to a continuous flow aerosol collector.

The majority of the work presented in this chapter was published in *Micro Total Analysis Systems*:

Mentele, M. M.; Noblitt, S. D.; Kraly, J. R.; Henry, C. S. Continuous Flow Interface for Microfluidic Devices. *Micro Total Analysis Systems, Proceedings of the MicroTAS Symposium 2010*, 1019-1021.

3.1 Introduction

There has been great interest in measuring the composition of atmospheric aerosols over the past decade due to their deleterious effects on human health and the environment.¹⁻⁴ Aerosols are suspensions of solid or liquid particles in the atmosphere that can originate from anthropogenic, biogenic, or geogenic sources.^{3,5} It remains

unclear whether certain aerosol components originate from one of these sources or are formed through physical or chemical transformations in the atmosphere. Our understanding of aerosols is limited largely due to the fact that their chemical composition varies considerably in time and space, leaving us with incomplete knowledge concerning physical and chemical properties, global and regional distributions, and the interactions they undergo in the atmosphere. For these reasons, they also represent the largest uncertainty in understanding how humans are changing our climate.⁶

There are several techniques commonly used for aerosol monitoring, with the traditional method being filter collection, in which the transfer of aerosols from a dispersed state in the air to a compact sample on a filter facilitates the storage, transport, and pre-treatment required for offline analysis, most commonly with gas or ion chromatography. Filter collection requires long sampling intervals, intensive sample preparation, and cannot capture real-time changes in particle chemistry. There is also the possibility of artifacts due to evaporation of volatile components, degradation of the sample over time, and interactions between particles, gases, and the substrate during sampling and storage.⁷⁻¹²

While filter samples can provide useful information on a long-time scale, real-time particle analysis is necessary to better understand the sources and transformations of atmospheric aerosols, as well as their effects on health and the environment.¹³ Aerosol mass spectrometry (AMS) is a technique that does provide real-time monitoring of aerosol size and composition.^{6,14-17} This equipment is expensive relative to most aerosol analysis instrumentation, and its large, bulky size makes transport for field studies

difficult. Also, mass spectra for unknown samples can be complicated and difficult to interpret due to high fragmentation of some species and the large variety of chemical components that are often present in ambient aerosols.^{14,17-21}

Chapter 1 described the online analysis approach of coupling traditional separation and detection instrumentation to an aerosol collector that dissolves particles into an aqueous stream. The most prevalent of these systems is the PILS-IC, which provides a semi-continuous method that is used to analyze inorganic cations and anions in ~2.5-30 min, with longer times often needed for organic acids.^{19,21-23} The analysis times are predominately determined by the speed of the IC, suggesting that an interface between the PILS and a more rapid separation technique could dramatically reduce the analysis times for PILS-based samplers.

Ion chromatography is one of the most common techniques used to determine aerosol composition; however, capillary electrophoresis has more recently been developed as a good alternative in terms of separation efficiency and rapid analysis.^{19,22-24} The ionic nature of many aerosol components make CE an appropriate technique for rapid aerosol composition determination and quantification. While not as common as the previously mentioned methods, it has been demonstrated that analysis of atmospheric anions and cations by CE provides a highly efficient separation with high accuracy and precision, and short analysis time.²⁵⁻²⁸ Another benefit of using CE for continuous measurement of aerosols is its capability to be converted into a miniaturized format. In an effort to make analysis more portable, Liu *et al.* and Noblitt *et al.* demonstrated that microfluidic CE (MCE) was also a suitable method for the analysis of anions in atmospheric aerosols.^{29,30} Noblitt *et al.* also reported on-line coupling between a water

condensation particle collector (WCPC) and a MCE system, marking the first on-line coupling of this promising technique for aerosol analysis.³¹ As discussed in the previous chapter, however, this coupling does not allow for real-time measurement because the WCPC does generate a continuous sample flow. Instead, MCE coupled with the PILS aerosol sampler would give semi-real-time analysis with the benefits of fast analysis time, portability, robustness, low cost, and minimal sample and reagent requirements.

Interfacing continuously flowing samples with MCE presents a challenge because it can be difficult to introduce hydrodynamic flow into micron-sized channels in one region of the microchip without creating flow in other areas of the microchip. Chapter 2 described continuous flow microfluidic devices developed by other groups, though none of those devices could be used for aerosol analysis without modification. Furthermore, complex devices require use of additional equipment to power valves and pumps incorporated into the microchips. The simpler design introduced here requires only one power supply, one detector, and a computer for data collection, and allows for simpler fabrication and operation. Minimal equipment requirement and ease of use are particularly important for the development of aerosol analysis devices, which are intended to be implemented in the field for weeks at a time and must be low cost to meet the needs of end-users.

Our device eliminates the need for valves through the use of an electric field and very thin channels, which increases hydrodynamic fluid resistance between the sample and separation channels. Only one applied potential is needed for device operation, and other than refilling buffer reservoirs periodically, the microchip can theoretically run unattended for long periods of time. In this report, the injection method of the new

microchip is discussed, and a quantitative model is used to predict flow behavior and optimize chip geometry. Separations of cations and anions commonly found in aerosols are carried out, and the performance of the microchip over a range of pump speeds is examined. Finally, the microchip was used to continuously sample from a PILS aerosol collector, demonstrating the potential of the PILS-microchip CE system.

3.2 Experimental

Materials

The following chemicals and materials were used for microchip fabrication: SU-8 3025 photoresist (MicroChem., Newton, MA), propylene glycol monomethyl ether acetate (Aldrich, St. Louis, MO), 4 inch thermal oxide silicon wafer (University Wafers, Boston, MA), Sylgard 184 elastomer base and curing agent (Dow Corning, Midland, MI), and 15 μm gold-plated tungsten wire (Goodfellow Cambridge Ltd, Huntingdon, Cambridgeshire, UK).

Analytes and buffer components include: fluorescein isothiocyanate (FITC) (Invitrogen, Eugene, OR), 2,2-Bis(hydroxymethyl)-2,2',2''-nitrotriethanol (Bis-Tris) and 3-(N,N-dimethylmyristylammonio)-propanesulfonate (TDAPS) (Fluka, Buchs, Switzerland), N-[2-Hydroxyethyl]piperazine-N'-[2-ethanesulfonic acid] (HEPES), potassium nitrate, sodium nitrate, ammonium nitrate, potassium chloride, and ammonium sulfate (Fisher, Fair Lawn, NJ), N-[tris(hydroxymethyl)methyl]-2-aminoethanesulfonic acid (TES), 18-crown-6, lithium trifluoromethanesulfonate, picolinic acid, N-(2-hydroxyethyl)piperazine-N'-(4-butane-sulfonic acid) (HEPBS), 1,3-propanedisulfonic acid disodium salt (PDS), and oxalic acid (Sigma-Aldrich, St. Louis, MO). Reagents used

in this study were ACS grade. All aqueous solutions were prepared from a Millipore Milli-Q purifier (Billerica, MA). Fluorescence images using a FITC sample were carried out in a 20 mM TES buffer solution. The buffer solution used for anion separations was 17 mM picolinic acid / 19 mM HEPBS with 19 mM TDAPS.³⁰ Cation separations were performed using a buffer comprised of 15 mM HEPES / 15 mM Bis-Tris with 2.5 mM 18-crown-6.

Instrumentation and data acquisition

The instrumental configuration has been described previously.³² A Dionex CD20 conductivity detector (Dionex, Sunnyvale, CA) was modified to allow the detection leads to connect to the microchip detection wires. A laboratory-built, floating high-voltage power supply (HVPS) was used to apply the electric field and to control injections.³³ The analog output (0-1 V) from the detector was monitored with a National Instruments USB-6210 DAQ and LabView 8.0 software. For most experiments the data collection rate was 8 Hz, with the only exception being a collection rate of 10 Hz during the PILS-microchip CE experiment. Fluorescence images were collected with a Nikon Eclipse TE2000-U microscope, equipped with an Exfo X-Cite 120 lamp and Photometrics Cool Snap HQ² camera. Metamorph 7.1.7 software was used to acquire fluorescence data.

The PILS operates by collecting aerosol particles from the atmosphere and then mixing this sample flow with a turbulent flow of steam. The supersaturated environment inside the PILS causes the aerosol particles to grow into droplets, which can then be collected by an impactor to produce a continuous liquid flow for online analysis of the collected aerosols.²³ Here, the PILS was interfaced to a microchip through a peristaltic

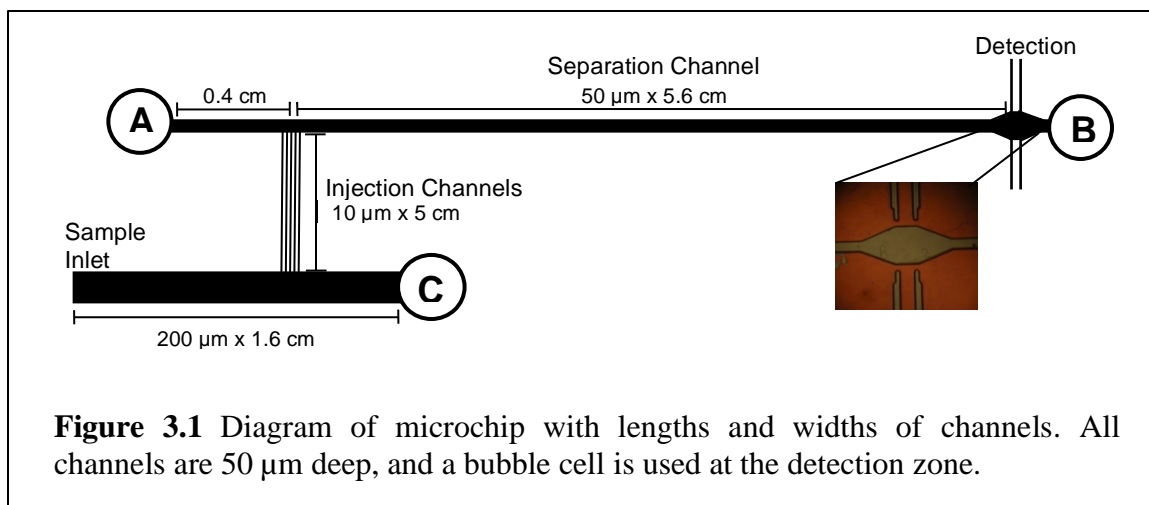
pump, which served to pull sample flow from the PILS and push it through the sample channel of the microchip. The pump controls the flow of sample and was set at 9.3 $\mu\text{L}/\text{min}$. The PILS heater and tip were set at 180°C and 90°C respectively. Air was continuously sampled for 5 hrs in Fort Collins, CO on April 15th, 2009.

Device fabrication

Fabrication of PDMS microchips and inclusion of 10 or 15 μm gold-plated tungsten wires were carried out according to established protocols.^{34,35} In brief, a mold was fabricated using a thermal oxide silicon wafer coated with a 50 μm thick layer of SU-8 3025 negative photoresist. The 50 μm layer was obtained by spin processing at 1800 rpm for 30 sec. The coated wafer was baked at 65°C for 3 min, followed by 95°C for 5 min. It was then exposed to UV light for 7 sec, and baked again at 65°C and 95°C for 2 and 6 min respectively. After it was developed with propylene glycol monomethyl ether acetate, the master was used to replica mold the microchip features in PDMS. A degassed mixture of Sylgard 184 elastomer and curing agent (10:1) was poured on the master and on a blank silicon wafer, and allowed to cure at 65°C for approximately 2 hrs. The cured PDMS was removed from the master and the blank wafer and reservoir holes were made using a 5 mm biopsy punch (Robbins Instruments, Chatham, NJ). A sample inlet hole was also made using a 1.5 mm biopsy punch. The detection wires were manually placed into the device and held in place with Scotch tape. The surfaces of the two PDMS pieces were rinsed with methanol, dried, and treated in an air plasma cleaner (Harrick) for 45 s at 18 W of power. The PDMS components were then immediately pressed together to form an irreversible seal. An FEP tube with an O.D. of 1/16'' and an I.D. of 0.008'' was placed into the sample inlet hole and sealed in place using PDMS around the tube. The exposed

ends of the wires were attached to 18 gauge copper wires glued to the outside of the microchip, which allowed for connection to the detection leads.

A schematic of the microchip design is shown in Figure 3.1. Five injection channels spaced 30 μm apart, each 10 μm wide and 0.5 cm long, connect the sample channel to the separation channel. The thin channels were implemented to suppress hydrodynamic flow between the continuous flow sample channel and the rest of the device. Multiple thin channels were used so that a sufficiently-sized sample plug forms, but a high flow resistance remains. The effective separation capillary length was 5.6 cm, with the entire buffer channel measuring 6 cm long and 50 μm wide. The dimensions of the sample channel were 200 μm by 1.6 cm, and the height of all the channels was 50 μm . The two detection wires were spaced 100 μm from each other, and were placed in tapered, bridged channels. A bubble cell was used with a detection zone that was 200 μm wide and had an expansion distance of 190 μm . The bubble cell has been shown to improve conductivity detection by reducing background noise and decreasing the possibility for detection wire fouling.³⁶



The number of thin channels was later varied, and it was found that one thin channel was capable of transferring a sufficient sample plug to the separation channel. Having only one $10\ \mu\text{m}$ channel made blockage of the thin channel more prevalent, however. Three thin channels did not lead to frequent blocking from fibers in the buffer solution, and a three thin channel design was used in experiments validating hydrodynamic flow modeling.

Device operation

Fluorescent imaging of a $1\ \mu\text{M}$ FITC sample was used to monitor the hydrodynamic and electroosmotic flow of sample and buffer, as well as the injection of sample into the separation channel. Figure 3.2a and b illustrates the voltages applied at the reservoirs during injection and separation, and the direction and type of dominant flow that results. A syringe pump at a flow rate of $10\ \mu\text{L}/\text{min}$ resulted in sample moving hydrodynamically (flow direction shown in red) through the sample channel at all times. During separation $1000\ \text{V}$ were applied at reservoir A, resulting in a field strength of $156\ \text{V}/\text{cm}$ in the segment of the separation channel that lies between the injection channels

and reservoir B; and ground was applied at reservoirs B and C. This resulted in a dominant electroosmotic flow (shown in blue) down the separation channel to reservoir B, and down the thin injection channels to reservoir C. Electroosmotic flow down the thin channels prevents sample leakage. During injection, reservoir A is grounded and electroosmotic flow ceases. Hydrodynamic flow from the sample channel pushes sample into the thin injection channels and the separation channel. When the voltage is reapplied at reservoir A, the electroosmotic flow returns so that the sample plug moves down the separation channel, and any remaining sample is pushed back down the thin channels. Fluorescent images of a FITC sample taken before, during, and after injection are shown in Figure 3.2c, d, and e.

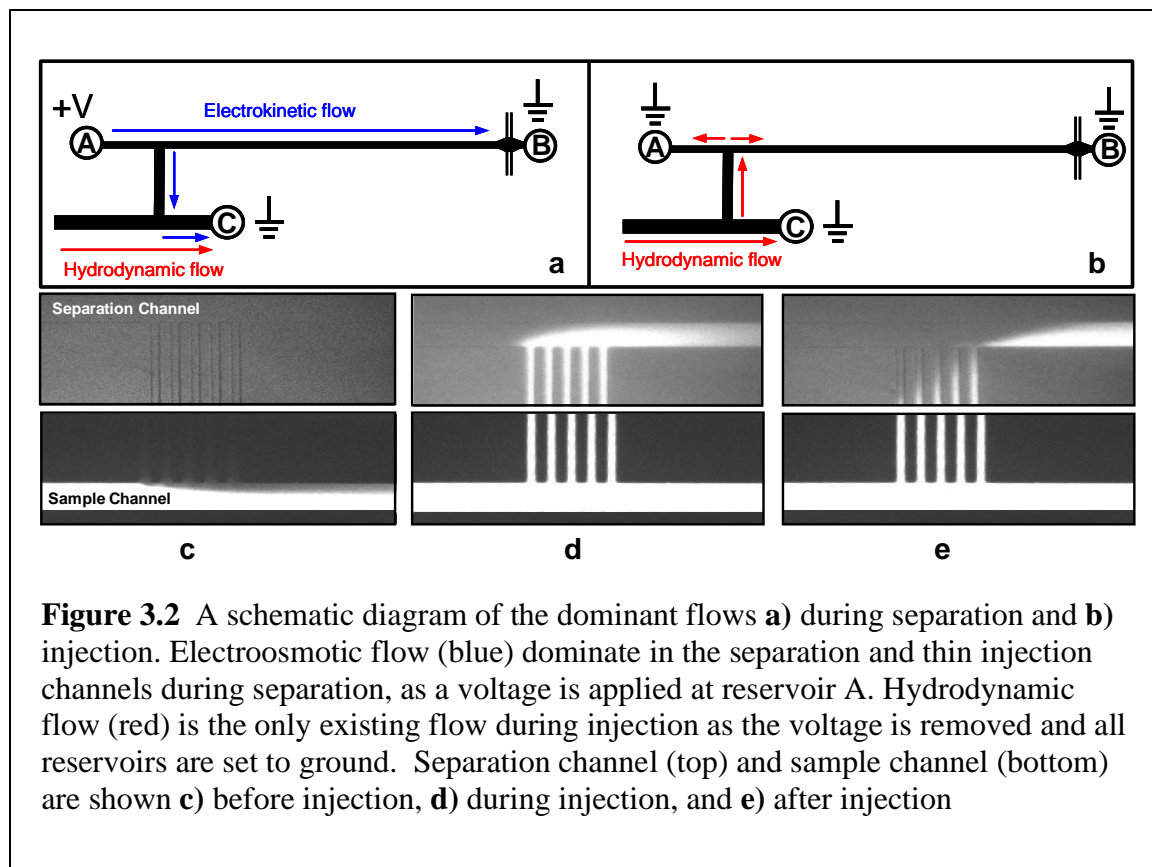


Figure 3.2 A schematic diagram of the dominant flows **a)** during separation and **b)** injection. Electroosmotic flow (blue) dominates in the separation and thin injection channels during separation, as a voltage is applied at reservoir A. Hydrodynamic flow (red) is the only existing flow during injection as the voltage is removed and all reservoirs are set to ground. Separation channel (top) and sample channel (bottom) are shown **c)** before injection, **d)** during injection, and **e)** after injection

3.3 Results and Discussion

Hydrodynamic flow modeling

Flow behavior in the microchip was modeled to take into account both hydrodynamic and electrophoretic flow. In order for the microchip to function properly, channel dimensions and incoming sample flow rate must be such that the linear hydrodynamic flow velocity (U) of sample moving up the injection channels is less than the electrokinetic flow velocity (V_E) of buffer moving down the injection channels ($U < V_E$). This condition yields the scenario seen in Figure 3.2a. Likewise, for injection to occur as demonstrated in Figure 3.2b, electrokinetic flow velocity down the injection channels must be less than the hydrodynamic linear flow velocity ($U > V_E$).

Hydrodynamic flow modeling was based on the analogy demonstrated by Harrison *et al.* between volume flow in a tube and the flow of current through a wire.³⁷ Specifically, Equation 3.1 is related to Ohm's Law equation:

$$\Delta P = \Phi r \rightarrow \Delta V = iR \quad (3.1)$$

so that the pressure difference (ΔP) is equivalent to the voltage drop (ΔV), volumetric flow rate (Φ) is equivalent to current (i), and flow resistance (r) is equivalent to electrical resistance (R). To obtain a model we can treat the network of channels in the microchip as a circuit (Figure 3.3), which allows us to directly apply Kirchoff's Laws and calculate the current (i) moving through the injection channels.

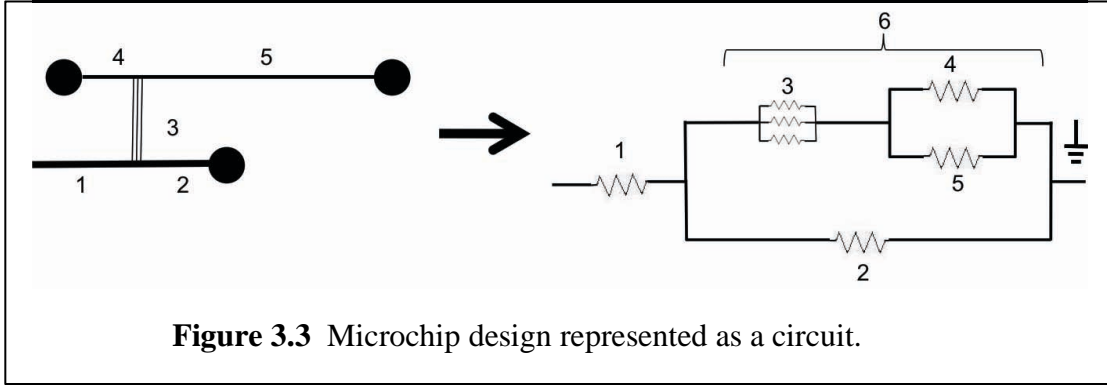


Figure 3.3 Microchip design represented as a circuit.

According to Kirchoff's Laws, voltage through a parallel circuit remains equal in each branch; therefore, $V_2 = V_6$, which can also be expressed as shown in Equation 3.2:

$$i_2 R_2 = i_6 R_6 \tag{3.2}$$

Kirchoff's Laws also state that current moving through a parallel circuit divides among the available paths but remains the same through a series circuit, which provides

Equation 3.3:

$$i_1 = i_2 + i_6 \tag{3.3}$$

Using Equation 3.3 to substitute for i_2 in Equation 3.2 yields Equation 3.4:

$$i_1 R_6 = i_6 R_6 + i_6 R_2 \tag{3.4}$$

The resistance of segment 6 (R_6) can be expressed by Equation 3.5:

$$R_6 = \frac{R_2 R_3}{R_2 + R_3} \tag{3.5}$$

This substitution allows Equation 3.4 to be re-expressed as:

$$i_1 \frac{R_2 R_3}{R_2 + R_3} = i_6 \frac{R_2 R_3}{R_2 + R_3} + i_6 R_2 \tag{3.6}$$

Since segment 3 represents the injection channels, it is the current through this segment (i_3) that needs to be solved for. Once again, because current through a series remains the same, we can say that the current moving through all of segment 6 is equal to the current

moving through segment 3, or $i_6 = i_3$. This fact gives us the final expression for current through the injection channels:

$$i_3 = \frac{i_1}{R_3 + \frac{R_4 R_5}{R_4 + R_5} + 1} \quad (3.7)$$

Resistances (R) were calculated via Equation 3.8³⁷

$$R = \frac{4\eta L}{(wd)^2 F} \quad (3.8)$$

where η is viscosity, L is length, w and d are half width and half depth, respectively, and F is the geometric form factor (Equation 3.9), which is dependent of the width and depth of channels.³⁷

$$F = \left\{ \frac{w}{3d} - \frac{64w^2}{\pi^5 d^2} \sum_{n=0}^{\infty} \frac{\tanh \left[\frac{(2n+1)\pi d}{2w} \right]}{(2n+1)^5} \right\} \quad (3.9)$$

Given that the current in segment 3 (i_3) is equivalent to its volumetric flow rate (Φ_3) according to Equation 3.1, the linear flow velocity (U) of sample moving up the injection channels can be determined using Equation 3.10:

$$U = \Phi/A \quad (3.10)$$

where A is the combined cross sectional area of the injection channels. As previously mentioned, the flow behavior is predicted by comparing linear flow velocity with electrokinetic velocity (V_{E3}). For example, sample leaking will not occur if $U_3 < E_3$ because this implies that the electrokinetic flow is pushing buffer down the injection channels. The electrokinetic velocity in the injection channels is dependent on the electroosmotic flow (μ_{EOF}), the ionic mobility (μ_{ek}) of the sample, and the electric field (E) present in those channels:

$$V_{E3} = (\mu_{eo} + \mu_{ek})E_3$$

□□□□

Given that linear flow velocity (U) is equal to distance/time, we were also able to use the hydrodynamic flow model to predict the time it takes sample to move through sections of the microchip. This provided an easy approach to validate the accuracy of the theoretical flow model. Specifically, the time it took FITC sample to move up the injection channels and reach the separation channel was measured and compared to the theoretical time. FITC sample was introduced into the microchip with a syringe pump, and the time to injection was measured for four different pump rates (U_1). Results from this study, shown in Table 3.1, demonstrate that the flow model developed here does accurately predict hydrodynamic and electrokinetic flow behavior in the microchip. The small deviation between some of the calculated and measured values is likely the result of variability in channel dimensions along the length of the thin injection channels.

Table 3.1 Measured and theoretical time it takes a FITC sample to move from the sample channel to the separation channel (0.5 cm) for 4 pump rates. Theoretical times were calculated by determination of U_3 using the hydrodynamic flow model.

Pump rate ($\mu\text{L}/\text{min}$)	Measured Time (sec) (n = 20)	Theoretical Time (sec)
10	1.03 ± 0.05	1.02
7	1.34 ± 0.08	1.47
4.8	2.22 ± 0.04	2.13
3	3.40 ± 0.07	3.45

Evaluation of separation performance

Device performance was evaluated using separations of standard cation and anion solutions. The cation solution contained NH_4^+ , K^+ , Na^+ , and Li^+ and the anion solution contained Cl^- , SO_4^{2-} , NO_3^- , $\text{C}_2\text{O}_4^{2-}$, and 1,3-propanedisulfonic acid (PDS) as an internal

standard. Each standard was prepared at an analyte concentration of 50 μM , and was introduced into the sample channel using a syringe pump. Figure 3.4 shows representative anion and cation separations. The anion separation yielded migration times of 98.57 ± 0.84 sec (Cl^-), 109.62 ± 0.56 sec (SO_4^{2-}), 116.99 ± 0.79 sec (NO_3^-), 128.56 ± 1.27 sec ($\text{C}_2\text{O}_4^{2-}$), and 137.50 ± 1.57 sec (PDS). These values correspond to relative standard deviations that range from 0.51 – 1.15 % with $n = 4$. Normalization of peak areas to PDS gave peak area ratios of 0.41 ± 0.02 (Cl^-), 1.31 ± 0.02 (SO_4^{2-}), 0.41 ± 0.04 (NO_3^-), and 0.50 ± 0.04 ($\text{C}_2\text{O}_4^{2-}$), with relative standard deviations ranging from 1.28 – 9.18 %. The cation separation yielded average migration times of 48.52 ± 0.09 sec (NH_4^+), 53.03 ± 0.11 s (K^+), 59.87 ± 0.11 s (Na^+), and 67.94 ± 0.12 s (Li^+). Peak area for NH_4^+ , K^+ , Na^+ , and Li^+ peaks were 48.52 ± 0.09 , 53.03 ± 0.11 , 59.86 ± 0.11 , 67.94 ± 0.12 , respectively. Good reproducibility was achieved, as relative standard deviations were ≤ 0.20 % for both migration times and peak areas.

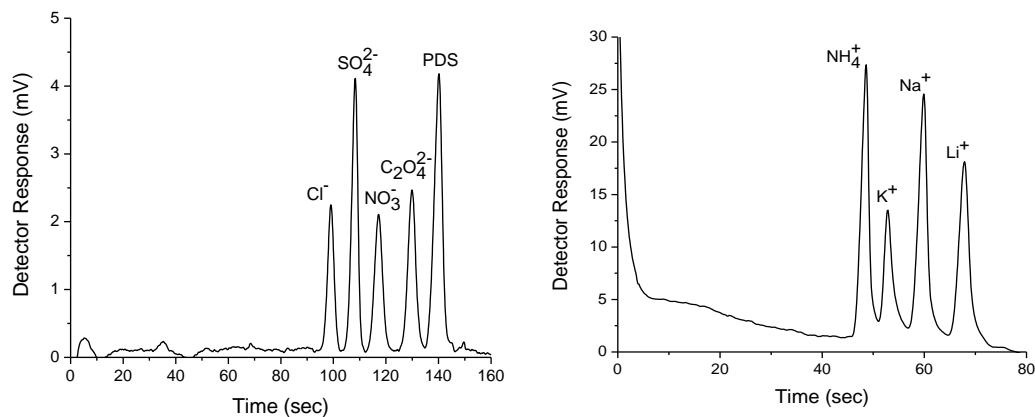


Figure 3.4 Electropherograms of anion separation (left) and cation separation (right). The anion separation was performed using 17 mM picolinic acid / 19 mM HEPBS with 19 mM TDAPS as the background electrolyte, a pump speed of 7 $\mu\text{L}/\text{min}$, a separation voltage of -1000 V, and a 5 sec injection time. Cations were separated with a background electrolyte of 15 mM HEPES / 15 mM Bis Tris with 25 mM 18-crown-6, a pump speed of 10 $\mu\text{L}/\text{min}$, a separation voltage of 950 V, and an injection time of 3 sec. All analytes were present in a 50 μM concentration.

In order to determine the extent to which the hydrodynamic pressure affects separation of analytes, the cation separation was performed at varying pump speeds. Figure 3.5 shows electropherograms at pump speeds ranging from 3 to 15 $\mu\text{L}/\text{min}$. As the pump rate was increased, shorter injection times were used to obtain a consistent sample plug volume. For example, during this experiment a 5 sec injection was used when the pump rate was set at 10 $\mu\text{L}/\text{min}$, while an 11 sec injection was used for a pump rate of 5 $\mu\text{L}/\text{min}$. It was observed that migration times decreased, indicating that the hydrodynamic pressure affects the movement of bulk solution in the separation channel, as was expected. Resolution begins to decrease at higher pump speeds as well. For example, Na⁺/ Li⁺ peak resolution decreased from 3.44 to 2.02, and NH₄⁺/ K⁺ resolution changed from 2.38 to 1.39 when the pump rate was changed from 3 to 10 $\mu\text{L}/\text{min}$.

Separation efficiencies remain fairly constant for the first three peaks (NH_4^+ , K^+ , and Na^+); however, it steadily decreases for the last peak, Li^+ as shown in Figure 3.6.

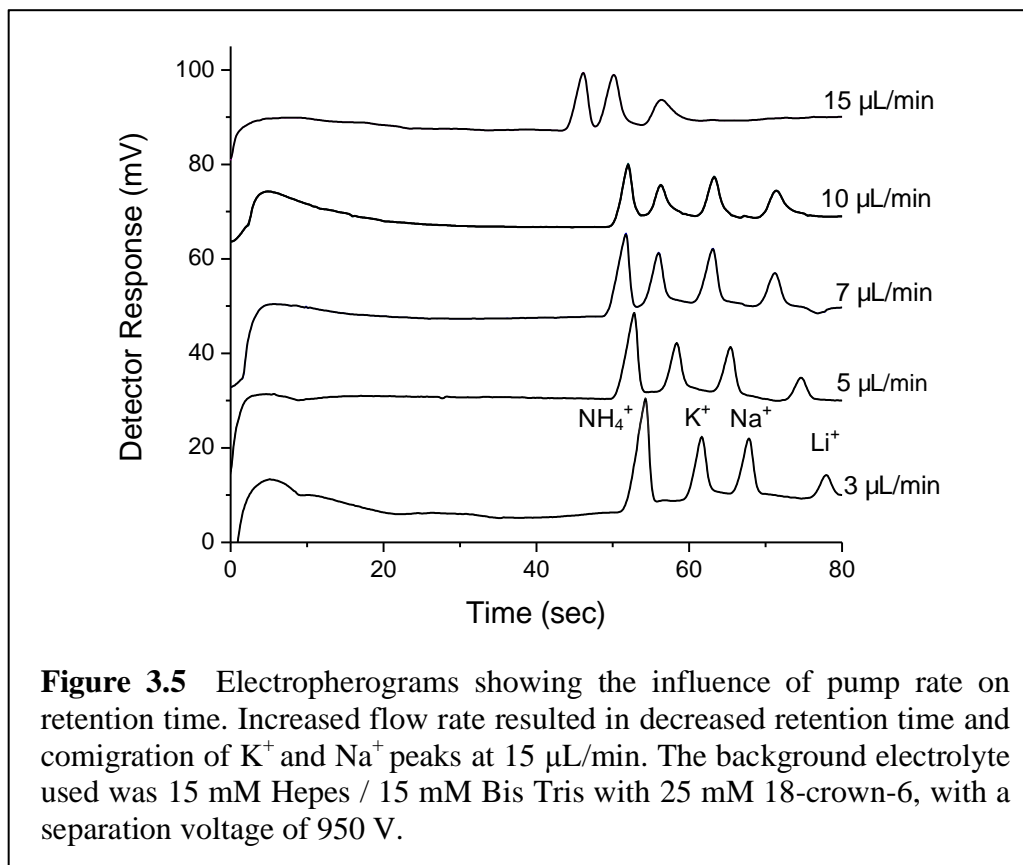
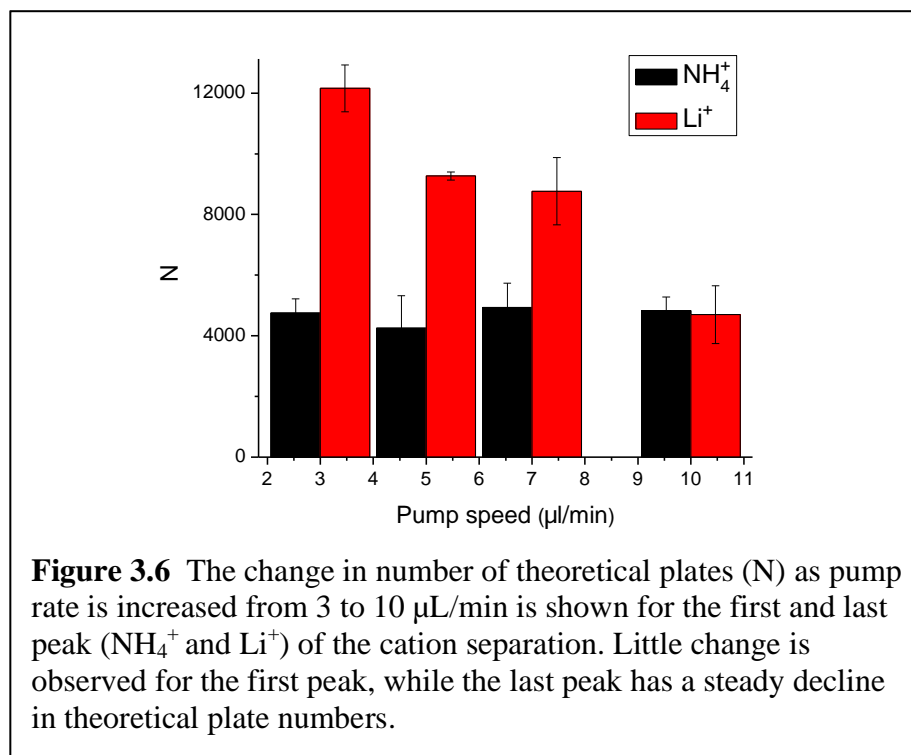


Figure 3.5 Electropherograms showing the influence of pump rate on retention time. Increased flow rate resulted in decreased retention time and comigration of K^+ and Na^+ peaks at 15 $\mu\text{L}/\text{min}$. The background electrolyte used was 15 mM Hepes / 15 mM Bis Tris with 25 mM 18-crown-6, with a separation voltage of 950 V.

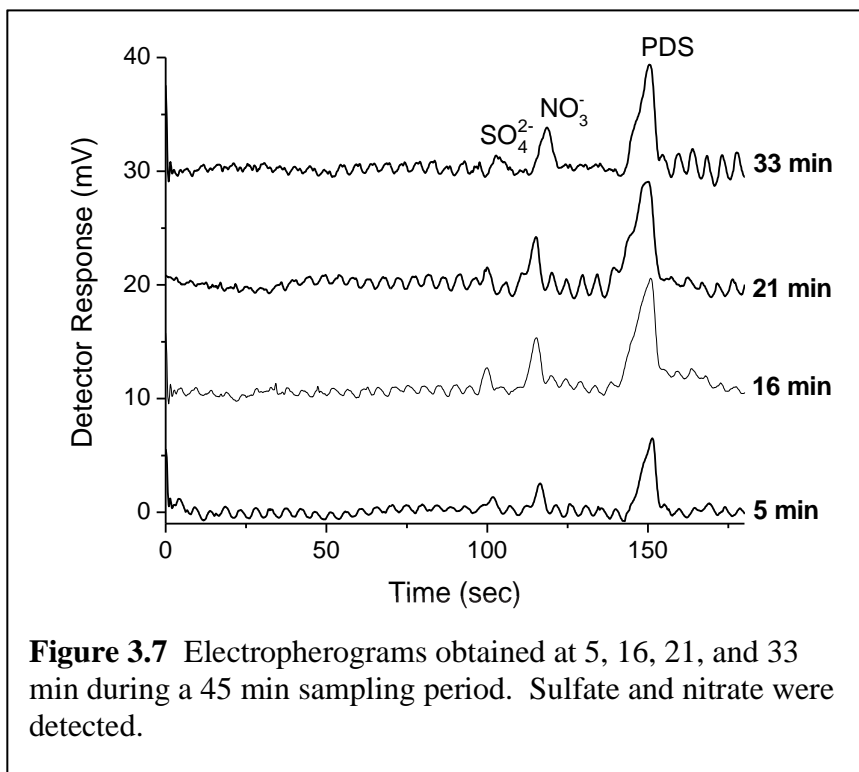


The loss of separation efficiency can be explained by the presence of Taylor dispersion due to a small hydrodynamic flow in the microchannel. CE separations are known to have exceptional separation efficiencies because of the flat flow profile associated with electroosmotic flow (EOF).³⁸ Hydrodynamic flow is characterized by a parabolic profile, which allows for more axial dispersion, thus degrading the separation efficiency.³⁸ It is understandable then, why the introduction of a hydrodynamic component to the separation channel would result in a decrease in separation efficiency. While it is important to be aware of these effects on separation performance, the loss in resolution and separation efficiency at high pump rates can be easily solved in the future if necessary. If higher pump rates are necessary, channel dimensions can be increased to

reduce hydrodynamic pressure. Likewise, pump rates lower than 3 $\mu\text{L}/\text{min}$ could be used if the sample channel was made smaller, and hydrodynamic pressure was increased.

Interfacing device to an aerosol sampler

To demonstrate the utility of this device for analysis of aerosols, the microchip was interfaced to a PILS aerosol collector. The PILS continuously collected aerosols from outside air, while the sample stream was fed into the microchip through use of a peristaltic pump. The pump rate was set at 9.3 $\mu\text{L}/\text{min}$, separation voltage was 1100 V, and a 4 sec injection time was used. Air was continuously sampled over a 45 min period, with individual analysis occurring at 200 sec intervals. Figure 3.7 shows the resulting electropherograms at 5, 16, 21, and 33 min. Nitrate and sulfate were detected, using PDS as an internal standard to account for sample dilution. The IC chromatograph showed the same peaks with an analysis time of 15 min. The oscillating baseline occurs due to the pulsing of the peristaltic pump, and presents an obvious problem. In the future, this disturbance will be minimized with a pulse dampener. Retention times for SO_4^{2-} , NO_3^- , and PDS were 100.99 ± 1.75 , 116.20 ± 1.96 , and 149.34 ± 0.76 respectively. The relative standard deviations for these retention times ranged from 0.5 – 1.7 % with $n = 6$. The migration times are slightly longer than those reported above for device characterization and the difference is most likely the result of differences in electroosmotic flow (EOF) and hydrodynamic flow rate.



3.4 Conclusion

It has been demonstrated that the proposed microchip is capable of performing separations while sampling from a continuous flow. Flow modeling allows us to optimize microchip dimensions to accommodate different sample flow rates and electric fields, and allows us to predict injection times. This design provided an interface between MCE and PILS, as was demonstrated by detection of sulfate and nitrate in ambient aerosols; however, it currently serves more as a proof of concept than as a usable system. Improvements are needed to make a more reliable device that can run for hours, and preferably days. More specifically, a cause for frequent, unexplained fouling of the detection wires needs to be determined and remedied, or perhaps contactless detection

employed. The totality of this work is expected to be published in the context of a field study with validation by IC.

3.5 References

- (1) Bernstein, J. A.; Neil, A.; Barnes, C.; Bernstein, I. L.; Bernstein, J. A.; Nel, A.; Peden, D.; Diaz-Sanchez, D.; Tarlo, S. M.; Williams, P. B., Health effects of air pollution. *The Journal of allergy and clinical immunology* **2004**, *114* (5), 1116-1123.
- (2) Lohmann, U.; Feichter, J., Global indirect aerosol effects: a review. *Atmos. Chem. Phys.* **2005**, *5* (3), 715-737.
- (3) Pöschl, U., Atmospheric Aerosols: Composition, Transformation, Climate and Health Effects. *Angewandte Chemie International Edition* **2005**, *44* (46), 7520-7540.
- (4) Solomon, P. A.; Norris, G.; Landis, M.; Tolocka, M., Chemical Analysis Methods for Atmospheric Aerosol Components. In *Aerosol measurement principles, techniques, and applications*, Baron, P. A.; Willeke, K., Eds. Wiley: New York, **2001**; pp 261-293.
- (5) Finlayson-Pitts, B. J.; Pitts, J. N., Jr., Tropospheric Air Pollution: Ozone, Airborne Toxics, Polycyclic Aromatic Hydrocarbons, and Particles. *Science* **1997**, *276* (5315), 1045-1051.
- (6) Prather, K. A.; Hatch, C. D.; Grassian, V. H., *Annu. Rev. Anal. Chem.* **2008**, *1*, 485-514.
- (7) Abdel-Salam, M., Aerosol Sampling Methods in Workplace and Ambient Environments. *J. Aerosol Medicine* **2006**, *19* (4), 434-455.
- (8) Eatough, D. J.; Long, R. W.; Modey, W. K.; Eatough, N. L., Semi-volatile secondary organic aerosol in urban atmospheres: meeting a measurement challenge. *Atmospheric Environment* **2003**, *37* (9-10), 1277-1292.
- (9) Lee, K. W.; Mukund, R., Filter Collection. In *Aerosol measurement principles, techniques, and applications*, Baron, P. A.; Willeke, K., Eds. Wiley: New York, **2001**; pp 197-228.
- (10) McMurry, P. H., A review of atmospheric aerosol measurements. *Atmospheric Environment* **2000**, *34*, 1959-1999.
- (11) Turpin, B. J.; Saxena, P.; Andrews, E., Measuring and simulating particulate organics in the atmosphere: problems and prospects. *Atmospheric Environment* **2000**, *34* (18), 2983-3013.
- (12) Chow, J. C., Measurement Methods to Determine Compliance with Ambient Air Quality Standards for Suspended Particles. *J. Air Waste Mang.* **1995**, *45* (320-382).
- (13) Sipin, M. F.; Guazzotti, S. A.; Prather, K. A., Recent Advances and Some Remaining Challenges in Analytical Chemistry of the Atmosphere. *Analytical Chemistry* **2003**, *75* (12), 2929-2940.
- (14) Allan, J. D.; Jimenez, J. L.; Williams, P. I.; Alfarra, M. R.; Bower, K. N.; Jayne, J. T.; Coe, H.; Worsnop, D. R., *Geophys. Res.* **2003**, 108.
- (15) DeCarlo, P. F.; Kimmel, J. R.; Trimborn, A.; Northway, M. J.; Jayne, J. T.; Aiken, A. C.; Gonin, M.; Fuhrer, K.; Horvath, T.; Docherty, K. S.; Worsnop, D. R.; Jimenez, J. L., Field-Deployable, High-Resolution, Time-of-Flight Aerosol Mass Spectrometer. *Analytical Chemistry* **2006**, *78* (24), 8281-8289.

- (16) Jimenez, J. L.; Jayne, J. T.; Shi, Q.; Kolb, C. E.; Worsnop, D. R.; Yourshaw, I.; Seinfeld, J. H.; Flagan, R. C.; Zhang, X.; Smith, K. A.; Morris, J. W.; Davidovits, P., Ambient aerosol sampling using the Aerodyne Aerosol Mass Spectrometer. *J. Geophys. Res.* **2003**, *108*.
- (17) Nash, D. G.; Baer, T.; Johnston, M. V., Aerosol mass spectrometry: An introductory review. *International Journal of Mass Spectrometry* **2006**, *258* (1-3), 2-12.
- (18) Jayne, J. T.; Leard, D. C.; Zhang, X.; Davidovits, P.; Smith, K. A.; Kolb, C. E.; Worsnop, D. R., Development of an Aerosol Mass Spectrometer for Size and Composition Analysis of Submicron Particles. *Aerosol Science and Technology* **2000**, *33* (1), 49 - 70.
- (19) Li, Z.; Hopke, P. K.; Husain, L.; Qureshi, S.; Dutkiewicz, V. A.; Schwab, J. J.; Drewnick, F.; Demerjian, K. L., Sources of fine particle composition in New York city. *Atmospheric Environment* **2004**, *38* (38), 6521-6529.
- (20) Wexler, A. S.; Johnston, M. V., Real-Time Single-Particle Analysis. In *Aerosol measurement principles, techniques, and applications*, Baron, P. A.; Willeke, K., Eds. Wiley: New York, **2001**; pp 365-385.
- (21) Peltier, R. E.; Sullivan, A. P.; Weber, R. J.; Brock, C. A.; Wollny, A. G.; Holloway, J. S.; de Gouw, J. A.; Warneke, C., Fine aerosol bulk composition measured on WP-3D research aircraft in vicinity of the Northeastern United States – results from NEAQS. *Atmos. Chem. Phys.* **2007**, *7* (12), 3231-3247.
- (22) Lee, T.; Yu, X.-Y.; Kreidenweis, S. M.; Malm, W. C.; Collett, J. L., Semi-continuous measurement of PM_{2.5} ionic composition at several rural locations in the United States. *Atmospheric Environment* **2008**, *42* (27), 6655-6669.
- (23) Orsini, D. A.; Sullivan, A.; Sierau, B.; Baumann, K.; Weber, R., Refinements to the particle-into-liquid smapler (PILS) for ground and airborne measurements of water soluble aerosol composition. *Atmospheric Environment* **2003**, *37*, 1243-1259.
- (24) Blanco-Heras, G. A.; Turnes-Carou, M. I.; López-Mahía, P.; Muniategui-Lorenzo, S.; Prada-Rodríguez, D.; Fernández-Fernández, E., Determination of organic anions in atmospheric aerosol samples by capillary electrophoresis after reversed pre-electrophoresis. *Electrophoresis* **2008**, *29* (6), 1347-1354.
- (25) Dabek-Zlotorzynska, E.; Dlouhy, J. F., Application of capillary electrophoresis in atmospheric aerosols analysis: Determination of inorganic and organic anions. *Journal of Chromatography A* **1994**, *671* (1-2), 389-395.
- (26) Dabek-Zlotorzynska, E.; Dlouhy, J. F., Application of capillary electrophoresis in atmospheric aerosol analysis: determination of cations. *Journal of Chromatography A* **1995**, *706* (1-2), 527-534.
- (27) Fukushi, K.; Takeda, S.; Chayama, K.; Wakida, S.-I., Application of capillary electrophoresis to the analysis of inorganic ions in environmental samples. *Journal of Chromatography A* **1999**, *834* (1-2), 349-362.
- (28) Timerbaev, A. R.; Dabek-Zlotorzynska, E.; A. G. T. van den Hoop, M., Inorganic environmental analysis by capillary electrophoresis. *Analyst* **1999**, *124* (6), 811-826.

- (29) Harper, M., A review of workplace aerosol sampling procedures and their relevance to the assessment of beryllium exposures. *Journal of Environmental Monitoring* **2006**, *8*, 598-604.
- (30) Noblitt, S. D.; Schwandner, F. M.; Hering, S. V.; Collett Jr, J. L.; Henry, C. S., High-sensitivity microchip electrophoresis determination of inorganic anions and oxalate in atmospheric aerosols with adjustable selectivity and conductivity detection. *Journal of Chromatography A* **2009**, *1216* (9), 1503-1510.
- (31) Noblitt, S. D.; Lewis, G. S.; Liu, Y.; Hering, S. V.; Collett, J. L.; Henry, C. S., Interfacing Microchip Electrophoresis to a Growth Tube Particle Collector for Semicontinuous Monitoring of Aerosol Composition. *Analytical Chemistry* **2009**, *81* (24), 10029-10037.
- (32) Noblitt, S. D.; Kraly, J. R.; VanBuren, J. M.; Hering, S. V.; Collett, J. L.; Henry, C. S., Integrated membrane filters for minimizing hydrodynamic flow and filtering in microfluidic devices. *Analytical Chemistry* **2007**, *79* (16), 6249-6254.
- (33) Garcia, C. D.; Liu, Y.; Anderson, P.; Henry, C. S., Versatile 3-channel high-voltage power supply for microchip capillary electrophoresis. *Lab on a Chip* **2003**, *3* (4), 324-328.
- (34) Duffy, D. C.; McDonald, J. C.; Schueller, O. J.; Whitesides, G. M., Prototyping of microfluidic systems in poly(dimethylsiloxane). *Analytical Chemistry* **1998**, *70*, 4974-4984.
- (35) Liu, Y.; Vickers, J. A.; Henry, C. S., Simple and Sensitive Electrode Design for Microchip Electrophoresis/Electrochemistry. *Analytical Chemistry* **2004**, *76* (5), 1513-1517.
- (36) Noblitt, S. D.; Henry, C. S., Improving the Compatibility of Contact Conductivity Detection with Microchip Electrophoresis Using a Bubble Cell. *Analytical Chemistry* **2008**, *80* (19), 7624-7630.
- (37) Attiya, S.; Jemere, A. B.; Tang, T.; Fitzpatrick, B.; Seiler, K.; Chiem, N.; Harrison, D. J., Design of an interface to allow microfluidic electrophoresis chips to drink from the fire hose of the external environment. *Electrophoresis* **2001**, *22* (2), 318-327.
- (38) O'Grady, J. F. K. Y. N., Patrick McDonnell, Aaron J. Mancuso, Kimberley A. Frederick, Detecting deviations from pure EOF during CE separations. *Electrophoresis* **2007**, *28* (14), 2385-2390.

CHAPTER 4: PAPER-BASED MICROFLUIDICS

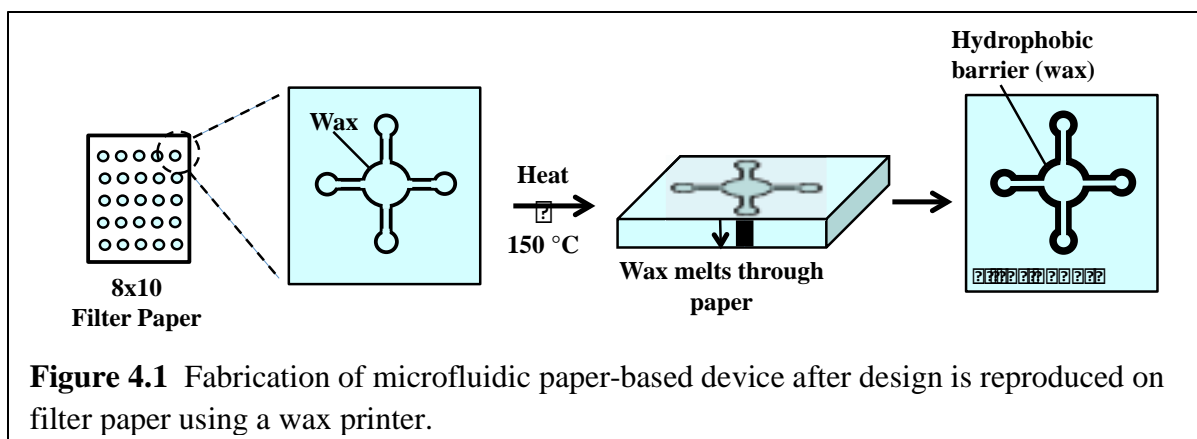
4.1 What is paper-based microfluidics?

Microfluidic paper-based analytical devices (μ PADs) are patterned hydrophilic paper substrates that serve as a microfluidic platform for multiplexed analyte detection. Flow circuits are created in paper by depositing hydrophobic material that serves as barriers. These barriers confine and direct flow of aqueous solutions, which move through the paper fiber network by capillary action.

μ PADs offer an attractive alternative to polymer devices in some cases as mass production costs are much lower and paper is readily available and disposable.¹ The low cost and simple operation of typical paper-based devices make this technology especially applicable as a health care diagnostic tool in developing countries, where advanced cleanroom facilities, expensive instrumentation, and trained personnel are not widely available.¹⁻³ To date, the most prevalent examples of μ PADs have been applied towards clinically relevant bio-analysis.⁴⁻⁷ Although, the attention that paper-based devices have recently attracted is fueling a great deal of innovative research that will expand the applications of μ PADs to include environmental monitoring, water and food safety, filtration systems, biosafety and biodefense, and military and homeland security.⁶⁻⁹

Paper-based devices can be fabricated through photolithography, wax screen printing, inkjet etching, or wax printing. Wax printing has become one of the most popular techniques, as it provides a rapid (~5 min) method for fabricating many devices

at once, requiring only a commercially available printer and hot plate, and is one of the least expensive methods. The wax printing method is demonstrated in Figure 4.1. A commercially available wax printer is used to reproduce a device design on cellulose paper. Heating the printed design on a hot plate at 150 °C melts the wax ink so that hydrophobic barriers form through the thickness of the paper.



The following chapters describe the development of a μ PAD for colorimetric detection of particulate metals. Colorimetric assays created for metal detection on paper will be demonstrated in Chapter 5. The properties of cellulose and capillary movement of fluids through paper will be described in Chapter 6, and the ability to exploit or modify fluid and reagent movement will be demonstrated. Chapter 7 will then provide the first example of a paper-based device used for multiplexed metal detection in an aerosolized sample.

4.2 References

- (1) Rezk, A. R.; Qi, A.; Friend, J. R.; Li, W. H.; Yeo, L. Y., Uniform mixing in paper-based microfluidic systems using surface acoustic waves. *Lab on a Chip* **2012**, *12* (4), 773-779.
- (2) Yager, P.; Edwards, T.; Fu, E.; Helton, K.; Nelson, K.; Tam, M. R.; Weigl, B. H., Microfluidic diagnostic technologies for global public health. *Nature* **2006**, *442* (7101), 412.
- (3) Chin, C. D.; Linder, V.; Sia, S. K., Lab-on-a-chip devices for global health: Past studies and future opportunities. *Lab on a Chip* **2007**, *7* (1), 41-57.
- (4) Abe, K.; Suzuki, K.; Citterio, D., Inkjet-Printed Microfluidic Multianalyte Chemical Sensing Paper. *Analytical Chemistry* **2008**, *80* (18), 6928-6934.
- (5) Lu, Y.; Shi, W.; Jiang, L.; Qin, J.; Lin, B., Rapid prototyping of paper-based microfluidics with wax for low-cost, portable bioassay. *Electrophoresis* **2009**, *30* (9), 1497-1500.
- (6) Martinez, A. W.; Phillips, S. T.; Butte, M. J.; Whitesides, G. M., Patterned Paper as a Platform for Inexpensive, Low-Volume, Portable Bioassays. *Angewandte Chemie International Edition* **2007**, *46* (8), 1318-1320.
- (7) Martinez, A. W. P., S. T.; Whitesides, G. M., Three-dimensional microfluidic devices fabricated in layered paper and tape. *PNAS* **2008**, *105* (50), 19606-19611.
- (8) Zhao, W.; van den Berg, A., Lab on paper. *Lab on a Chip* **2008**, *8* (12), 1988-1991.
- (9) Bruzewicz, D. A.; Reches, M.; Whitesides, G. M., Low-Cost Printing of Poly(dimethylsiloxane) Barriers To Define Microchannels in Paper. *Analytical Chemistry* **2008**, *80* (9), 3387-3392.

CHAPTER 5: COLORIMETRIC DETECTION OF METALS ON PAPER

5.1 Introduction

Detection and quantification of metals carried by aerosols in many occupational settings has become important due to the extensive list of negative health effects associated with particulate metal exposure. For example, worker exposure to heavy metals has been identified as a priority research area by the National Institute for Occupational Safety and Health (NIOSH).¹ The current methods of occupational exposure assessment for metals require that filter samples be collected and sent out for analysis. There is a need to develop better methods for analysis of metals in aerosols that reduce the overall analysis time and cost while also allowing on-site measurement. The work presented here and in following chapters demonstrates a method for quantifying particulate metals using paper-based microfluidic devices. This chapter describes colorimetric assays developed for metal detection on paper, and evaluates their suitability for analysis of mixed-metal samples.

Metals have historically lent themselves to colorimetric detection, a technique carried out relatively easily on paper substrates. Analytical chemists have long used chemical tests carried out in drops of solution on filter paper, commonly referred to as spot tests. A familiar example is the use of indicator papers to rapidly determine pH through detection of hydronium or hydroxide ions. In the early 1920s, investigations into whether it was feasible to carry out colorimetric reactions on paper led to the discovery

that many common qualitative inorganic tests executed in test tubes displayed great sensitivity when they were carried out as spot reactions on filter paper.² Later studies demonstrated that in cases where water insoluble colorimetric reagents were used, lower detection limits were obtained with spot reactions than when the same tests were conducted in a test tube.³ There are several explanations for the enhancement of assay sensitivity on paper containing insoluble reagents: 1) the reagent solid is finely dispersed throughout the capillaries of the paper, providing an excess of reaction sites; 2) the diffusion and dilution that accompany reagent and analyte mixing in solution are avoided; and 3) sharply defined color spots result because products remain at the site of formation.³ Chapter 6 will demonstrate how the paper surface can be easily modified to limit mobility of water-soluble reagents and products so that they also yield sharply defined, intense color spots.

The attractive qualities of simple, colorimetric spot tests have been exploited for common products such as glucose test strips and pregnancy tests. However, use of such assays has been largely limited to qualitative analysis because of difficulties associated with assessing small changes in color intensity. While colorimetric spot tests cannot rival the quantitative capabilities of sophisticated instrumentation, new developments in paper-based microfluidic technology and image analysis have re-introduced this chemistry as a simple and inexpensive quantitative detection technique.

While it has been suggested that metal detection would be a good application for paper-based microfluidic devices, very few examples of this have actually been reported. Apilux, *et. al*, performed electrochemical detection of Au^{3+} with simultaneous colorimetric detection of Fe^{3+} on a paper-based device for gold-refining waste samples.⁴

Nie, *et. al* reported electrochemical detection of Pb^{2+} in the presence of Zn^{2+} . Besides these two reports, paper-based metal detection has been limited to spot tests with relatively simple samples containing few interfering metals; or a series of pre-treatment steps carried out in solution are required for more complex metal samples prior to metal detection on paper.^{2,5,6} In order for a paper-based microfluidic device to be employed in assessing particulate metal exposure, assays must first be developed that can be used with complex mixed-metal samples. Ideally, interferences from other metals should be eliminated without the need for washing or other post-assay treatments.

With the goal of using a paper-based device form metal detection in mind, a variety of colorimetric assays were established as a precursor to measuring particulate metals in occupational health settings. Filter paper is the preferred substrate for spot reactions due to its capillarity and absorptive effects. The assays described here were performed on Whatman grade 1 filter paper, most often inside reservoirs created through a wax printing method which will be described in Chapter 7. The assays presented in this chapter were based on a broad selection of literature describing spot tests or solution-based tests, some dating as far back as the 1930s. In most cases, procedures and reagents described in the literature were significantly altered to suit our application, and additional reagents were introduced to hinder interference from other metals. The six assays described below show varying levels of development. After six paper-based assays were established, three were chosen for use on the device described in Chapter 7 based on their suitability for quantitative detection and the desired application. Reagent volumes, detection limits, and calibrations curves are very dependent on paper grade and type, as well as device dimensions; therefore, this chapter describes general assay procedures for

detection of cadmium, lead, manganese, iron, nickel, and copper on paper. Colorimetric reagents were always used in stoichiometric excess relative to the metal ions they detect. More specific procedural details and results for iron, nickel, and copper detection will be described in Chapter 7. Even though use of several of the assays presented here was not continued, the following discussions help demonstrate how assays and reagents should be chosen for metal detection on paper-based devices. As it is anticipated that these efforts will be continued in the Henry group, the examples provided here will continue to be used and provide guidance for future paper-based metal assays.

5.2 General Assay Procedures

All assays described here were performed on Whatman Grade 1 filter paper using pipets to apply reagents and samples. In cases where assays were carried out inside reservoirs on paper, the wax printing method described in Chapter 4 was implemented to create the hydrophobic reservoir barriers. Metal salts used to test for potential interferences were manganese chloride tetrahydrate, zinc nitrate hexahydrate, vanadium(III) chloride, lead(II) nitrate, chromium(III) chloride, cobalt(II) chloride, and aluminum sulfate, and were selected because of their common presence in aerosols.⁷⁻⁹

Detection of Cadmium

The reagent, ferrous dipyriddy iodide, was prepared by sonicating an aqueous solution containing 1.6 mM 2,2-dipyridine, 0.5 mM $\text{FeSO}_4 \cdot 7\text{H}_2\text{O}$, and 60 mM KI for 30 min. Any precipitate was filtered off, leaving a saturated solution of $\text{Fe}(2,2\text{-dipyridyl})_3 \cdot \text{I}_2$ with an excess of I^- . A 1000 ppm Cd^{2+} standard solution was prepared from

$\text{Cd}(\text{NO}_3)_2 \cdot \text{H}_2\text{O}$. A 30 % ammonia solution was used to hinder Cu^{2+} interference. Reagent and sample solutions were pipetted onto filter paper, and resulting differences in product formation due variation in method order were noted.

Detection of Lead

A saturated solution of rhodizonic acid was prepared by dissolving sodium rhodizonate in tartrate buffer (pH 2.8). A 1000 ppm Pb standard solution was prepared from $\text{Pb}(\text{NO}_3)_2$. Rhodizonic acid solution was added to filter paper and allowed to dry. The standard Pb^{2+} solution was then added to the same spot and immediate formation of a bright pink color resulted. A 5 % HCl solution was applied to the pink spot, resulting in formation of a blue-violet color. Once maximum color intensity of the blue-violet product was reached, a blow dryer was used to remove excess HCl, which is believed to be responsible for the rapid degradation of the blue-violet complex.¹⁰

Detection of Manganese

A solution of 3,3',5,5'-tetramethylbenzidine (TMB) (1 mg/mL) was prepared in 0.1 M HCl. A 500 ppm Mn^{2+} standard solution was prepared from $\text{MnCl}_2 \cdot 4\text{H}_2\text{O}$. The assay was performed in reservoirs on filter paper, which was prepared for manganese detection by drying NaOH (pH 12.8) on the paper, followed by addition of TMB solution. The Mn^{2+} solution was added, which resulted in formation of a blue color that quickly changes to yellow. A 7.5 M phosphoric acid solution was then added to the yellow spot, causing it to turn brown. The brown color will either change back to yellow over time or remain depending on the amount of acid added. Paper was allowed to dry

completely between each addition of reagent and before sample was applied. Possible interferences from the following metal ions were studied: Ni^{2+} , Cu^{2+} , Fe^{2+} , Zn^{2+} , V^{3+} , Pb^{2+} , Cr^{3+} , Co^{2+} , Al^{3+} .

Detection of Iron

An acetate buffer was prepared with 15.0 g sodium acetate trihydrate and 11.75 mL glacial acetic acid in 50 mL water, resulting in a 6.3 M acetate solution of pH 4.5. Both 1,10-phenanthroline (8 mg/mL) and hydroxylamine (0.1 g/mL) were prepared as separate solutions, each in the acetate buffer. A 1000 ppm Fe standard solution was prepared with FeCl_2 . Assays were carried out in reservoirs on paper that was impregnated with hydroxylamine followed by 1,10-phenanthroline. Paper was allowed to dry completely between addition of each reagent. Possible interferences from the following metal ions were studied: Ni^{2+} , Cu^{2+} , Mn^{2+} , Zn^{2+} , V^{3+} , Pb^{2+} , Cr^{3+} , Co^{2+} , Al^{3+} .

Detection of Nickel

Water-insoluble dimethylglyoxime (dmg) was prepared as a 60 mM solution in methanol. A 1000 ppm Ni^{2+} standard solution was prepared from NiSO_4 . Assays were carried out in reservoirs on paper which was impregnated with reagents prior to addition of nickel sample. The dmg solution was added to the paper, followed by an ammonium hydroxide solution (pH 9.5). Paper was allowed to dry completely between each addition of reagent and before addition of sample solutions. Possible interferences from the following metal ions were studied: Mn^{2+} , Cu^{2+} , Fe^{2+} , Zn^{2+} , V^{3+} , Pb^{2+} , Cr^{3+} , Co^{2+} , Al^{3+} .

Detection of Copper

Two different assays were developed for the detection of copper. The first employed the colorimetric reagent dithiooxamide and the second was based on the reaction of copper ions with bathocuproine. Both are described here.

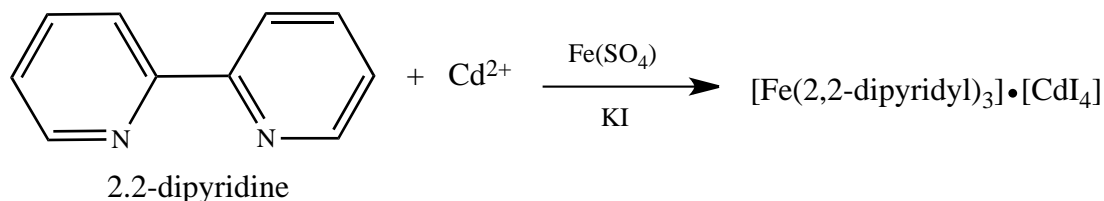
Dithiooxamide: Dithiooxamide was dissolved in acetone to yield a 10 mg/mL solution. Two different buffers were tested for this assay, each adjusted to pH 4.5. The first was an acetic acid/sodium acetate buffer prepared from 2.5 g sodium acetate trihydrate and 2.5 mL glacial acetic acid in a total volume of 10 mL. This buffer was later replaced with a 20 % malonic acid solution. Alcoholic solutions of ethylenediamine ranging from 10-20 % were prepared and used to mask interferences from other metal ions. A standard 1000 ppm Cu^{2+} solution was prepared from $\text{CuSO}_4 \cdot 5\text{H}_2\text{O}$. Reagents were applied to reservoirs on paper prior to addition of Cu^{2+} in the following order: pH 4.5 buffer solution (acetate or malonic acid), ethylenediamine, dithiooxamide. Paper was allowed to dry completely between addition of reagents. Interferences from the following metal ions were studied: Ni^{2+} , Mn^{2+} , Fe^{2+} , Zn^{2+} , V^{3+} , Pb^{2+} , Cr^{3+} , Co^{2+} , Al^{3+} .

Bathocuproine: A solution of 50 mg/mL bathocuproine was prepared in chloroform. An acetic acid/NaCl buffer (10 mM, pH 4.5) provided the univalent anion (Cl^-) and established the pH for the assay. Hydroxylamine (0.1 g/mL) was used for reduction of Cu^{2+} to Cu^+ . A 1000 ppm Cu solution was prepared from $\text{CuSO}_4 \cdot 5\text{H}_2\text{O}$. Reagents were applied to reservoirs on paper prior to addition of Cu^{2+} solution in the following order: hydroxylamine, acetic acid/NaCl buffer, bathocuproine. The paper was allowed to dry completely between each addition of reagent.

5.3 Results and Discussion

Detection of Cadmium

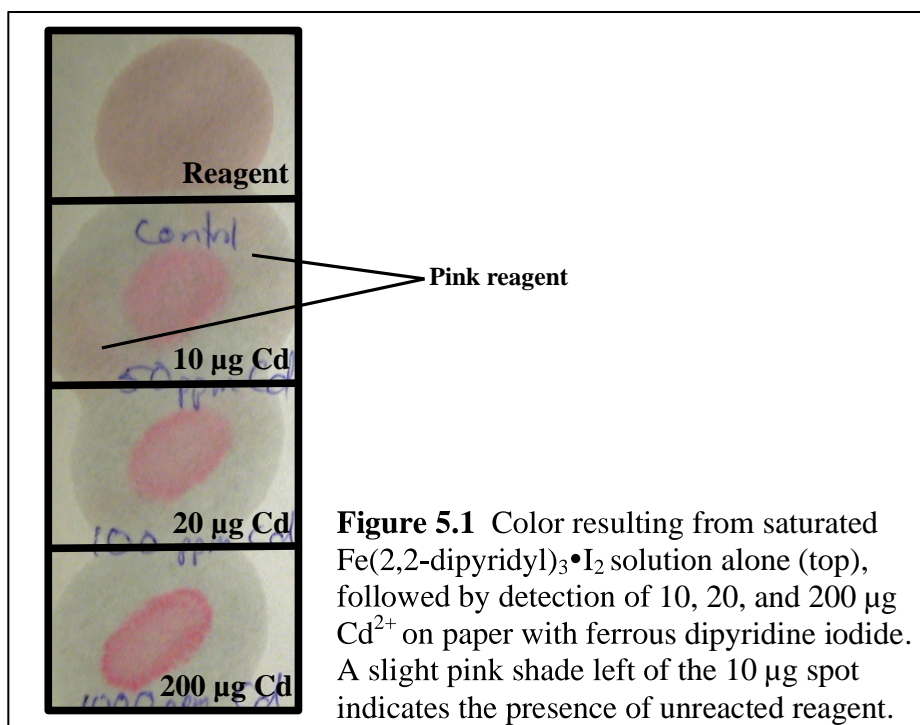
Detection of Cd^{2+} was accomplished through use of ferrous dipyriddy iodide, $\text{Fe}(2,2\text{-dipyriddy})_3 \cdot \text{I}_2$. The base 2,2-bipyridine forms a remarkably stable complex with ferrous salts: $[\text{Fe}(2,2\text{-dipyriddy})_3]^{2+}$.¹¹ This cation can combine with complex ions, such as $[\text{CdI}_4]^{2-}$, resulting in formation of the red precipitate $\text{Fe}(2,2\text{-dipyriddy})_3 \cdot \text{CdI}_4$. The red precipitate, which reveals the presence of cadmium, was formed on paper by employing a saturated solution of $[\text{Fe}(2,2\text{-dipyriddy})_3]\text{I}_2$ containing excess I_2 as a reagent.^{2,11} This reagent solution contains all of the ions required for formation of the red precipitate according to the reaction:



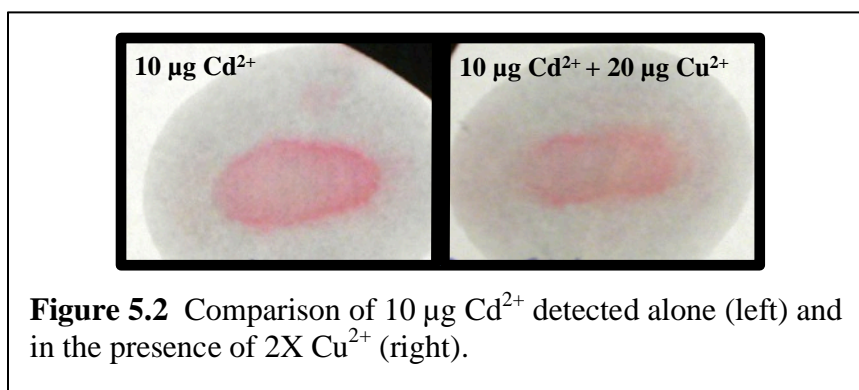
Cu^{2+} interferes with this assay under neutral or acidic conditions by forming cuprous iodide, which forms a colored product with 2,2-dipyridine. The presence of ammonia limits interferences by forming inactive copper and zinc compounds, $\text{Cu}(\text{NH}_3)_4^{2+}$ and $\text{Zn}(\text{NH}_3)_4^{2+}$.² $\text{Cd}(\text{NH}_3)_4^+$, however, reacts readily with the reagent. Additional metal ions interfere by forming slightly soluble or complex iodides that also form red precipitates containing 2,2-dipyridine. These include ions of silver, thallium, lead, and to a lesser extent, bismuth, mercury, and tin. In an ammoniacal solution lead, mercuric, bismuth, and tin ions form insoluble oxides that can be filtered out of the sample prior to cadmium detection. This type of sample pretreatment may not be

desirable for all applications, especially if multiplexed analysis includes detection of one of these metals.

The reagent solution of saturated $\text{Fe}(\text{2,2-dipyridyl})_3 \cdot \text{I}_2$ is red itself, and forms a pink spot on paper, which can make the red precipitate difficult to see at low concentrations. The order in which the reagent and sample are added affected this as well. For example, Figure 5.1 shows the reagent spot on paper and detection of 10, 20, and 200 μg of Cd^{2+} when the Cd^{2+} solution was pipetted onto paper prior to addition of reagent. It was seen that when added in this order, reagent ions will react at the site of dried Cd^{2+} . Also, as the reagent ions precipitate out with Cd^{2+} , the pink color due to the reagent solution fades with increasing Cd^{2+} . This can be observed by comparing results from 200 μg to 10 μg Cd^{2+} in Figure 5.1. There is still a slight pink color outside the red precipitation spot for the 10 μg Cd^{2+} sample due to unreacted reagent, while no color is seen outside the precipitate of the 200 μg sample.



The same spot test procedure was performed for 3 samples: 1) 10 $\mu\text{g Cd}^{2+}$, 2) 20 $\mu\text{g Cu}^{2+}$, and 3) 10 $\mu\text{g Cd}^{2+}$ with 20 $\mu\text{g Cu}^{2+}$. After samples had dried on the filter paper, 20 μL of the ammonia solution was added to each, followed by 20 μL of the colorimetric reagent solution. The Cu^{2+} spot showed no difference from the reagent spot, indicating that the ammonia was preventing Cu^{2+} from forming a colored complex with the reagent ions. A visual comparison of the Cd^{2+} spot versus the $\text{Cd}^{2+}/\text{Cu}^{2+}$ spot is shown in Figure 5.2. The presence of twice the mass of Cu^{2+} relative to Cd^{2+} did result in color fading.



The images presented thus far show colorimetric detection of Cd^{2+} when reagent is added to filter paper already containing the metal ion sample. It is more convenient for commercial purposes, however, to develop a paper-based detection device impregnated with colorimetric reagent so that detection is accomplished simply upon addition of sample. As mentioned previously, the order of sample and reagent application affects the outcome of this spot test. When the $\text{Fe}(2,2\text{-dipyridyl})_3 \cdot \text{I}_2$ reagent is dried onto paper prior to sample addition, the pink color of the reagent remains in the background even after the cadmium precipitate is formed (Figure 5.3). As Cd^{2+} levels decrease, distinguishing the red precipitation product from the pink background becomes more difficult.

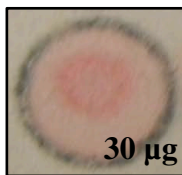
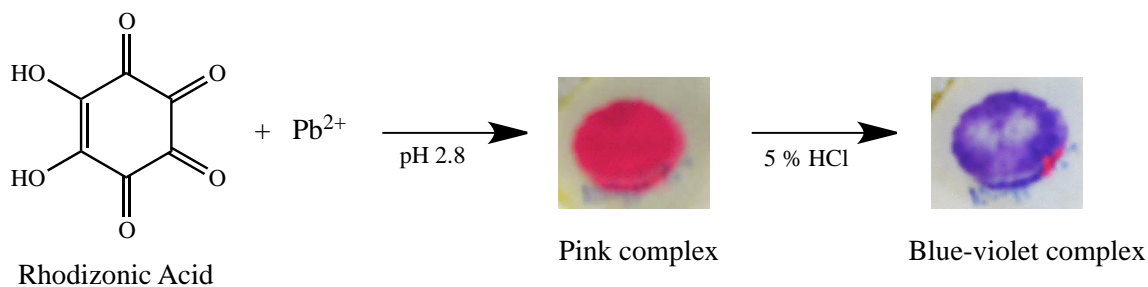


Figure 5.3 Detection of 30 µg Cd²⁺ on paper pre-treated with ferrous dipyriddy iodide.

The cadmium assay was excluded from further use due to difficulties in discerning the red product from the pink reagent on paper; however, it is likely that further optimization will make this a viable candidate for the device and application that will be described in Chapter 7. More specifically, techniques for treatment of the paper surface that will be introduced in Chapter 6 may be employed to concentrate the red cadmium precipitate by immobilizing it into a smaller area. If immobilized there is also the possibility that the water-soluble excess reagent could be pushed to the edge of the detection reservoir, leaving the red precipitate behind after product formation.

Detection of Lead

The assay employed for colorimetric detection of lead on paper was based on the use of sodium rhodizonate in forensics as a convenient field test for verification of the presence or absence of lead deposits.^{10,12} Rhodizonic acid reacts with Pb²⁺ at pH 2.8 to form a bright pink complex, and upon addition of dilute HCl, also forms a blue-violet lead compound following the reaction:



Formation of the pink color can be indicative of the presence of Pb^{2+} ; however, several other metals also form similarly colored compounds with rhodizonic acid. In order for this test to be definitive for presence of Pb^{2+} , appearance of the pink complex must be followed by formation of the blue-violet product upon treatment with 5 % HCl.^{10,12}

The mechanism by which these two reactions take place is still not well understood, largely due to the lack of information regarding the chemical structures of the two colored Pb^{2+} compounds. When synthesized in the laboratory, both compounds form fine powders that are insoluble in solvents that do not decompose them.¹⁰ This has made structure determination by single crystal X-ray diffraction impossible; and although data obtained from solid state IR and NMR spectroscopic studies have proven the compounds contain lead and rhodizonate, no clues have been provided as to the structural arrangement, identity of donor atoms, or tautomeric form in which the ligand exists.¹⁰ It has been suggested that there is very little coordinate covalent bond character in the interaction between rhodizonate ligands and the metals they bind. This claim was supported by studies demonstrating that the stability of rhodizonate-metal compounds markedly increases as the dielectric constant of the solvent (H_2O) is decreased through addition of acetone or ethanol.¹³ A strong dependence of compound stability on dielectric constant of the solvent is typical of compounds formed primarily through electrostatic interactions.¹³

Of the metal ions that have been shown to react with rhodizonate, lead, barium, and copper(II) form the most stable colored compounds; although, even these are susceptible to rapid decomposition. Selective detection of lead is dependent on formation of the blue-violet compound shown above; however, the color fades within 30 sec of formation due to instability of the product. It has been suggested in the literature that excess HCl is responsible for this decomposition, and that using a blow-dryer to remove HCl from paper after maximum color intensity has been reached will prolong life of the product.¹⁰ Upon exploiting this suggestion and decreasing the volume of 5 % HCl added to the reaction spot, color fading was delayed slightly. The best results were obtained by adding a NaOH solution immediately after the blue-violet color began to form to neutralize the acid, and then using the blow-dryer on the reaction spot. With this procedure, fading was substantially decreased and the color remained on paper for several days. These results were not consistent, however, as color intensity was completely dependent (within a matter of seconds) on when the NaOH was added and drying accomplished.

The inability to obtain quantitative data from this assay due to inconsistent color formation was the most important factor considered in excluding this assay from further use, but it is not the only disadvantage encountered. An ideal paper-based device would be impregnated with all necessary reagents prior to use, and reagents would need to remain stable for shipping and short-term storage. The procedure described above requires addition of reagents at various steps of the reaction, meaning that reagent solutions would have to be sent out with devices and there would be the possibility of user error. In addition, sodium rhodizonate, is unstable when exposed to air or light.^{10,13}

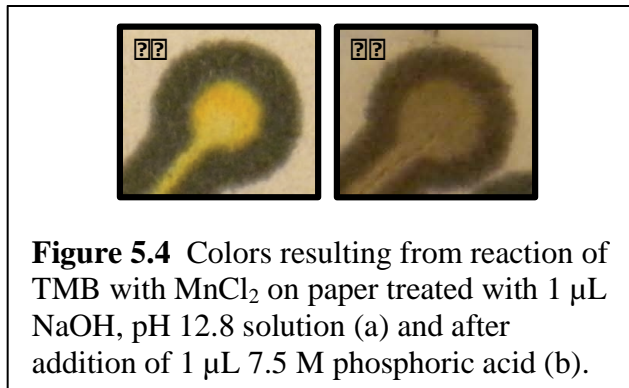
While this assay provides an excellent method for determining whether or not lead is present on a surface, the disadvantages listed here make it unsuitable for the application described in this dissertation.

Detection of Manganese

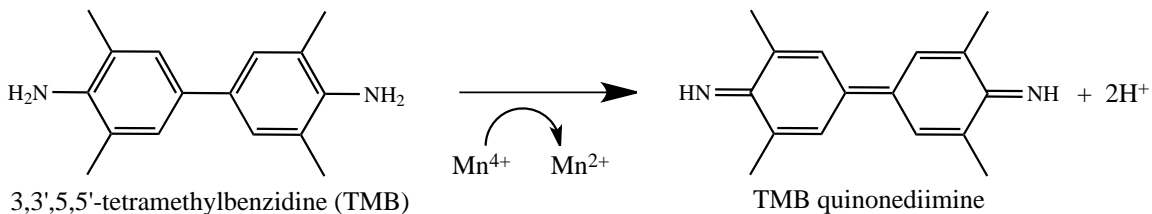
The assay for manganese detection on paper was created from a solution-based colorimetric test that employs the reagent 3,3',5,5'-tetramethylbenzidine (TMB) for detection of manganese in sea and drinking water, and later in photosynthetic membranes.^{14,15} Details for the reaction by which a colored product forms from reaction of manganese ions and TMB have not been described, but are suggested here. TMB, shown in the reaction below, is a chromogenic agent known to form various colored oxidation products, and has been widely used in detection of blood sugar, urine glucose, peroxide enzyme, and various antibodies in clinical or forensics samples.¹⁶ When TMB was used for detection of manganese, oxidation of manganese to the 4+ state was necessary for color formation and was accomplished by establishing a pH > 12 on the reaction spot with NaOH. Under these conditions, and in the presence of TMB, a yellow product appears at the reaction site when manganese ions are introduced. When this solution-based assay was presented in the literature, the product was described as having a maximum absorbance at 450 nm.¹⁵ Investigations into oxidation of TMB by various other compounds, such as horseradish peroxidase, lead to reports of a yellow quinonediimine oxidation product of TMB with an absorbance maximum ranging from 450-465 nm.¹⁷⁻¹⁹ Furthermore, one account describes a brown solution with absorbance

maxima at 380, 465, and 650 nm resulting from oxidation of TMB with periodate. It was determined that this brown solution contained a mixture of TMB oxidation products.¹⁷

The oxidation product color has been shown to be greatly dependent on pH, an occurrence that was observed for the manganese assay as well.^{17,18} Under initial conditions of pH 12.8, addition of MnCl_2 to the reaction spot resulted in formation of the yellow product, which then turned brown upon addition of 7.5 M phosphoric acid. An example of the two colored products with and without addition of acid is shown in Figure 5.4. Depending upon the amount of acid added, the product either remains brown or changes back to yellow as it dries. In either case, once dried the product remains stable indefinitely.



Based on the similarities existing between the TMB oxidation products described in previous literature and the products formed in the assay demonstrated here, it was determined that the yellow color indicative of manganese is due to a two-electron oxidation of TMB by Mn^{4+} according to the reaction:

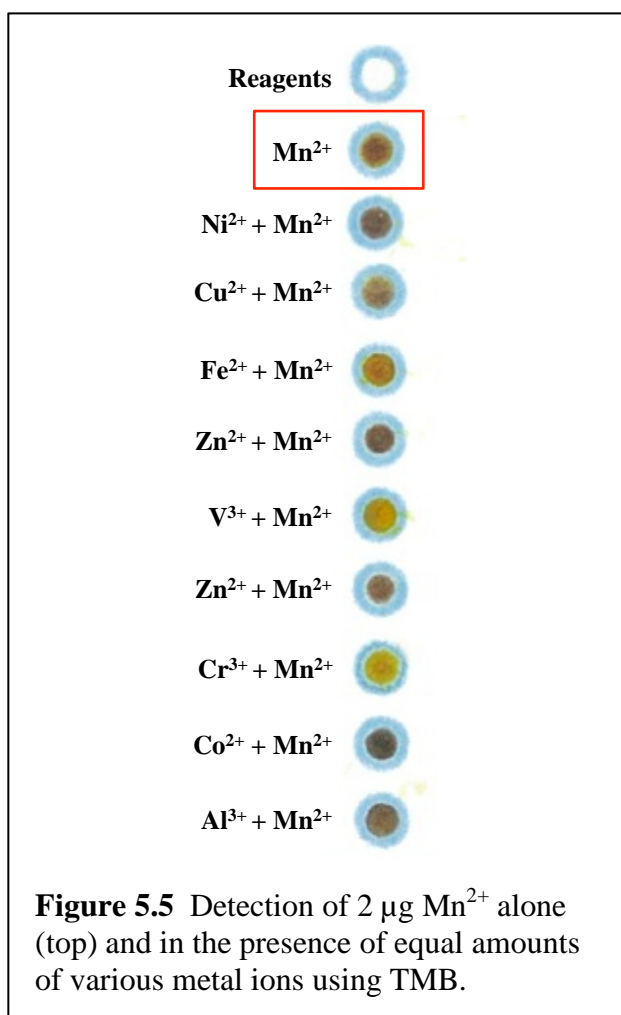


This is further supported by the fact that even the most stable form of Mn^{4+} , MnO_2 , has a standard reduction potential (E°) of +1.23 V. This reduction potential should be sufficient for oxidation of TMB, known to have modest reduction potentials in a variety of conditions (e.g. 0.27 V in ethanol/phthalate buffer, \sim 0.7 V in methanol/benzene mixtures).

Since color formation is dependent on oxidation of TMB, it was expected that interference to the assay could result from other oxidizing agents, including other metal cations with high reduction potentials (E°) such as Au^{3+} ($E^\circ = 1.50$ V) and Co^{3+} ($E^\circ = 1.82$ V).²⁰ Interferences from various metal ions were tested, first alone with TMB, and then together with Mn^{2+} at a 1:1 ratio. Of the ions studied, only V^{3+} and Co^{2+} reacted alone with TMB, forming purple-brown products. When present with Mn^{2+} , all metal ions had an effect on product color, as can be seen in Figure 5.5. Relative to color produced from Mn^{2+} alone, darker brown or purple colors resulted in the presence of Ni, Zn, Pb, Co, and Al ions; while the presence of Fe, Cu, V, and Cr ions yielded lighter hues of brown, orange, or yellow. The degree of interference from so many metal cations made this assay unrealistic for manganese detection. Also, the need to adjust pH to favor a single oxidation products leads to the same drawbacks encountered for the lead assay. Namely, a reagent, in this case a highly concentrated acid solution, has to be added to the reaction zone after sample is introduced, defeating the purpose of a ready-to-use paper device assay.

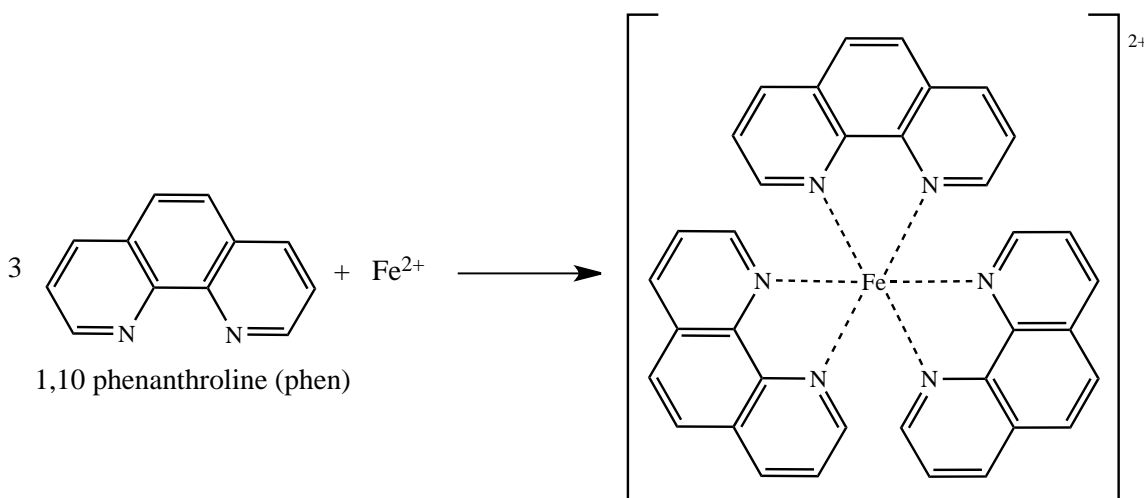
Several other assays exist for colorimetric detection of manganese, and investigations into their use is recommended over attempts to solve the interference issues of this assay. Use of two reagents commonly employed for manganese detection in

the past, benzidine and o-tolidine, is discouraged as both are carcinogenic. Another common test for manganese is oxidation to the violet permanganate compound; however, conditions for this assay also oxidize Cr^{3+} to brightly colored chromate.² More selective assays have been described using 1-(2-pyridylazonaphthol) or formaldoxime; however, as solution-based tests, absorbance measurements were difficult to obtain due to insolubility of the reagents and their colored products.²¹ As insoluble reagents and products are more likely to improve paper-based colorimetric detection rather than hinder it, these reagents may prove successful for manganese detection on paper.



Detection of Iron

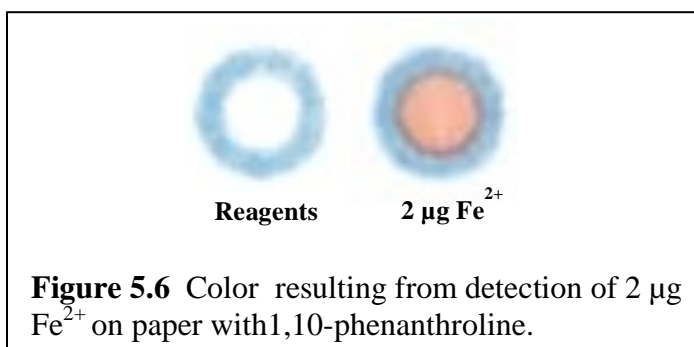
Iron was determined through detection of the red/orange ferriin complex $[\text{Fe}(\text{phen})_3]^{2+}$ formed by the reaction of Fe^{2+} with 1,10-phenanthroline (phen) under acidic conditions:^{5,22}



Iron(III) does not react under these conditions; however, reduction of Fe^{3+} by ascorbic acid or hydroxylamine allows for measurement of total Fe. Hydroxylamine hydrochloride was used in this assay to serve two purposes: 1) it reduces Fe^{3+} to Fe^{2+} ; and 2) hydroxylamine acts as a masking agent by complexing the possible interfering metals Ni, Zn, Cd, and Co.²³ Acetic acid solutions of varying pH were tested, and it was found that treating the assay area with a solution of pH 4.5 results in the greatest product color intensity.

The orange $[\text{Fe}(\text{phen})_3]^{2+}$ product is shown in Figure 5.6. Interferences to this assay from the following metal ions were studied: Ni^{2+} , Mn^{2+} , Cu^{2+} , Zn^{2+} , V^{3+} , Pb^{2+} , Cr^{3+} , Co^{2+} . Solutions of these ions were first tested alone with 1,10-phenanthroline under the same reaction conditions described above, and none yielded a colored product. Interference was then tested with each at a 1:1 ratio with Fe^{2+} . A slight loss in color

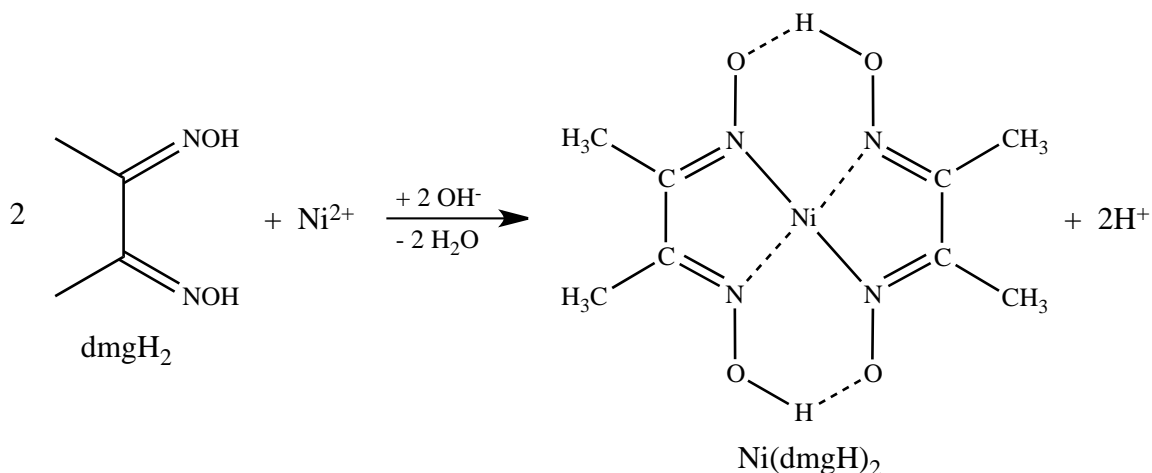
intensity occurred in the presence of Mn^{2+} , Cu^{2+} , Cr^{3+} , and Co^{2+} at this ratio; however, increasing the excess of 1,10-phenanthroline in the reaction zone solved this problem. It was assumed that these cations were complexing small amounts of 1,10-phenanthroline, but not forming colored products.



The 1,10-phenanthroline assay for detection of iron is amenable for use on a paper substrate due to the stability of reagents and product and the ease with which the orange color can be observed. Moreover, the lack of interference from other metals make this assay ideal for quantitative iron measurements in mixed metal samples, such as those collected for particulate metal exposure assessment. When carried out on a more complex paper-device, high mobility of the product on paper became an issue. Chapter 6 will discuss this as an example for how reagents that change paper surface properties can be used to improve paper-based detection, and further use of this assay will be described in Chapter 7.

Detection of Nickel

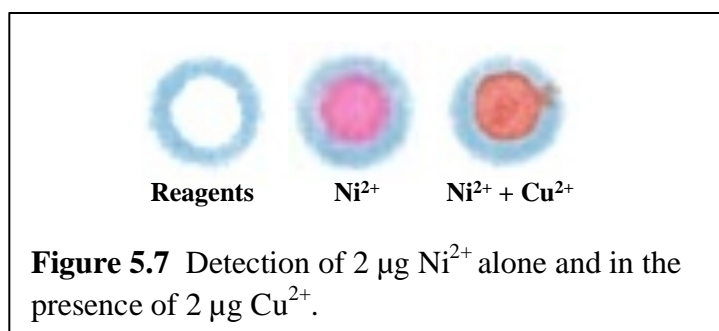
The assay used for nickel detection was based on the bright pink complex formed from the reaction of Ni^{2+} with dimethylglyoxime (dmg):²⁴⁻²⁶



This reaction occurs due to donation of electron pairs on the nitrogen atoms of dmgh to Ni²⁺, which requires the loss of a proton from one oxime group (NOH) of each dmgh molecule. Since complexation of Ni²⁺ by dmgh involves the loss of a proton, the rate and extent of complexation are pH dependent.^{24,26} It has been reported that this reaction does not take place below pH 6, and that the most rapid complexation of Ni²⁺ with DMG occurs at pH 9.²⁶ For the spot test developed here, paper treated with ammonium hydroxide solutions ranging in pH from 8-11 showed immediate color formation, and variation of pH within this range did not result in a measurable difference of color intensity. The pink Ni(dmgh)₂ product is shown in Figure 5.7.

In a study of possible interferences from Fe²⁺, Mn²⁺, Cu²⁺, Zn²⁺, V³⁺, Pb²⁺, Cr³⁺, Co²⁺, and Al³⁺, issues were found with Cu²⁺ and, to a lesser extent, Fe²⁺. When present as the only metal, Cu²⁺ did not form a colored product with dmgh₂ under these assay conditions; however, when present at a 1:1 ratio with Ni²⁺ it causes the pink nickel reaction product to develop a reddish-orange hue and increases color intensity measurements. An example of this effect is shown in Figure 5.7. This change in hue may be due to formation of one or several Cu-dmgh species, as the Cu(dmgh)₂ complex has

been described as brown, and reports of Cu-dmg interactions in ammoniacal solutions have resulted in violet products.^{2,27} The fact that Cu^{2+} did not form a colored product with dimethylglyoxime or ammonia in the absence of Ni^{2+} also suggests that under these assay conditions, the presence of additional metal cations may promote formation of the colored Cu-dmg products. Masking interference from Cu was attempted through the use of tartrate, though it was effective at eliminating interferences when Cu was present at a 1:1 ratio with nickel. Although, it was found that Cu did not affect the assay when present at levels four times lower than that of Ni. There are reports of sodium thiosulfate being used to mask Cu^{2+} , and further investigation into this reagent is recommended for improving nickel detection when Cu is present at levels similar to Ni.^{28,29}



Interference from Fe^{2+} occurred in a manner opposite to what was observed with Cu^{2+} . A sample containing only Fe^{2+} was able to react with dmgH_2 to produce a faint brown-red product; however, when present at a 1:1 ratio with Ni^{2+} , interference from Fe^{2+} was slight and could be eliminated by adding excess dmgH_2 to the assay area. Stability constants, often reported as $\log K$, for Fe-dmg complexes have not been reported for conditions that would allow for a direct comparison between it and the Ni complex; although, it may be assumed that $\log K$ for the brown-red Fe-dmg complex is low enough

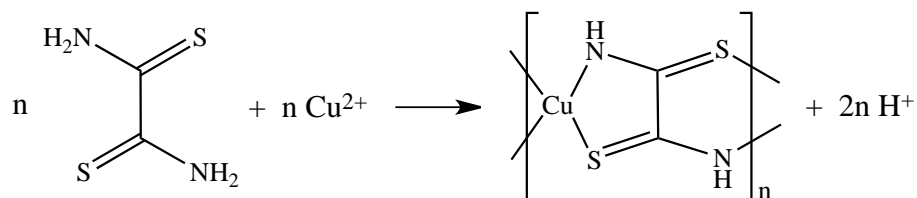
relative to that of $\text{Ni}(\text{dmgH})_2$, that the dmgH_2 ligand favors complexation with Ni^{2+} over Fe^{2+} . This would explain why interference to the Ni assay from Fe^{2+} is minimal when both cations are present at a 1:1 ratio. In cases where Fe content is several times greater than that of Ni, sodium fluoride was employed to mask interferences from Fe^{2+} .^{28,29} In Chapter 7 it will be shown that nickel was determined quantitatively in the presence of high levels of Fe without interference when sodium fluoride was used as a masking agent.

The use of tartrate or citrate has often been suggested in the literature to inhibit interferences from Fe, Cu, Mn, Co, and Cr ions.^{2,30-32} Tartrate was shown in this work to be effective at eliminating color formation from Fe but, as mentioned previously, did little to inhibit interference from copper. Moreover, the presence of tartrate significantly diminished color intensity of the $\text{Ni}(\text{dmgH})_2$ product, as can be seen in Figure 5.8. In order to preserve lower detection limits for Ni detection, the use of tartrate as a masking agent is discouraged unless absolutely necessary. Acetate can also be employed to mask interferences from Co, Mn, and Zn, and does not affect the $\text{Ni}(\text{dmgH})_2$ product. In Chapter 7 it will be demonstrated that a mixture of acetate and fluoride ions were capable of masking interferences from all metals present in an aerosolized ash sample. Cr levels in the ash sample were about 12 times greater than that of Ni, Fe levels were about two times greater, and all other metals, including the possible interferences Cu, Co, Zn, and Mn, were present at levels at least ten times lower than Ni. Unless acetate proves to be ineffective as these metal levels increase relative to nickel, its use as a masking agent is preferable to tartrate.

The dmg assay for detection of Ni was found to be ideal for use on a paper-based microfluidic device due to the stability of reagents employed and of the Ni(dmgH)₂ product, as well as the high visibility of the bright pink product. In addition, because the product is only slightly water-soluble, it concentrates itself on paper in one spot rather than spreading through the paper and diluting the color intensity. Currently, no interferences are seen when the assay is performed in the presence of several other metals as long as Cu levels are low relative to Ni. In many cases, no further optimization would be necessary, as Cu is often not as abundant as Ni in many occupational settings, such as in the steel industry, where occupational exposure to metals is commonly studied. In order to expand the utility of this assay for metal exposure studies, however, additional masking agents for Cu may be needed in the future.

Detection of Copper

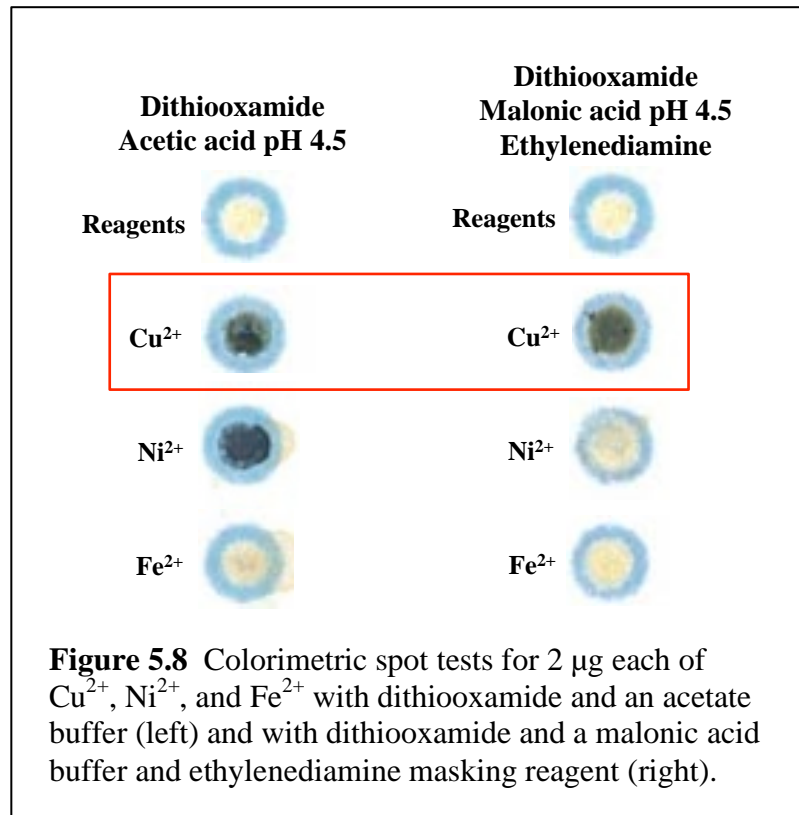
Two colorimetric reagents were examined for detection of Cu. The first was dithiooxamide, also known as rubeanic acid, which reacts instantly with Cu²⁺ to form a solid, black coordination polymer according to the following reaction:³³⁻³⁵



Dithiooxamide is soluble in acetone, yielding a yellow solution, and once impregnated in paper, the solid reagent remains stable for months.³⁶ Co, Ni, Fe, and Ag salts also produce colored precipitates upon reaction with dithiooxamide; however, malonic acid and ethylenediamine can be utilized to sequester interfering ions, thus

inhibiting their interference.^{2,5,37} The selectivity of this assay can be tuned by adjusting the pH because most metal ions only form stable complexes with dithiooxamide above pH 7. The reaction between Cu^{2+} and dithiooxamide remains efficient at pH levels as low as 3, however. For this reason, the reaction spot was treated with buffer adjusted to pH 4.5 for this assay.

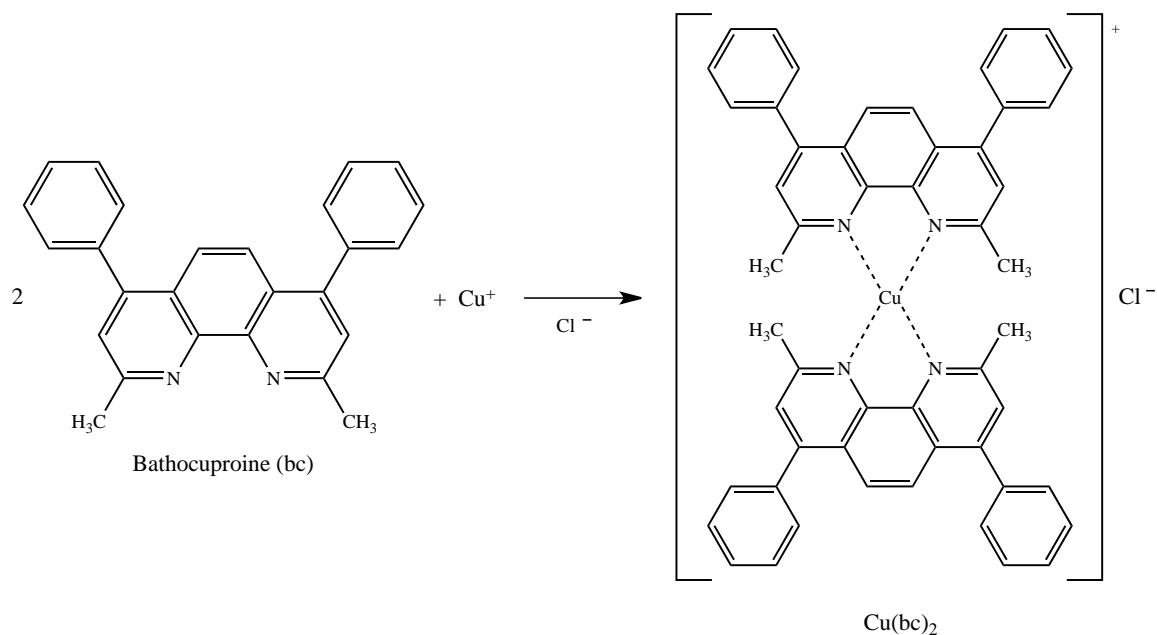
The black Cu(II)-dithiooxamide product is shown in Figure 5.8. The assay was first carried out by drying acetate buffer (pH 4.5) on the reaction spot before the colorimetric reagent was applied, and the following metal ions were tested for reaction with dithiooxamide under these conditions: Ni^{2+} , Mn^{2+} , Fe^{2+} , Zn^{2+} , V^{3+} , Pb^{2+} , Cr^{3+} , Co^{2+} , Al^{3+} . The reaction spots on the left of Figure 5.8 demonstrate that Ni^{2+} forms a black product with dithiooxamide that would greatly interfere with copper detection, and the Fe^{2+} test also showed slight black coloring. This study was repeated, but with malonic acid (pH 4.5) and ethylenediamine solutions replacing the acetate buffer. Reaction spots on the right side of Figure 5.8 show that under these conditions Fe^{2+} no longer caused black precipitate formation, and the product resulting from Ni^{2+} was almost entirely inhibited. Of the other metals tested, only Co^{2+} produced a colored product (orange) upon reaction with dithiooxamide; however, it was later found that presence of this orange color did not affect intensity measurements of the black Cu(II)-dithiooxamide complex. Further interference studies were carried out using malonic acid and ethylenediamine in which detection of Cu^{2+} was performed in the presence of each of the aforementioned metals, one at a time. A slight loss of color was seen when V^{3+} or Co^{2+} were present at a 1:1 ratio with Cu^{2+} . Increasing the amount of dithiooxamide impregnated in the paper solved this problem.



Two major advantages of this assay were: 1) the stability of all reagents both in solution and dried on paper, as well as the stability of the colored product, and 2) the dark color of the product that allows for easy visualization at lower levels. Ultimately, interferences from Ni continued to result in falsely high intensity measurements and use of the dithiooxamide assay was discontinued.

The colorimetric assay utilizing bathocuproine (bc) was chosen to replace dithiooxamide for detection of copper, and demonstrated improved selectivity. Bathocuproine is a derivative of 1,10-phenanthroline. The presence of methyl groups on this ligand prevents chelation with Fe²⁺; however, it does readily complex Cu⁺, forming an orange, slightly water-soluble product.^{38,39} Presence of a negatively charged, univalent

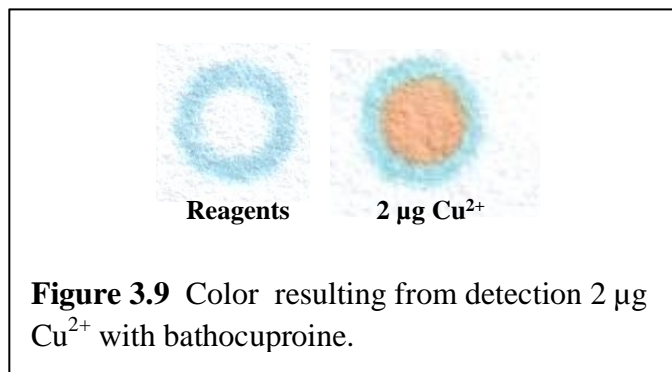
anion, such as Cl^- , is necessary as it provides stabilization of the Cu-bathocuproine complex. This is demonstrated by the following reaction:^{38,40}



In order to detect total copper, hydroxylamine was used for reduction of Cu^{2+} to Cu^+ . Bathocuproine is only soluble in organic solvents such as chloroform and benzene, and areas of paper impregnated with bathocuproine become hydrophobic. Chapter 6 will discuss how modifications were made to the reagent to overcome problems associated with hydrophobicity of the detection area on paper.

Color resulting from formation of the $\text{Cu}(\text{bc})_2$ complex is shown in Figure 5.9. The standard copper sample was a solution of a Cu^{2+} salt, which is not expected to be complexed by bathocuproine. The color formation seen in Figure 5.9 not only proves success of the assay, but also demonstrates that hydroxylamine was efficient at reducing Cu^{2+} to Cu^+ . No interferences were seen from Fe, Ni, Mn, Zn, V, Pb, Cr, Co, Ba, Cd, Ag, or Al ions present in an aerosolized fly ash sample, even though levels of Ni, Fe, and Cr

were present at levels ~5 times, ~10 times, and ~50 times higher than copper levels, respectively.



Aside from initial issues resulting from hydrophobicity of the reagent (described in Chapter 6), no disadvantages to this assay were discovered. Bathocuproine proved to be selective for Cu²⁺, as interference from other metals was not observed, and the reagents used, as well as the orange product were found to be stable on a paper substrate. This assay replaced the dithiooxamide test for Cu in the paper-based device introduced in Chapter 7, and details of this assay performed on that device will be presented then.

5.8 Conclusion

Colorimetric detection of Cd, Mn, Pb, Fe, Ni, and Cu was accomplished on a filter paper substrate. The assays for Fe, Ni, and Cu detection were chosen to be employed in a paper-based device for particulate metal detection based primarily on the following criteria: 1) the ease with which color formation is observed, 2) stability of reagents and colored product, and 3) the degree of interference from other metals. Improvements to assays or alternatives for detection of Cd and Mn were suggested. Investigations into additional colorimetric assays for Pb and other metals, such as V, Co,

and Cr are expected to increase utility of the device presented in Chapter 7. The discussions presented here provide a better understanding of the types of reagent and product properties that yield the most successful quantitative colorimetric assays on paper, as well as the types of reaction mechanisms that tend to be less susceptible to interference from other metals. For example, the Mn assay demonstrated that assays based on oxidation of the colorimetric reagent are likely to have interferences from metal cations with high reduction potentials. As much of the past literature discussing these assays either applies to solution-based detection or is outdated and contradictory, this chapter will serve as an extremely useful tool for further development of multiplexed metal detection on paper-based devices.

5.8 References

- (1) NIOSH *National Transportation, Warehousing, and Utilities Agenda*; NORA Transportation, Warehousing, and Utilities Sector: **2008**.
- (2) Feigl, F., *Spot tests in inorganic analysis*. Elsevier Pub. Co.: Amsterdam, **1972**.
- (3) Clarke, B. L.; Hermance, H. W., Paper as a Medium for Analytical Reactions: I. Improvements in the Spot Test Technic. *Industrial & Engineering Chemistry Analytical Edition* **1937**, 9 (6), 292-294.
- (4) Apilux, A.; Dungchai, W.; Siangproh, W.; Praphairaksit, N.; Henry, C. S.; Chailapakul, O., Lab-on-Paper with Dual Electrochemical/Colorimetric Detection for Simultaneous Determination of Gold and Iron. *Analytical Chemistry* **2010**, 82 (5), 1727-1732.
- (5) Butts, P. G.; Gahler, A. R.; Mellon, M. G., Colorimetric Determination of Metals in Sewage and Industrial Wastes. *Sewage and Industrial Wastes* **1950**, 22 (12), 1543-1562.
- (6) Luis, P.; Carducci, C. N., Improved spot test for traces of nickel with dimethylglyoxime in the presence of interferences. *Microchimica Acta* **1971**, 59 (1), 124-130.
- (7) Chester, R.; Nimmo, M.; Fones, G. R.; Keyse, S.; Zhang, Z., Trace metal chemistry of particulate aerosols from the UK mainland coastal rim of the NE Irish sea. *Atmospheric Environment* **2000**, 34 (6), 949-958.
- (8) EPA *Profile of the Fabricated Metal Products Industry*; Office of Enforcement and Compliance Assurance: Washington, DC, **1995**.
- (9) EPA *Metal Plating Waste Minimization*; Waste Management Office, Office of Solid Waste: Arlington, VA, **1995**.
- (10) Bartsch, M. R.; Kobus, H. J.; Wainwright, K. P., An Update on the Use of the Sodium Rhodizonate Test for the Detection of Lead Originating from Firearm Discharges. *Journal of Forensics Science* **1996**, 41, 1046-1051.
- (11) Feigl, F.; Miranda, L. I., Selective Spot Reaction for Cadmium. *Industrial & Engineering Chemistry Analytical Edition* **1944**, 16 (2), 141-142.
- (12) Dillon, J. H., The Sodium Rhodizonate Test: A Chemically Specific Chromophoric Test for Lead in Gunshot Residues. *The Association of Firearm and Tool Mark Examiners Journal* **1990**, 22 (3), 251-256.
- (13) Chalmers, R. A.; Telling, G. M., A reassessment of rhodizonic acid as a qualitative reagent. *Microchimica Acta* **1967**, 55 (6), 1126-1135.
- (14) Semin, B.; Seibert, M., A simple colorimetric determination of the manganese content in photosynthetic membranes. *Photosynthesis Research* **2009**, 100 (1), 45-48.
- (15) Serrat, F. B., 3,3',5,5'-Tetramethylbenzidine for the Colorimetric Determination of Manganese in Water. *Mikrochimica Acta* **1998**, 129, 77-80.
- (16) Liu, M.; Zhang, Y.; Chen, Y.; Xie, Q.; Yao, S., EQCM and in situ FTIR spectroelectrochemistry study on the electrochemical oxidation of TMB and the effect of large-sized anions. *Journal of Electroanalytical Chemistry* **2008**, 622, 184-192.
- (17) Beklemishev, K. M.; Stoyan, A. T., Sorption-Catalytic Determination of Manganese Directly on a Paper-based Chelating Sorbent. *Analyst* **1997**, 122 (10).

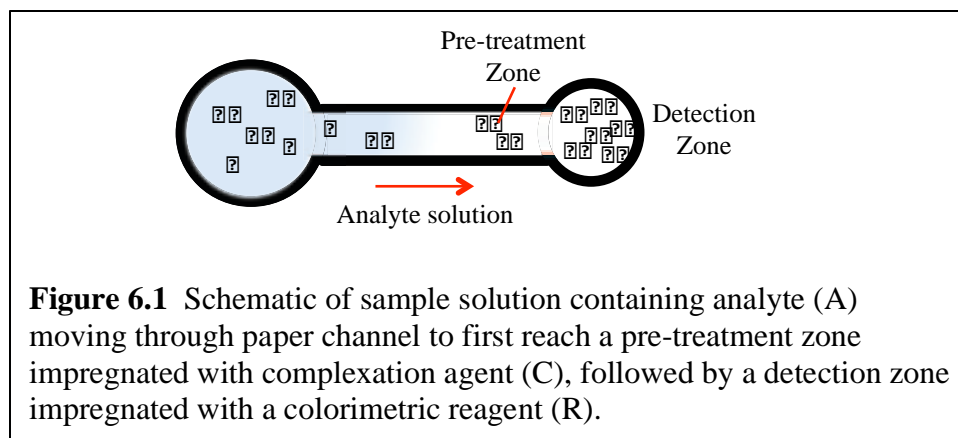
- (18) Jang, G.-G.; Roper, D. K., Balancing Redox Activity Allowing Spectrophotometric Detection of Au(I) Using Tetramethylbenzidine Dihydrochloride. *Analytical Chemistry* **2011**, 83 (5), 1836-1842.
- (19) Josephy, P. D.; Eling, T.; Mason, R. P., The horseradish peroxidase-catalyzed oxidation of 3,5,3',5'-tetramethylbenzidine. *The Journal of Biological Chemistry* **1982**, 257 (7), 3669-3675.
- (20) Bard, A. J.; Faulkner, L. R., *Electrochemical methods fundamentals and applications*. Wiley: New York, **2001**.
- (21) Chiswell, B.; O'Halloran, K. R., Comparison of three colorimetric methods for the determination of manganese in freshwaters. *Talanta* **1991**, 38 (6), 641-647.
- (22) Brandt, W. W.; Dwyer, F. P.; Gyarfás, E. D., Chelate Complexes of 1,10-Phenanthroline and Related Compounds. *Chemical Reviews* **1954**, 54 (6), 959-1017.
- (23) Hughes, M. N.; Shrimanker, K., Metal complexes of hydroxylamine. *Inorganica Chimica Acta* **1976**, 18 (0), 69-76.
- (24) Bambenek, M. A.; Pflaum, R. T., The Reaction of Nickel with Dioximes. *Inorganic Chemistry* **1963**, 2 (2), 289-292.
- (25) Booth, E.; Strickland, J. D. H., The Compounds Formed between Nickel(II) and Dimethylglyoxime by Alkaline Oxidation. *Journal of the American Chemical Society* **1953**, 75 (12), 3017-3019.
- (26) Gazda, D. B.; Fritz, J. S.; Porter, M. D., Determination of nickel(II) as the nickel dimethylglyoxime complex using colorimetric solid phase extraction. *Analytica Chimica Acta* **2004**, 508 (1), 53-59.
- (27) Caton, J. E.; Banks, C. V., Hydrogen bonding in some copper(II) and nickel(II) vic-dioximes. *Inorganic Chemistry* **1967**, 6 (9), 1670-1675.
- (28) Dedkova, V. P.; Shvoeva, O. P.; Savvin, S. B., Test Determination of Cu(II), Ni(II), and Cr(VI) in a Single Sample. *Journal of Analytical Chemistry* **2001**, 56 (8), 758-762.
- (29) Schmitt, D.; Stein, A.; Baumer, W. Indicator for the detection of nickel ions. 1973.
- (30) University, T. S., The Gravimetric determination of nickel. *Chem 222 lab manual* **2011**.
- (31) Jozic, M.; Peer, T.; Malissa, H., Rapid Test Methods for the Field Screening of Heavy Metals in Soil Samples. *Water, Air, & Soil Pollution* **2009**, 199 (1), 291-300.
- (32) Farag, A. B.; El-Wakil, A. M.; El-Shahawi, M. S., Detection and semiquantitative determination of nickel with dimethylglyoxime-loaded foam. *Talanta* **1982**, 29 (9), 789-790.
- (33) Nagels, P.; Mertens, R.; Desseyn, H. O., Electrical properties of Cu(II)-N,N'-dimethyldithiooximide polymers. *Synthetic Metals* **2002**, 128, 1-6.
- (34) Kitagawa, H.; Nagao, Y.; Fujishima, M.; Ikeda, R.; Kanda, S., Highly proton-conductive copper coordination polymer, H₂dtoaCu (H₂dtoa=dithiooxamide anion). *Inorganic Chemistry Communications* **2003**, 6 (4), 346-348.
- (35) Zotti, G.; Mengoli, G.; Decker, F., Electrodeposition and Photoelectrochemical Properties of Dithiooxamido Copper (II) Films Onto Copper Electrodes. *Molecular Crystals and Liquid Crystals* **1985**, 121 (1-4), 337-340.

- (36) Delavault, R., Simplified Field Test For Copper. *Journal of Geochemical Exploration* **1977**, 8, 537-540.
- (37) West, P. W., Selective Spot Test for Copper. *Industrial & Engineering Chemistry Analytical Edition* **1945**, 17 (11), 740-741.
- (38) Moffett, J. W.; Zika, R. G.; Petasne, Evaluation of bathocuproine of the spectrophotometric determination of copper(I) in copper redox studies with applications in studies of natural waters. *Analytica Chimica Acta* **1985**, 175, 171-179.
- (39) Smith, G. F.; Wilkins, D. H., New Colorimetric Reagent Specific for Copper. *Analytical Chemistry* **1953**, 25 (3), 510-511.
- (40) Hulthe, P., A bathocuproine reagent-paper for the rapid semi-quantitative determination of copper in the 1 to 70 p.p.m. range. *Analyst* **1970**, 95 (1129), 351-355.

CHAPTER 6: ADVANCING PAPER-BASED DEVICES - NOVEL METHODS OF CONTROLLING CHEMISTRY ON PAPER

6.1 Introduction

The previous chapter described the development of paper-based assays for metal detection that were minimally susceptible to interference from other metals. These assays were demonstrated as spot tests, meaning a sample solution was pipetted directly onto the prepared assay area. In a paper-based microfluidic device, the idea is typically for sample to be applied in one area of the device and then be carried by capillary action through the paper fibers to a detection zone impregnated with reagents for colorimetric detection. When sample is introduced in this way, reaction zones can also be created along the sample path that allow for pre-treatment, which includes oxidation/reduction or complexation of interfering compounds as was described previously. A simple schematic of this concept is demonstrated in Figure 6.1, in which an aqueous analyte (A) solution is introduced at one end of a channel and flows past a pre-treatment zone containing a complexation agent (C) to reach the detection zone containing the colorimetric reagent (R).

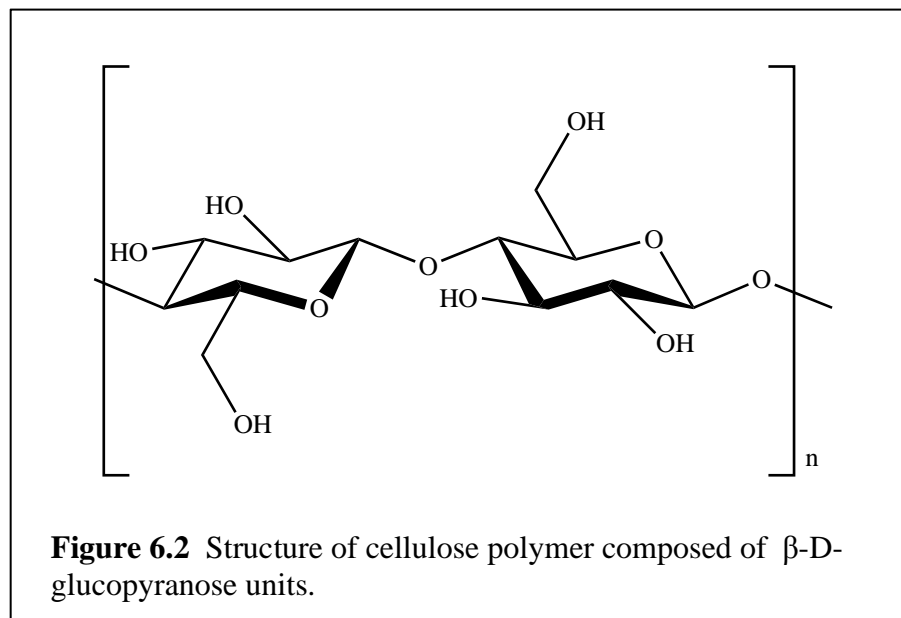


Fluid movement through paper fibers and the behavior of different reagents on paper can be better understood by considering the basic structure and properties of cellulose. Cellulose is a homopolymer composed of β -D-glucopyranose units which are linked together through glycosidic bonds (Figure 6.2).^{1,2} The three hydroxyl groups of each monomer are responsible for the hydrophilic nature of pure cellulose. The completely linear polymer molecules aggregate through Van der Waals forces and extensive intra- and inter- molecular hydrogen bonding to form fibers.^{1,2} A paper network consists of randomly laid cellulose fibers that also interact with each other through hydrogen bonding as wetted fibers dry in contact with each other. The result is a complicated arrangement of narrow pores between fibers that allows water to absorb and move through paper by capillary action.^{1,2} The rate of capillary movement of fluids through paper can be described by the Washburn equation:

$$\frac{dl}{dt} = \frac{\gamma r \cos \theta}{4\eta l} \quad (6.1)$$

where dl/dt is the rate of penetration of the capillary, l is the distance penetrated into a cylindrical capillary of radius r in time t , θ is the contact angle between the surface and a liquid with surface tension γ and viscosity η .² From this equation, it is seen that liquids

with higher surface tension and lower viscosity will have the greatest rate of capillary flow in paper. For example, water, which is known for wicking through paper by capillary action, has a surface tension of 0.0728 N/m and a viscosity of 1 mPa s at 20 °C. As a comparison, methanol, which has very poor wicking action, also has a low viscosity (0.593 mPa s) but its surface tension is more than three times smaller than that of water at 0.0227 N/m at 20 °C.



Interactions between cellulose paper and other chemicals are dominated by hydrogen bonding over electrostatic repulsion or attraction from unprotonated hydroxyl groups. Predicting the degree of such interactions is unrealistic, as the processing of cellulose in papermaking can oxidize surface hydroxyl groups to carboxylic groups and even contact with a liquid causes modifications in paper structure due to disruption of hydrogen bonds, relaxation of fibers, and shrinking or expanding of pores.² Fillers and other additives used in papermaking can affect significant changes in the physical

properties of paper. For example, capillary flow of water in common printer paper is quite low, largely because fillers used in its production eliminate pores between fibers. Alternatively, Whatman filter paper is free of all additives and has excellent absorption and capillarity properties which make it a popular substrate for paper-based microfluidic devices.

This chapter demonstrates the ability to control reaction conditions and movement of reagents and products in a paper-based microfluidic device. Polyelectrolytes were used to immobilize reagents and products that were carried away from the detection zone by water, and a solubilizing agent was used to overcome sample flow problems that arise when hydrophobic reagents are impregnated into a zone. In addition, it was shown that drastically different pH zones can be created in paper without negatively affecting one another. These techniques expand the multiplexed detection capabilities of paper-based devices, as they demonstrate how a wide range of chemistries and capillary flow modifications can be carried out on a single device.

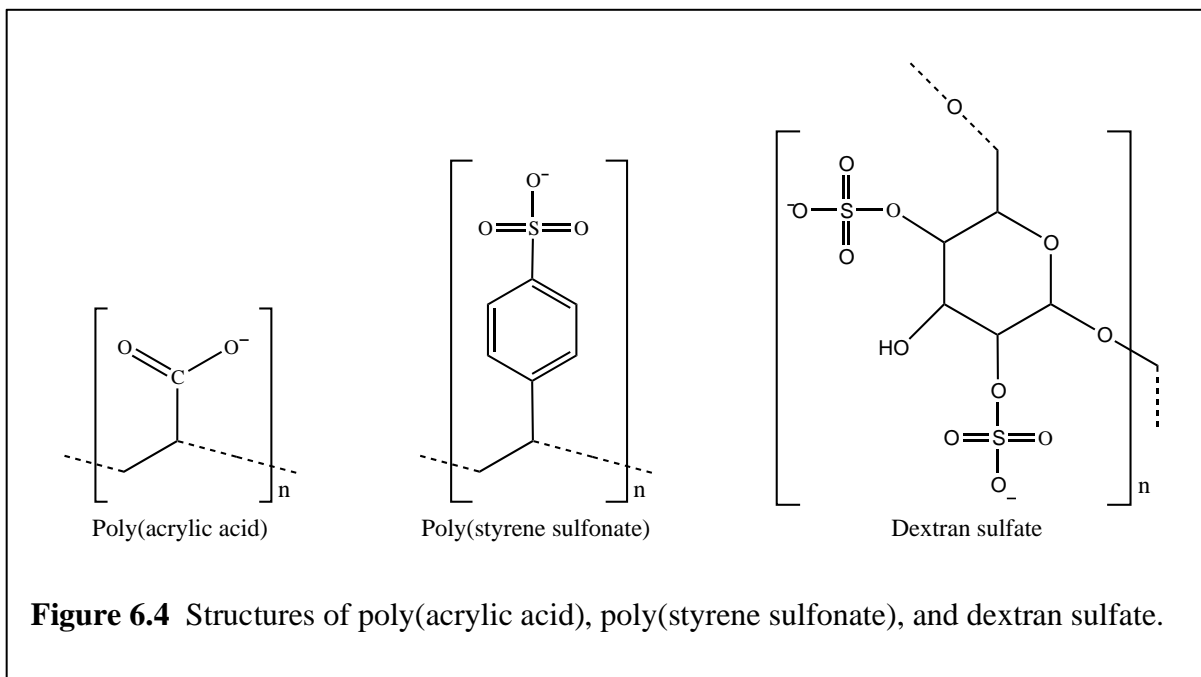
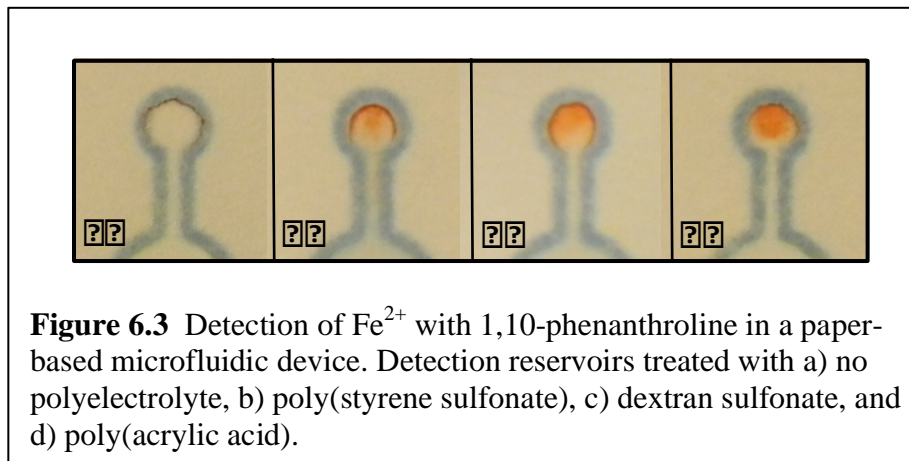
6.2 Controlling mobility of compounds on paper

It was mentioned in the previous chapter that the use of water-insoluble colorimetric reagents tends to yield sensitive spot test assays because their products remain at the site of formation, resulting in sharply defined, intense color spots. It was found throughout this work that immobility of reagents and products on paper was especially advantageous, if not imperative, when assays were carried out on microfluidic devices which use water to carry sample through the paper zones. While it is desirable for water to carry analytes through the paper, immobilization of reagents keeps different zones

from blending into one another as sample solution moves past them, and immobilization of product concentrates color intensity.

The importance of product immobilization was better understood when the iron assay described in Chapter 5 was employed in a device detection zone rather than as a simple spot test. The reagent used for detection iron was 1,10-phenanthroline, which is moderately soluble in water under acidic conditions, as is the orange complex formed with Fe^{2+} .^{3,4} As demonstrated in the schematic of Figure 6.1 above, 1,10-phenanthroline was dried onto the detection zone, and an aqueous sample solution was added to a sample reservoir at the center of a paper device. Upon reaching the detection zone, water carrying Fe^{2+} also carried 1,10-phenanthroline and/or the orange $\text{Fe}(\text{phen})_3^{2+}$ product to the detection reservoir borders, making visualization of the product difficult. This effect is shown in Figure 6.3a. In an attempt to solve this problem, the detection zone was coated with a negatively charged polyelectrolyte with the purpose of increasing the charge density at the paper surface. It was hypothesized that the orange product could be immobilized if there were stronger interactions between the negatively charged paper fiber surfaces and the positively charged iron complex. Three polyelectrolytes were tested for this purpose: poly(acrylic acid) (MW ~ 1,000,000), poly(styrene sulfonate) sodium salt (MW ~ 70,000), and dextran sulfate sodium salt (MW ~ 500,000). Structures of these polymer molecules are shown in Figure 6.4. Detection zones (3 mm diameter) were prepared by applying 1 μL of polyelectrolyte solution (~0.05 mM polymer chain) and allowing it to dry before adding the other reagents. A solution containing 5 μg Fe^{2+} was pipetted onto the sample reservoir and 10 μL additional water was added to carry sample to the detection zone. Results from this test, shown in Figure 6.3, demonstrated that

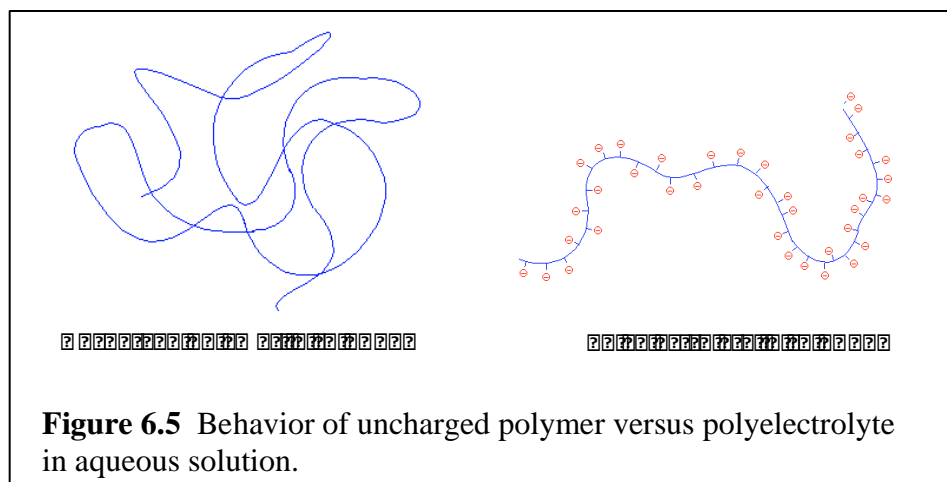
retention of the orange product was accomplished, with the greatest immobilization effects from the polyelectrolytes occurring in the following order: poly(acrylic acid) > dextrose sulfate > poly(styrene sulfonate).



The pKa for poly(acrylic acid) is ~ 4 , while pKa's for dextrose sulfate and poly(styrene sulfonate) approach negative values.⁵⁻⁷ Under the iron assay conditions, in

which the detection zone pH is ~ 4.5 , all three polyelectrolyte molecules should be increasing the negative charge density relative to the cellulose. Since poly(acrylic acid) is partially protonated at pH 4.5 and shielding of negative charge by sodium ions is possible for the other two polyelectrolyte sodium salts on paper, it is difficult to predict which of these three yield the greatest negative charge density at the detection zone. The degree to which each polyelectrolyte immobilized the orange product seemed to be most affected by the viscosity of the polyelectrolyte solution applied to paper. The poly(acrylic acid) solution was by far the most viscous of the three and resulted in the greatest immobilization of product. Further investigations into this aspect are warranted in the future.

Polyelectrolytes exhibit unusual behavior in aqueous solutions that greatly affects viscosity.^{1,2} Uncharged polymer molecules in aqueous solution tend to be tangled into random coils, while acidic polyelectrolytes, such as poly(acrylic acid), are covered in negative charges which repel each other, causing the polymer chain to stretch out (Figure 6.5). The expanded polyelectrolyte chains increase solution viscosity because they take up more space and are more effective at resisting flow of the solvent molecules around them. It is suggested here that when sample solution reaches the detection zone, not only is the orange product held to some degree by attraction to the negatively charged chains, but viscosity is increased as the water dissolves dried polyelectrolyte molecules. This significantly slows capillary flow of the solution, thus aiding in immobilization of the orange product while the remaining water evaporates.



Further tests showed that flow can be blocked completely by increasing the amount of poly(acrylic acid) in a zone. This has led to the idea of possibly creating a polyelectrolyte “gate” in paper microfluidic channels that blocks solution from entering a certain area of the device, but can then be removed when needed. When high concentrations of NaCl are present in a polyelectrolyte solution, viscosity is greatly reduced. This occurs because excess Na^+ ions are able to reduce the effective negative charge along the chain, allowing it to revert back to its coiled conformation. It is possible that a polyelectrolyte “gate” blocking capillary flow in a paper channel could be “opened” by adding a concentrated solution of NaCl to the zone, thus reducing viscosity so that solution can pass.

6.3 Reducing hydrophobicity in a zone

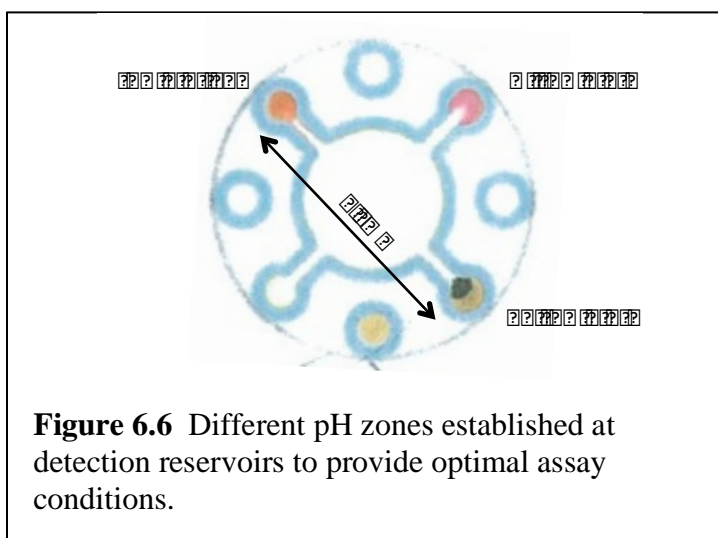
The bathocuproine reagent used for detection of copper is hydrophobic, and deposition in the detection zone results in a hydrophobic area that blocks flow of aqueous sample solution. Detection zone hydrophobicity was reduced by adding poly(ethylene

glycol) to the bathocuproine chloroform solution, with optimal solution concentrations determined to be 50 mg/mL bathocuproine and 40 mg/mL polyethylene glycol (PEG 400). Lower levels of PEG relative to bathocuproine were not sufficient to reduce hydrophobicity, while levels higher than 40 mg/mL lead to inconsistent color formation. PEG is commonly used as a solubilization reagent in the pharmaceutical and food industries. It is miscible with both water and chloroform, which is the solvent used to dissolve bathocuproine, and when deposited on paper along with bathocuproine, the polarity it adds to the detection zone allows for the aqueous sample solution to come in contact with the hydrophobic reagent.

6.4 Controlling pH in different zones of a device

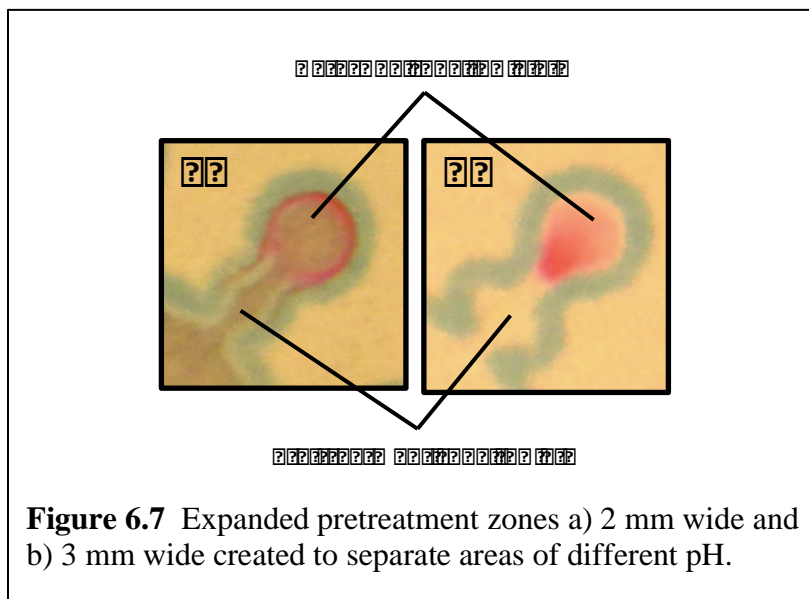
Among the reagents dried onto to a device are those needed to set the pH of a specific zone. In a device that performs multiplexed detection it is especially important that the pH at one detection zone does not effect the pH at another, as optimal pH conditions for each assay may vary drastically. The ability to control pH at each detection zone by drying the appropriate buffer or acid/base solution is demonstrated by the example of simultaneous detection of Ni^{2+} , Cu^{2+} , and Fe^{2+} by dimethylglyoxime (dmg), dithiooxamide, and 1,10-phenanthroline, respectively (Figure 6.6). In this experiment, the optimal pH for Fe and Cu detection was set by drying solutions of hydroxylamine (for Fe) and malonic acid (for Cu), each with a pH of 4.5, onto their respective detection zones; and an ammonium hydroxide solution of pH 9.8 was dried onto the nickel detection zone. As was described in the previous chapter, this assay for iron detection is only successful under acidic conditions; likewise, the pink $\text{Ni}(\text{dmgH})_2$ complex only

forms under basic conditions. Appropriate color formation in each detection zone shows that pH was controlled in these different areas of the device without affecting one another. It should be noted that the actual pH of the paper after application of reagents was never determined. Instead, reported pH values are those of the solutions used to set pH, and optimization of pH for an assay was based on results yielded when solutions of various pH were dried onto a zone.



Establishing unique pH zones for each detection reservoir was not difficult due to the distance between them, but in some cases it may be necessary or useful to have different pH zones right next to one another. One instance of this arose in the nickel assay, where acetic acid was used to mask interferences from other metals. Adding the 10 mM acetic acid solution (pH 4) to the nickel detection zone lowered the pH there so that the pink product did not form. The pre-treatment zones mentioned above were developed at this point, not only to solve this issue, but also to improve pre-treatment of sample in general. Pre-treatment zones, shown in Figure 6.7, were created in the channels, just

before the detection reservoirs and were expected to serve two functions: 1) to allow for additional time and area for analytes to be oxidized/reduced if appropriate and for interfering metals to be complexed by masking agents; 2) to separate detection zones from dried reagents that will change assay pH. The first pre-treatment zones created measured ~2 mm at their widest point, and the acetic acid masking agent was dried onto this area. Figure 6.7a shows that this slight widening of the channels was not effective at keeping acetic acid in the pre-treatment zone from affecting the nickel assay. The pink color indicative of Ni^{2+} was only able to form along the edges of the reservoir, and the hue of the product was changed to a more red color. The pre-treatment zone was then expanded to ~3 mm wide and a 1 mm straight channel was added between this zone and the detection zone (Figure 6.3b). With this modification, conditions in the detection zone appeared unaffected by the acetic acid in the pre-treatment zone and this device design was adopted for use in all subsequent work.



6.5 Conclusion

The ability to immobilize reagents and products on paper and to control pH in specific zones of a paper-based device was demonstrated here. These techniques allow colorimetric assays to move beyond simple spot tests, and instead be employed in paper-based devices that exploit fluid movement through paper to achieve more advanced analysis. The separation of pH zones allows for multiplexed detection and sample pre-treatment on a single device, while reagent and product immobilization result in improved limits of detection. Further investigation into tuning the mobility of reagents and capillary flow of solutions in paper is likely to continue the expansion paper-based device capabilities. Using the techniques described here, colorimetric spot tests described in Chapter 5 were able to be employed in a paper-based microfluidic device for detection of particulate metals. This device, capable of multiplexed detection from an aerosolized sample, will be demonstrated in the following chapter.

6.6 References

- (1) Gardner, D. J.; Optorto, G. S.; Mills, R.; Samir, A. S., Adhesion and surface issues in cellulose and nanocellulose. *Journal of Adhesion Science and Technology* **2008**, *22*, 545-567.
- (2) Sahin, H. T.; Arslan, M. B., A study on physical and chemical properties of cellulose paper immersed in various solvent mixtures. *International Journal of Molecular Sciences* **2008**, *9*, 78-88.
- (3) Adhikamsetty, R. K.; Gollapalli, N. R.; Jonnalagadda, S. B., Complexation kinetics of Fe²⁺ with 1,10-phenanthroline forming ferriin in acidic solutions. *International Journal of Chemical Kinetics* **2008**, *40* (8), 515-523.
- (4) Van Meter, F. M.; Neumann, H. M., Solvation of the tris(1,10-phenanthroline)iron(II) cation as measured by solubility and nuclear magnetic resonance shifts. *Journal of the American Chemical Society* **1976**, *98* (6), 1382-1388.
- (5) Sakiyama, T.; Takata, H.; Toga, T.; Nakanishi, K., pH-sensitive shrinking of a dextran sulfate/chitosan complex gel and its promotion effect on the release of polymeric substances. *Journal of Applied Polymer Science* **2001**, *81* (3), 667-674.
- (6) Nge, T. T.; Yamaguchi, M.; Hori, N.; Takemura, A.; Ono, H., Synthesis and Characterization of Chitosan/Poly(acrylic acid) Polyelectrolyte Complex. *Journal of Applied Polymer Science* **2001**, *83* (5), 1025-1035.
- (7) Guthrie, J. P., Hydrolysis of esters of oxy acids: pK_a values for strong acids. *Can. J. Chem.* **1978**, *56*, 2342-2354.

CHAPTER 7: MICROFLUIDIC PAPER-BASED ANALYTICAL DEVICE FOR DETECTION OF PARTICULATE METALS

Employing the colorimetric assays and techniques demonstrated in the previous two chapters, a microfluidic paper-based device was developed for detection of particulate metals in occupational settings. This work represents the first example of multiplexed metal detection on paper from a real, aerosolized sample. It also demonstrates the use of filters as a sample system, eliminating the need for filter digestion.

The work presented in this chapter was submitted to *Analytical Chemistry*:

Mentele, M. M.; Cunningham, J.; Koehler, K.; Volckens, J.; Henry, C. S. Microfluidic Paper-Based Analytical Device for Particulate Metals. *Anal. Chem.* **2012**, (in press).

7.1 Introduction

Morbidity and mortality from occupational respiratory diseases are estimated to cost ten billion dollars each year in the U.S.^{1,2} World-wide, such diseases are associated with approximately 425,000 annual occupationally-related mortalities.³ More specifically, occupational exposure to particulate metals affects millions of workers, primarily in areas of manufacturing, construction (welding, cutting, blasting), and transportation (combustion, utility maintenance, and repair services).⁴ The health effects associated with exposure to airborne metals are extensive and include cancers of the respiratory, hematopoietic, renal, nervous, hepatic, and digestive systems, immune

disorders, birth and developmental defects, neuropathy, nephropathy, and specific respiratory diseases such as asthma, bronchitis, COPD, and emphysema.⁵⁻¹⁰

Yet, despite the high incidence and prevalence of occupational respiratory disease, the paradigm for assessing exposure to aerosolized metals has remained largely unchanged over the last 25 years.¹¹ Current exposure assessment methods for particulate metals, designed to support monitoring for regulatory compliance, are both cost and time intensive. These methods call for collection of an 8-hour filter sample taken from a worker's breathing zone, after which time, the filter sample is shipped to a laboratory for chemical analysis.^{12,13} The standard turnaround time from shipment to analysis is 5-10 business days, meaning that a single exposure assessment requires approximately two weeks time for completion from sample collection to outcome reporting. The process is highly inefficient, especially from the standpoint of risk communication, as an industrial hygienist must return to the worksite two weeks later to disseminate testing results to management and workers. To exacerbate the issue, method detection limits suffer because of sample dilution during digestion and dissolution with acidic reagents. The lack of sensitivity especially hampers task-based exposure assessment, for which sampling times may need to be as low as tens of minutes. Such limitations can make it impossible to determine the source or activity associated with an elevated level of exposure. Furthermore, analysis costs, typically in excess of several hundred dollars per sample, limit the number of samples that can be collected. Consequently, there is a need to improve the sensitivity and efficiency of particulate metal measurement methods in occupational settings while also reducing the overall cost. This need will grow as permissible exposure limits trend towards lower levels.¹⁴

An ideal exposure assessment method would allow for shorter collection times and combine sampling and analysis into a single event, saving valuable time. Here, in an effort to reach this goal, a method has been developed using microfluidic paper-based analytical devices (μ PADs) with colorimetric detection to measure particulate metals on air sampling filters. First introduced in 2007 by the Whitesides group¹⁵, μ PADs consist of a patterned, hydrophilic paper substrate that serves as a platform for multiplexed analyte detection. Liquid moves through the paper fibers by capillary action, and channels are created in paper by depositing a hydrophobic material, such as photoresist or wax to confine and direct liquid flow. Paper is an attractive substrate for microfluidic devices; it is abundant, inexpensive, disposable, easy to use, store, and transport, has a high surface area for visualization, and is easy to modify chemically.¹⁵⁻¹⁸ Moreover, the availability of a variety of wax and inkjet printing techniques has made fabrication and functionalization of μ PADs relatively simple and inexpensive.¹⁹⁻²¹ For example, the cost of the device presented here is \$0.013 including the cost of the paper, the wax ink, the chemical reagents, and the printer amortized over its estimated lifetime. Both quantitative and qualitative analyses can be carried out with μ PADs using colorimetric detection. Cameras and scanners, in conjunction with imaging software, have been used to measure the size and intensity of color spots on μ PADs, and these portable, relatively inexpensive technologies allow for electronic transmission of data from the field to the laboratory.^{17,22-25}

Here, colorimetric assays were developed on a paper-based device for the detection of Fe, Ni, and Cu. Both the device and assays were designed so that detection of each metal could take place simultaneously and in the presence of possible interfering

metals. An acid digestion method was also established in which the particulate sample is digested directly on a collection filter in under 2 minutes and without any dilution. Both qualitative and quantitative data analyses were used to determine the amount of metal present. Visual comparison of color intensity and area allow for estimation of sampled metals mass within about 5 μg . Quantitative analysis of color intensity allowed for more sensitive measurements and limits of detection as low as 1 μg . These data were obtained using imaging software that selects specific color hues of reaction products and then converts these values to greyscale intensity. Measurements of metals in standard solutions and a resuspended incineration ash sample were in good agreement with actual values, with errors ranging from 0.2 – 0.6 μg (7.7 – 9.3 %).

7.2 Experimental

Fabrication and Design of μPAD

The μPAD presented here was fabricated using the previously reported wax printing technique.²⁰ The device design was created using drawing software (CorelDRAW) and was then printed onto Whatman Grade 1 filter paper (VWR) using a Xerox Phaser 8860 wax printer. The printed devices were placed on a hot plate at 150 °C for 120 s, which caused the wax to permeate through the paper, forming the three-dimensional hydrophobic barriers that control liquid flow. One side of the devices was covered with clear packing tape to prevent solution leaking out from underneath the paper during the assay.

Colorimetric Detection of Metals

Standard solutions: Iron(III) chloride hexahydrate, nickel(II) sulfate hexahydrate, and copper(II) sulfate pentahydrate (Sigma-Aldrich, St. Louis, MO) were used as standards for the Fe, Ni, and Cu assays, respectively. Additional metal salts were used to test potential interferences: manganese chloride tetrahydrate, zinc nitrate hexahydrate, vanadium(III) chloride, lead(II) nitrate, chromium(III) chloride, cobalt(II) chloride, and aluminum sulfate (Sigma-Aldrich, St. Louis, MO). Fe, Ni, and Cu standards were each prepared as 1000 ppm metal solutions. For the assays carried out in the presence of other metals, two solutions were prepared: 1) a solution containing 1000 ppm Fe and Ni with 250 ppm Cu, resulting in a ratio of 4:1 (Fe, Ni : Cu), and 2) a solution containing 70 ppm each of Mn, Zn, V, Pb, Cr, Co, and Al.

Fe Assay: An acetate buffer for the Fe assay was prepared with 15.0 g sodium acetate trihydrate and 11.75 mL glacial acetic acid in 50 mL water, resulting in a 6.3 M acetate solution of pH 4.5. Both 1,10-phenanthroline (8 mg/mL) and hydroxylamine (0.1 g/mL) were prepared as separate solutions, each in the acetate buffer. The μ PAD was prepared for detection of Fe by first adding 1 μ L hydroxylamine solution to the detection reservoir, which was enough volume to spread solution into the channel reservoir. After this solution had dried, 0.35 μ L of poly(acrylic acid) (0.7 mg/mL) was added to the detection reservoir, followed by two 0.4 μ L aliquots of 1,10-phenanthroline also in the detection reservoir. The device was allowed to dry completely between each addition of reagent.

Ni Assay: A 60 mM solution of dimethylglyoxime (dmg) was prepared in methanol. The μ PAD was prepared for detection of Ni by five 0.4 μ L aliquots of dmg to the detection reservoir, followed by two 0.4 μ L aliquots of ammonium hydroxide (pH 9.5). The device was allowed to dry completely between each addition of reagent.

Cu Assay: A solution of 50 mg/mL bathocuproine (bc) with 40 mg/mL PEG 400 was prepared in chloroform. The μ PAD was prepared for detection of Cu by adding 1 μ L hydroxylamine (0.1 g/mL), followed by 0.5 μ L acetic acid/NaCl buffer (10 mM, pH 4.5) to the detection reservoir. Two 0.5 μ L aliquots of the bathocuproine/PEG solution were then added to the detection reservoir. The device was allowed to dry completely between each addition of reagent.

Addition of standard samples: Standard solutions were added to the μ PAD using the following method. Solutions were first pipetted onto 10 mm punches of Whatman 1 filter paper. After both the punches and the detection reservoirs on the device had dried, the punches were placed on top of the μ PAD sample reservoir. The punch and μ PAD were covered with a piece of polydimethylsiloxane (PDMS). This cover contained holes over the detection and sample reservoirs and helped to move sample evenly and efficiently down the flow channels by applying uniform pressure across the device.

Particulate metal collection and digestion

An industrial incineration ash sample (RTC-CRM012) certified for metals was purchased from LGC Standards (Teddington, UK). A suspension of 0.1% ash in water

was prepared and nebulized into 0.8 m³ aerosol chamber. The average concentration in the chamber, as measured by an aerosol photometer (TSI, Model 8250), was 3.2 mg m⁻³. A sequential mobility particle sizer (Grimm, SMPS+C) and an aerosol particle sizer (TSI, Model 3321) monitored the aerosol size distribution. The aerosol size distribution was approximately lognormal with mean = 0.056 μm and geometric standard deviation (GSD) = 1.41. Aerosolized ash sample was then collected onto Whatman 1 filters (47 mm diameter) at an air flow rate of 10 L/min for 4 hrs, yielding 0.2 mg ash per cm² on the filter. Following sample collection, 10 mm diameter punches were taken from the collection filters using a biopsy punch. Microwave-assisted acid digestion of particulate metal samples was carried out by adding 5 μL concentrated nitric acid, followed by 30 μL water to the filter punches. The punches were then placed in a household microwave oven (1,100 Watts) on high power for a total of 45 s. The microwave was stopped every 15 s and an additional 30 μL water was added to punches to promote continued digestion. Finally, 8 μL of sodium bicarbonate (0.5 M) was added to neutralize the acid on the filter punches, which were then transferred to the μPAD by the method described above.

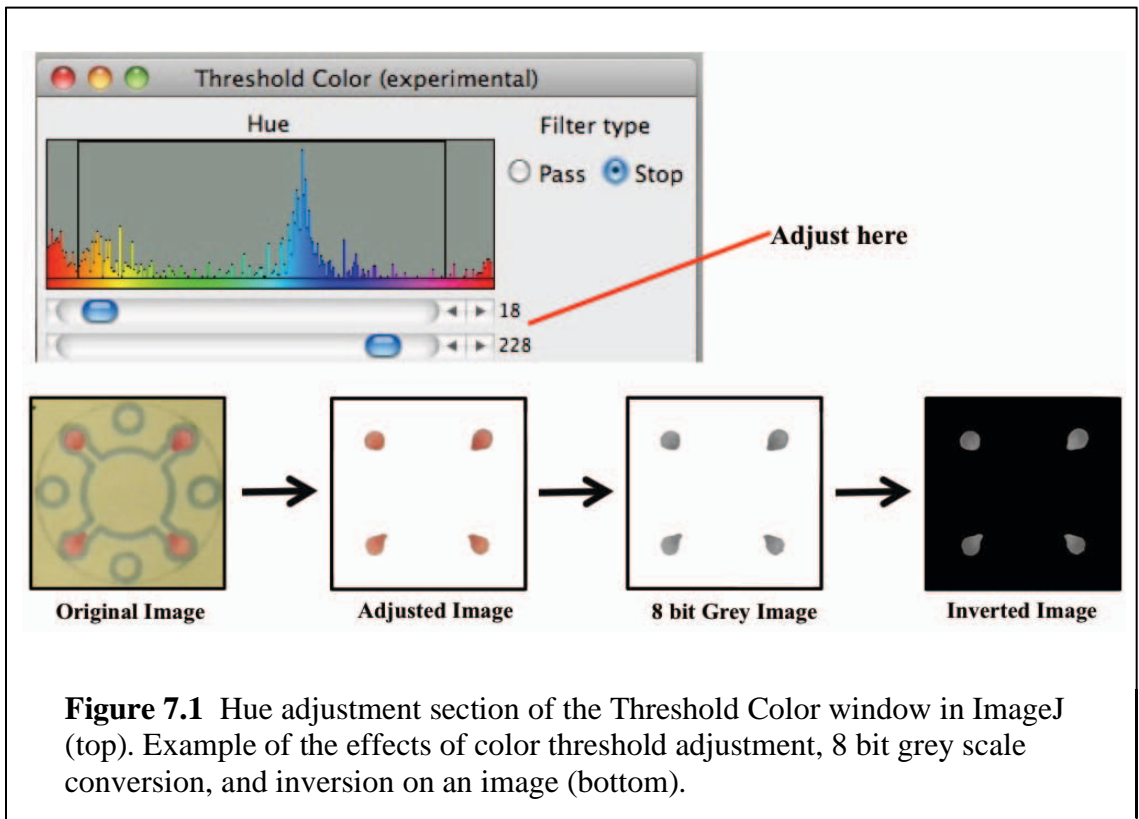
Quantitative Image Processing

Images of the paper devices were scanned (XEROX DocuMate 3220) and stored in JPEG format at 300 dpi. Average grey intensity of color formation at the detection reservoirs was measured using the public domain software ImageJ (National Institutes of Health). This process is described in detail here:

JPEG images were opened with ImageJ in RGB color format. Adjustment of the color threshold was achieved as follows:

1. The “Color Threshold” window is accessed through the ImageJ menu by selecting “Image” → “Adjust” → “Color Threshold.”
2. At the bottom of this window HSB is selected, which allows adjustment of hue, saturation, and brightness.
3. The hue was adjusted by moving the sliders directly below the “Hue” spectrum until only the color of interest is visible (Figure 7.1).

Images were then converted to 8-bit grey scale (“Image” → “Type” → “8-bit”) and inverted (“Edit” → “Invert”) so that intensity measurements yield a positive slope when plotted versus metal amounts. Images of a single device at each step of the processing are shown in Figure 7.1.



The mean grey value was measured by first selecting “mean grey value” and “limit to threshold” in the “Set measurements window,” found from the ImageJ menu by selecting “Analyze” → “Set measurements”. Each area to be measured was selected using the wand tool, which automatically finds the edge of an object and traces its shape. Grey intensity of the outlined area is measured selecting “Analyze” → “Measure.”

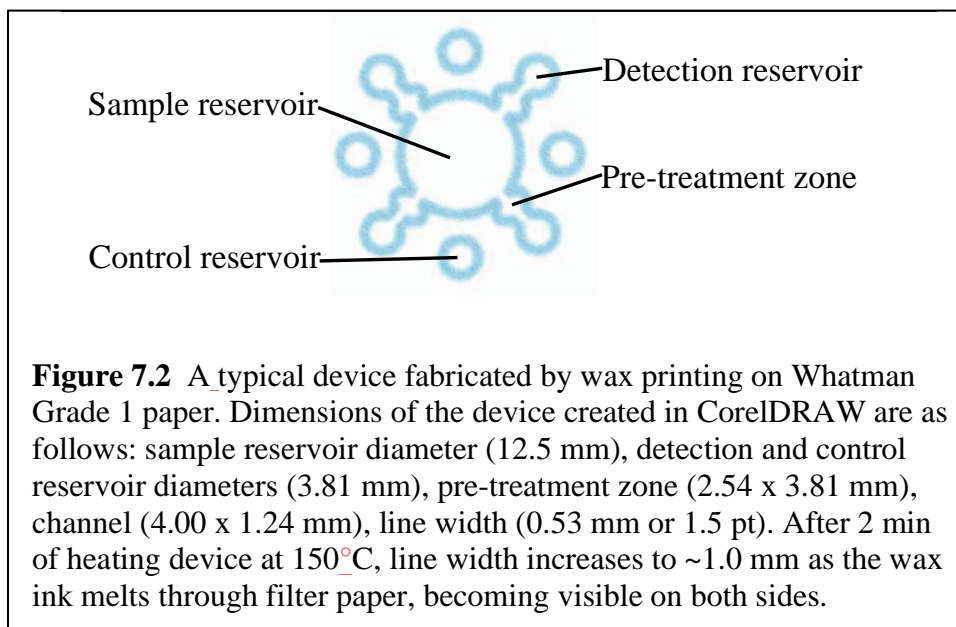
Once optimized, the threshold ranges set for each assay were fixed as follows: Fe (18-255), Ni (10-210), Cu (38-255). Data were imported into ORIGIN for subsequent analysis.

7.3 Results and Discussion

Device design

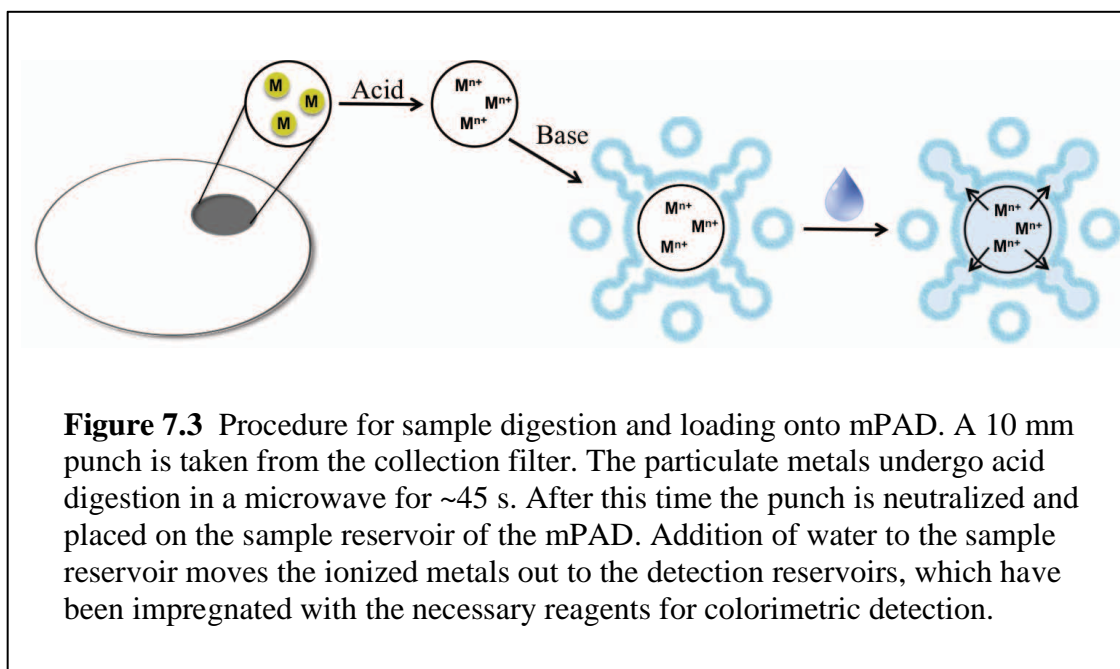
One advantage of μ PADs is the ability to store reagents at various points along the flow channels to carry out different chemistries on samples. Here, reagents, buffers, and surface modifiers were impregnated into specific areas of the paper device, creating zones where metal samples can be pre-treated prior to detection. Thus, despite the unique set of conditions required by each colorimetric assay, multiplexed detection can be carried out on a single μ PAD. The mPAD design (Figure 7.2) includes a central sample reservoir surrounded by four channels that lead to detection reservoirs. The channels also contain pre-treatment zones that can be used for the addition of reagents needed to either oxidize/reduce metals or to complex metals that interfere with a specific assay. An elliptical shape was used for this zone so that sufficient volumes of reagents could be added without leaking into the detection or sample reservoirs. By impregnating the pretreatment zones with masking agents and/or reductants as needed, interfering metals

were complexed and analytes were reduced to the appropriate oxidation state before sample reached the detection reservoirs. Additionally, polyelectrolytes were used when needed to modify the surface of the detection reservoirs. Depending on their properties, they served either to slow mobility of the fast moving colored product, or to increase hydrophilicity in the reservoir when a hydrophobic reagent had been applied.



Generally, a sample can be loaded directly onto the center of the μ PAD; however, this application requires digestion of particulate metals prior to detection. Rather than employ conventional methods of acid digestion, which dilute the sample and can be time consuming, acid digestion of particulate metals was accomplished directly on the air sampling filter after collection. It was initially intended that the μ PADs would be placed within the air sampler itself, so that metals could be collected directly onto the center reservoir and subsequently digested and detected. Acid digestion could not be carried out directly on the device, however, due to acidic fumes that drastically lowered the pH in the

detection reservoirs. Instead, a method was developed in which the acid digestion is carried out on punches taken from a collection filter. Punches are then placed on the center reservoir and sample is transferred from the filter punch to the device upon the addition of the PDMS lid and water. A schematic of this process is illustrated in Figure 7.3. Two other benefits were gained by this modification. Because air no longer had to be drawn through the device's sample reservoir to collect particulates, a smaller reservoir could be used. Sample detection limits were greatly lowered with a smaller sample reservoir due to more efficient movement of sample into the detection reservoir; less sample is lost to the paper when travel distances are shorter. In addition, because filter punches are used, virtually any filter-based air sampling device can be coupled to μ PAD detection, affording this technology wider application.



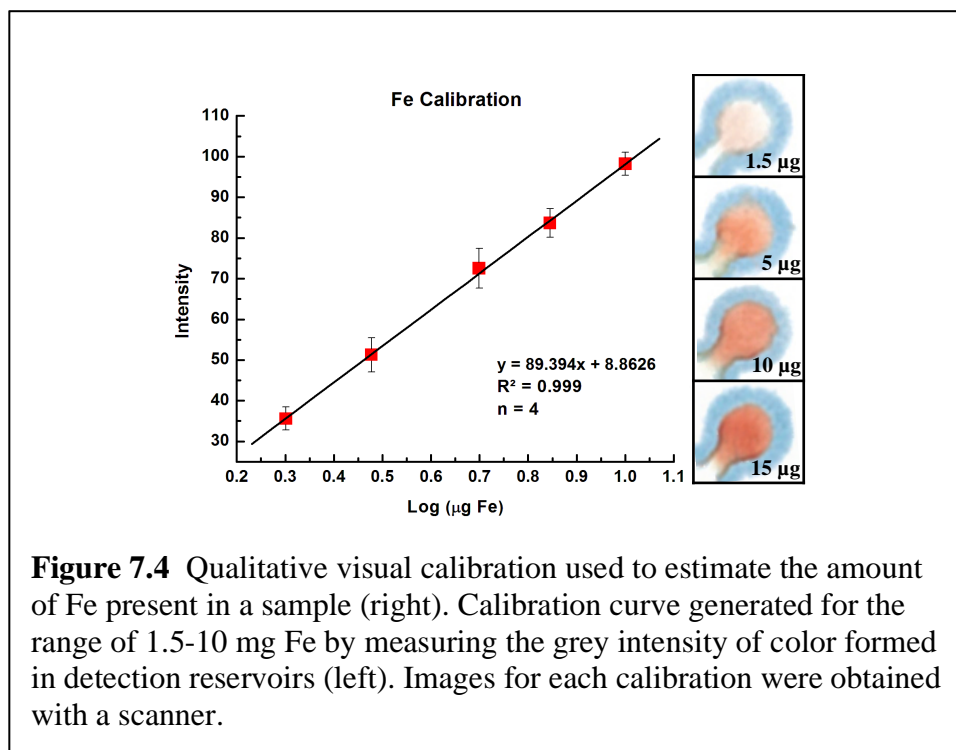
Control reservoirs are present on the device so that any colored compounds are not confused as product. These reservoirs are only needed as a visual control, however,

because the color threshold adjustment performed with the imaging software filters out unwanted color in the detection zone. Of course, this technique is successful as long as the reagent color does not mask the final product or have the same hue as the product. The wax ink used to define the borders and flow channels of the μ PAD contains a light blue dye, as the hue of this printed color is far different from the hue of the pinks and oranges produced in the assays.

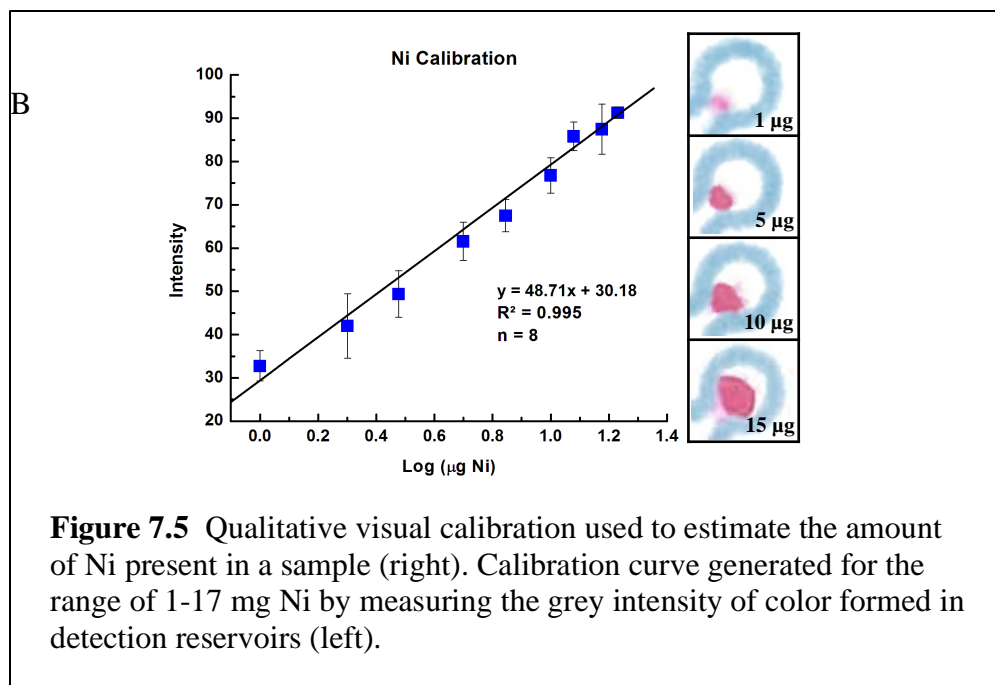
Colorimetric Assays

Fe was determined through detection of the red/orange ferrioxalate complex $[\text{Fe}(\text{phen})_3]^{2+}$ formed by the reaction of Fe(II) with 1,10-phenanthroline.²⁶ The presence of hydroxylamine on the device serves two purposes: 1) reducing Fe(III) to Fe(II), and 2) hydroxylamine acts as a masking agent by complexing possible interfering metals Ni, Zn, Cd, and Co.²⁷ However, the mobility of $[\text{Fe}(\text{phen})_3]^{2+}$ in paper was so high that it caused the colored product to move completely to the edge of the detection reservoirs, making quantitative analysis problematic. To solve this problem, the detection reservoir was coated with poly(acrylic acid) prior to addition of all reagent and buffer solutions. Poly(acrylic acid) has low mobility in paper, and its negative charges serve to keep the positively-charged complexation product from moving once formed. Both qualitative and quantitative calibrations for Fe are shown in Figure 7.4. The lowest amount of Fe on the filter punch that could be detected reproducibly was 1.5 μg , and the linear range was determined to be 1.5 – 10 μg Fe. Above the upper limit, the product begins to saturate the surface and the signal intensity does not increase linearly with concentration. Above 20 μg , no change in signal intensity was seen. Besides quantification, the Fe assay can

sometimes be useful as a control for the device. In many of the work environments at risk for high concentrations of particulate metals, levels of aerosolized Fe are quite high relative to other metal constituents; therefore, a negative result for Fe could indicate a faulty device.



Dimethylglyoxime (dmg), used for the detection of Ni, produces a bright pink Ni(II) complex.²⁸⁻³⁰ An ammonium hydroxide solution (pH 9.5) dried onto to the detection reservoir was effective at keeping the optimal pH of ~9 for the assay.²⁸ Qualitative and quantitative calibrations for Ni are shown in Figure 7.5. Amounts as low as 1 µg were detected reproducibly on the filter punch, with a linear range of 1 – 17 µg. The signal intensity was completely saturated above 20 µg.



Bathocuproine (bc), which forms an orange complex with Cu(I), was chosen for detection of Cu because it does not complex Fe and is the most sensitive of all the cuproines commonly used for Cu detection.^{31,32} Hydroxylamine was added to the pretreatment and detection zones for reduction of Cu^{2+} to Cu^+ .³³ A 10 mM acetic acid/NaCl buffer (pH 4.5) was used to set the pH at the detection reservoir and also because the Cl^- ion stabilizes the orange $\text{Cu}(\text{bc})_2$ complex.³⁴ The hydrophobicity of bathocuproine initially caused a problem, as it blocked aqueous sample from entering the detection reservoir. This issue was overcome by adding polyethylene glycol (PEG) to the bathocuproine solution. The presence of dried PEG on the device reduced the hydrophobicity in the detection reservoir caused by the bathocuproine and allowed sample to flow into the reservoir. The qualitative and quantitative calibrations for Cu are shown in Figure 7.6. This assay allowed for reproducible detection of Cu as low as 1 μg ,

with a linear range of 1 – 15 μg . The signal intensity was completely saturated above 17 μg .

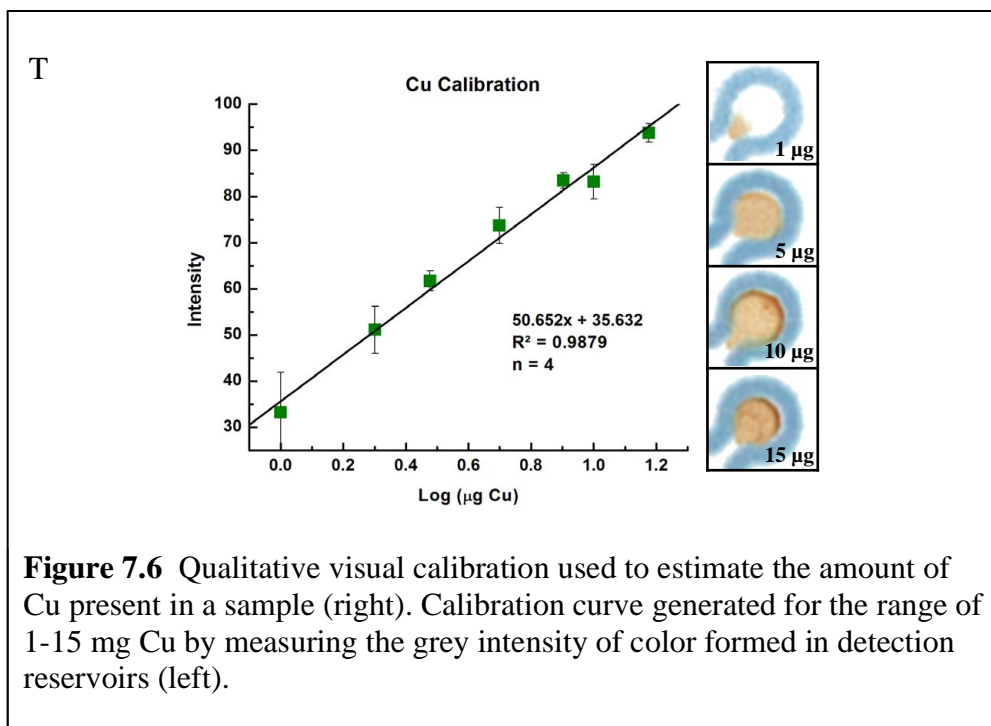


Table 7.1 demonstrates how the minimum detectable levels reported here compare to the permissible exposure limits (PELs) set by the Occupational Safety and Health Administration (OSHA).¹⁰ To allow for direct comparison, minimum detectable limit values are shown as a time weighted average (TWA) for an 8-hour workday, at a collection rate of 4 L/min. This is the collection rate commonly used for exposure assessment, as it is a mimic of human breath rate. With the detection limits reported for Fe and Ni, levels more than 100X less than the PELs set by OSHA were detectable with the μPAD . Likewise, the Cu detection limit results in detectable levels ~16X less,

proving that this method would be sensitive enough for assessing unsafe particulate metal exposure.

Table 7.1 A comparison between the minimal detectable levels and permissible exposure limits set by OSHA. Time weighted averages of minimum detectable levels are based on a 4 L/min collection rate.

Metal	μPAD Detection Limits		OSHA 8-hr PEL ^{††}
	MDL (μg) [†]	TWA (μg/m ³) [‡]	(μg/m ³)
Fe	1.5	9	1,000
Ni	1	6	1,000
Cu	1	6	100

[†] MDL – Minimum detectable level for a 10mm filter punch.

[‡] TWA – Minimum detectable air concentrations as an 8-hour time-weighted average

^{††} PEL – Permissible Exposure Limit, based on an 8-hr sample

The qualitative calibrations for each metal show an obvious difference in color intensity and/or area of color between each 5μg increment. Using the calibration images as a reference, metal amounts can be estimated within about 5 μg if within the linear range. This qualitative analysis would obviously not suffice for an assessment report; however, it could immediately reveal unsafe levels of particulate metal. In the following discussion of standard samples, quantitative measurements are used to show agreement with actual metal amounts, but it can also be seen that the intensities and areas of the colors in the detection reservoirs remain consistent with the qualitative calibrations.

To evaluate potential interferences from other metals, Fe, Ni, and Cu were each determined in the presence of Mn, Zn, V, Pb, Cr, Co, and Al. These metals were chosen because they are likely to be present in occupational settings.³⁵⁻³⁷ For these assays,

solutions containing all of the aforementioned metals were pipetted onto filter punches. Initially, these assays were carried out with equal amounts of Fe, Ni, and Cu, and the ratio of each of these three metals to the other seven interfering metals was 10:1. It was found that when equal amounts of Cu and Ni were present, Cu interfered with the Ni assay by increasing its color intensity. Samples containing Cu at a ratio of 1:4 with Fe and Ni, however, showed no interference to the Ni assay. This specific multiplexed set of assays, therefore, would be most suitable in occupational environments where Ni is more abundant in the air than Cu. This limitation acknowledged, we are currently working to address this shortcoming with additional complexation agents. For this study, 2.5 and 5.0 μg of Fe and Ni were each determined from a solution comprised of equal amounts of Fe and Ni, 4X less Cu, and 10X less of each of the interfering metals. Detection of 5.0 μg Fe and Ni from this study is shown in Figure 7.7a. When the effects of other metals were studied for the Cu assay, the analyte solution still contained 4X more Fe and Ni than Cu, but the amount of the seven other metals was 10X less than that of Cu. The quantitative results in Table 7.2 show that the measured values for detection of 2.5 and 5.0 μg of each of the three metals agree with the actual values, with errors ranging from 0.2 – 0.5 μg .

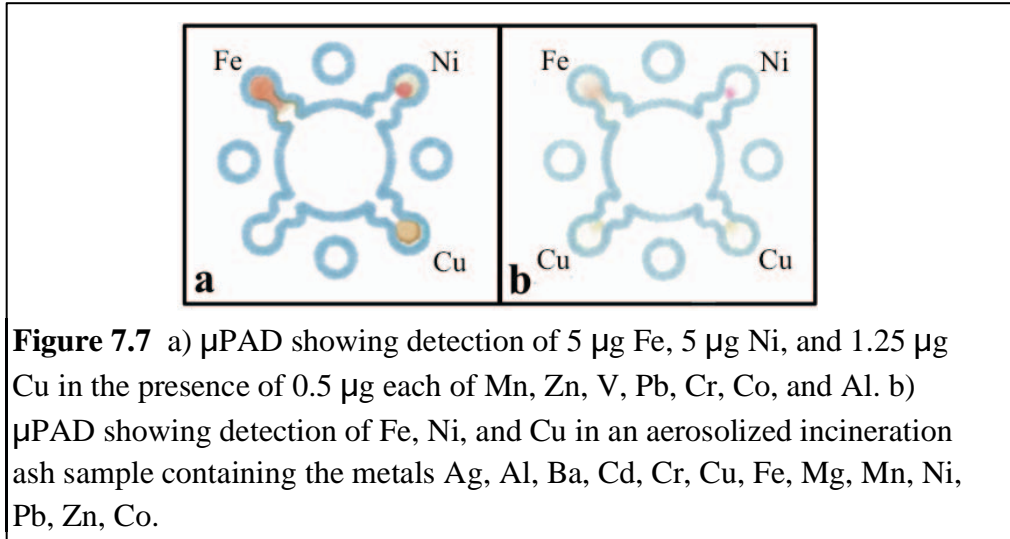


Table 7.2 Actual and measure amounts of Fe, Ni, and Cu present in standard solutions also containing levels 10 x less of the metals Al, Cr, Co, Pb, Zn, Mn, and V.

Metal	Actual (ug)	Measured (μ g) n = 4
Fe	2.5	2.6 \pm 0.3
	5	5.2 \pm 0.3
Ni	2.5	2.4 \pm 0.4
	5	5.4 \pm 0.3
Cu	2.5	2.6 \pm 0.2
	5	5.4 \pm 0.5

An incineration ash sample, certified for the metals Ag, Al, Ba, Cd, Cr, Cu, Fe, Mg, Mn, Ni, Pb, Zn, Co and V, was purchased to simulate a real sample. The sample was aerosolized in a chamber and collected onto Whatman 1 filters over a 4 hour period. Acid digestion was carried out on 10 mm punches taken from the filters, and determination of Fe and Ni was accomplished on the μ PAD (Figure 7.7b). Copper levels in the sample were too low to detect; however, they fall well below limits set for exposure, as discussed

below. Agreement between actual and measured values is shown in Table 7.3 and proves that the acid digestion method is effective in completely digesting particulate metals and that detection without interference is possible with more complex samples.

Table 7.3 Actual and measured levels of Fe, Ni, and Cu from a filter sample of re-suspended incineration ash. Measured values represent metal present on 10 mm punches taken from the collection filter.

Metal	10 mm Punch	
	Actual (ug)	Measured (µg)
Fe	2.58	2.3 ± 0.6 (n=5)
Ni	1.2	1.0 ± 0.4 (n=5)
Cu	0.27	Too low

7.4 Conclusion

The µPAD developed here provides an inexpensive way to assess occupational exposure to particulate metals. With this on-site method, unsafe metal levels can be determined almost immediately following sample collection, unlike the current method in which workers may be exposed to dangerous levels for several weeks before they are notified. The digestion of sample without dilution permitted metal detection at levels well below those allowed by OSHA, which indicates that shorter collection times can be performed to study task-specific exposures. Moreover, with the existence of colorimetric assays for a wide variety of metals, the µPADs can be tailored for specific work environments. While only detection of Fe, Ni and Cu was discussed here, the device can easily be modified to accommodate detection of other metals. Also, individual assays can often be optimized to eliminate specific interferences that are known to exist at high levels in a particular work environment.

7.5 References

- (1) Leigh, J. P. M., S. B.; Fahs, M. , *Costs of Occupational Injuries and Illnesses*. University of Michigan Press.: Ann Arbor, MI, **2000**.
- (2) Leigh, J. P. e. a., Costs of occupational COPD and asthma. *Chest* **2002**, *121* (1), 264-272.
- (3) Nelson, D. I. e. a., The global burden of selected occupational diseases and injury risks: Methodology and summary. *Am. J. Ind. Med* **2005**, *48* (6), 400-418.
- (4) BLS *Bureau of Labor Statistics National Employment Matrix*. ; **2008**.
- (5) Liu, J. G., R. A.; Waalkes, M. P. , Toxic Effects of Metals (7th Edition). In *Casarett and Doull's Toxicology*, Klaassen, C. D., Ed. McGraw-Hill: **2007**.
- (6) Chang, C.-C.; Hwang, J.-S.; Chan, C.-C.; Wang, P.-Y.; Hu, T.-H.; Cheng, T.-J., Effects of Concentrated Ambient Particles on Heart Rate Variability in Spontaneously Hypertensive Rats. *Journal of Occupational Health* **2005**, *47* (6), 471-480.
- (7) Chen, L. C.; Hwang, J.-S., Effects of Subchronic Exposures to Concentrated Ambient Particles (CAPs) in Mice: IV. Characterization of Acute and Chronic Effects of Ambient Air Fine Particulate Matter Exposures on Heart-Rate Variability. *Inhalation Toxicology* **2005**, *17* (4-5), 209-216.
- (8) Coyle, Y. M.; Minahjuddin, A. T.; Hynana, L. S.; Minna, J. D., An ecological study of the association of metal air pollutants with lung cancer incidence in Texas. *Journal of Thoracic Oncology* **2006**, *1* (7), 654-661.
- (9) Franklin, M.; Koutrakis, P.; Schwartz, P., The role of particle composition on the association between PM_{2.5} and mortality. *Epidemiology* **2008**, *19* (5), 680-689.
- (10) Wild, P.; Bourgard, E.; Paris, C., Lung cancer and exposure to metals: the epidemiological evidence. *Methods in Molecular Biology* **2009**, *472*, 139-167.
- (11) Vincent, J. H. e. a., Application of Recent Advances in Aerosol Sampling Science Towards the Development of Improved Sampling Devices: The Way Ahead. *Journal of Environmental Monitoring* **1999**, *1*, 285-292.
- (12) Ashley, K.; Howe, A. M.; Demange, M., Sampling and analysis considerations for the determinatin of hexavalent chromium in workplace air. *Journal of Environmental Monitoring* **2003**, *5*.
- (13) Harper, M., A review of workplace aerosol sampling procedures and their relevance to the assessment of beryllium exposures. *Journal of Environmental Monitoring* **2006**, *8*, 598-604.
- (14) Profile of the Iron and Steel Industry. In *EPA sector notebooks [electronic resource]*, United States. Environmental Protection Agency, E.; Compliance, A., Eds. EPA: Washington, DC **1995**.
- (15) Martinez, A. W.; Phillips, S. T.; Butte, M. J.; Whitesides, G. M., Patterned Paper as a Platform for Inexpensive, Low-Volume, Portable Bioassays. *Angewandte Chemie International Edition* **2007**, *46* (8), 1318-1320.
- (16) Bruzewicz, D. A.; Reches, M.; Whitesides, G. M., Low-Cost Printing of Poly(dimethylsiloxane) Barriers To Define Microchannels in Paper. *Analytical Chemistry* **2008**, *80* (9), 3387-3392.
- (17) Martinez, A. W. P., S. T.; Whitesides, G. M., Three-dimensional microfluidic devices fabricated in layered paper and tape. *PNAS* **2008**, *105* (50), 19606-19611.

- (18) Zhao, W.; Ali, M. M.; Aguirre, S. D.; Brook, M. A.; Li, Y., Paper-Based Bioassays Using Gold Nanoparticle Colorimetric Probes. *Analytical Chemistry* **2008**, *80* (22), 8431-8437.
- (19) Abe, K.; Suzuki, K.; Citterio, D., Inkjet-Printed Microfluidic Multianalyte Chemical Sensing Paper. *Analytical Chemistry* **2008**, *80* (18), 6928-6934.
- (20) Carrilho, E.; Martinez, A. W.; Whitesides, G. M., Understanding Wax Printing: A Simple Micropatterning Process for Paper-Based Microfluidics. *Analytical Chemistry* **2009**, *81* (16), 7091-7095.
- (21) Lu, Y.; Shi, W.; Jiang, L.; Qin, J.; Lin, B., Rapid prototyping of paper-based microfluidics with wax for low-cost, portable bioassay. *ELECTROPHORESIS* **2009**, *30* (9), 1497-1500.
- (22) Klasner, S.; Price, A.; Hoeman, K.; Wilson, R.; Bell, K.; Culbertson, C., Paper-based microfluidic devices for analysis of clinically relevant analytes present in urine and saliva. *Analytical and Bioanalytical Chemistry* **2010**, *397* (5), 1821-1829.
- (23) Li, X.; Tian, J.; Shen, W., Quantitative biomarker assay with microfluidic paper-based analytical devices. *Analytical and Bioanalytical Chemistry* **2010**, *396* (1), 495-501.
- (24) Wang, W.; Wu, W.-Y.; Zhu, J.-J., Tree-shaped paper strip for semiquantitative colorimetric detection of protein with self-calibration. *Journal of Chromatography A* **2010**, *1217* (24), 3896-3899.
- (25) Apilux, A.; Dungchai, W.; Siangproh, W.; Praphairaksit, N.; Henry, C. S.; Chailapakul, O., Lab-on-Paper with Dual Electrochemical/Colorimetric Detection for Simultaneous Determination of Gold and Iron. *Analytical Chemistry* **2010**, *82* (5), 1727-1732.
- (26) Brandt, W. W.; Dwyer, F. P.; Gyarfás, E. D., Chelate Complexes of 1,10-Phenanthroline and Related Compounds. *Chemical Reviews* **1954**, *54* (6), 959-1017.
- (27) Hughes, M. N.; Shrimanker, K., Metal complexes of hydroxylamine. *Inorganica Chimica Acta* **1976**, *18* (0), 69-76.
- (28) Gazda, D. B.; Fritz, J. S.; Porter, M. D., Determination of nickel(II) as the nickel dimethylglyoxime complex using colorimetric solid phase extraction. *Analytica Chimica Acta* **2004**, *508* (1), 53-59.
- (29) Bambenek, M. A.; Pflaum, R. T., The Reaction of Nickel with Dioximes. *Inorganic Chemistry* **1963**, *2* (2), 289-292.
- (30) Booth, E.; Strickland, J. D. H., The Compounds Formed between Nickel(II) and Dimethylglyoxime by Alkaline Oxidation. *Journal of the American Chemical Society* **1953**, *75* (12), 3017-3019.
- (31) Smith, G. F.; Wilkins, D. H., New Colorimetric Reagent Specific for Copper. *Analytical Chemistry* **1953**, *25* (3), 510-511.
- (32) Penner, E. M.; Inman, W. R., Determination of nickel in high-purity niobium, tantalum, molybdenum and tungsten metals by chloroform extraction of nickel(III) dimethylglyoximate. *Talanta* **1963**, *10* (9), 997-1003.
- (33) Bjorklund, L. B.; Morrison, G. M., Determination of copper speciation in freshwater samples through SPE-spectrophotometry. *Analytica Chimica Acta* **1997**, *343* (3), 259-266.

- (34) Hulthe, P., A bathocuproine reagent-paper for the rapid semi-quantitative determination of copper in the 1 to 70 p.p.m. range. *Analyst* **1970**, 95 (1129), 351-355.
- (35) Smodis, B.; Davidsson, L.; International Atomic Energy, A., *Assessment of levels and "health-effects" of airborne particulate matter in mining, metal refining and metal working industries using nuclear and related analytical techniques*. International Atomic Energy Agency: Vienna, **2008**.
- (36) De Barros Carreira Menezes, M. A.; Pereira Maia, E. C.; De V. S. Sabino, C.; Batista, J. R.; Neves, O. F.; Albinati, C.; Filho, S. S.; De M. Mattos, S. V., Workplace and Occupational Health The First Metal Evaluation Using Nuclear and Analytical Techniques in the State of Minas Gerais-Brazil. In *Assessment of Levels and "Health-Effects" of Airborne Particulate Matter in Mining, Metal Refining, and Metal Working Industries Using Nuclear and Related Analytical Techniques*, Agency, I. A. E., Ed. International Atomic Energy Agency: Vienna, Austria, **2008**; pp 17-40.
- (37) Estokova, A.; Stevulova, N.; Kubinocova, L., Particulate Matter Investigation In Indoor Environment. *Global NEST Journal* **2010**, 12 (1), 20-26.

CHAPTER 8: CONCLUSION AND FUTURE DIRECTIONS

8.1 Conclusions

The work presented in this doctoral dissertation only begins to demonstrate how vastly diverse the field of microfluidics can be. While the two devices described here were both utilized for measurement of aerosol components, the differences in complexity, capability, and cost are evident. A PDMS device developed for quantification of cations and anions in atmospheric aerosols was capable of performing CE separations and conductivity detection while sampling from a continuous flow. This is one of the few examples of a microfluidic device used for aerosol analysis, and is the only example of an MCE device interfaced to a continuous flow aerosol sampler. Microfluidic devices made with PDMS or similar plastic materials achieve advanced separations through CE, and can incorporate components such as valves, pumps, and mixers, which expand their utility. There are some disadvantages to using PDMS-type microchips, however. Additional equipment in the form of power supplies, detectors, amplifiers, and computers is most often required, which decreases their portability and increases their expense. Moreover, the fabrication is more involved; thus, reliable devices can be difficult to construct without the proper manufacturing facilities.

It seems that the disadvantages often encountered in using PDMS devices make evident the benefits provided by paper-based devices, though the converse to this is also true. In the work presented in Chapter 7, a microfluidic paper-based device was

presented for quick and simple detection of particulate metals in occupational settings. Colorimetric assays with minimal susceptibility to interference were developed and employed on this μ PAD. An efficient sample digestion technique carried out directly on a filter was created, eliminating the sample dilution that typically accompanies digestion of the entire filter. Due to the advantages of low cost and simple fabrication and operation, paper-based devices have the potential to be used by a broad range of populations, including those of developing countries. Furthermore, these advantages will make it easier for paper-based devices to be brought to a commercial market. They can in no way replace the more complex PDMS devices, however. Separation capabilities on paper are very limited compared to what can be achieved with PDMS devices. The methods of detection that can be employed on paper are limited as well. Given that the advantages and disadvantages possessed by each type of device seem to be mirror images of one another, the choice between “paper or plastic” is entirely dictated by the application.

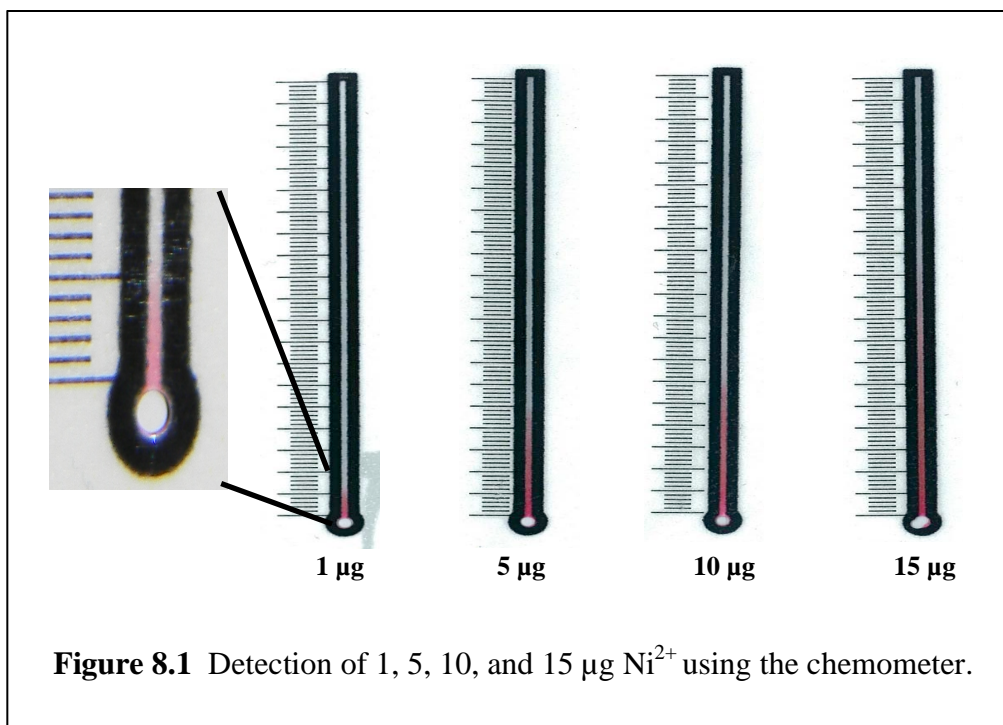
The capabilities offered by microfluidic technology have led to its exploitation in a broad range of fields. It remains a prominent, fast-moving area of research, continually finding use in new applications. Despite its many advantages, however, microfluidic technology is still at an early stage of development and requires further improvements before it can become more widely available to the public. While it has not yet lived up to the hype generated at its conception, the fundamentals of the field are strong and the proven potential is motivation for further development of microfluidic technology.

8.2 Future Directions

The work accomplished regarding paper-based assays and device development in this dissertation has helped lead to the development of several new projects involving

detection on paper substrates. Work on detection of particulate metals for occupational exposure assessment is being continued, and moving in several directions. The obvious next steps are the development of additional colorimetric metal assays for use on the current device, and further validation of the method through field studies. Samples will be collected in an occupational environment known to generate particulate metals, and measurements achieved using the μ PAD will be compared to results from ICP-AES analysis of the same filter samples. Once established as a reliable method for exposure assessment, the combination of assays on a device can be tailored to meet more specific needs of various work sectors.

A novel μ PAD, referred to as the chemometer, has been developed and is also being considered for measurement of particulate metals. This paper-based device, shown in Figure 8.1, also employs colorimetric detection but provides an even simpler method of quantification. Reagents are evenly applied along the length of the paper channel and allowed to dry. When an aqueous analyte solution is added to the sample reservoir it will move up this channel, forming a colored product. The analyte will continue to react with the colorimetric reagent until it has been diminished in the sample solution. With this technique, level of analyte is quantified by the length of color formed in the channel. Figure 8.1 demonstrates detection of 1, 5, 10, and 15 μg of Ni^{2+} .



Paper-based devices capable of electrochemical detection are being developed, and these are also likely to be used for metal detection. Incorporating both colorimetric and electrochemical detection on a single device allow for detection of metals and other analytes that can not be reliably quantified colorimetrically.

Use of paper substrates in the Henry lab is not being limited to metal detection. One of the first paper-based assays developed was for detection of the pathogen, *Listeria monocytogenes*. This project was taken over by Jana Jokerst and has yielded a publication and become the basis of a startup company. The example shown in Chapter 7 demonstrating collection filters used as a sample system is also being applied for analysis of dried blood spots by a PDMS microchip. It is likely that the list of applications for paper-based devices will continue to grow in the Henry lab, as so far their use has yielded at least two very successful projects and paper is never hard to come by.

APPENDIX 1: ORIGINAL PROPOSAL

Au-Based Nanoreactors for the Oxidation of Carbon Monoxide

Abstract

Oxide-supported Au nanoparticles have been shown to be promising low-temperature oxidation catalysts, particularly for removal of carbon monoxide (CO) in various commercial applications. The development of a superior catalyst for CO oxidation by exploiting the catalytic properties of Au nanoparticles trapped within hollow nanocrystals is proposed here. Catalytic activity is expected to be improved, as 1) size of Au nanoparticles can be controlled and stabilized, 2) interactions between Au and the oxide support will be maximized, and 3) degradation of the catalyst through secondary reactions will be minimized. Nanoreactors will be prepared through the synthesis of Au nanoparticles isolated inside Co_3O_4 hollow nanospheres. Transmission electron microscopy (TEM) and x-ray diffraction (XRD) will be used for characterization of the nanoparticles at each synthetic step. Catalytic activity for CO oxidation will be studied in a fixed bed flow reactor, with the conversion of CO detected by gas chromatography (GC).

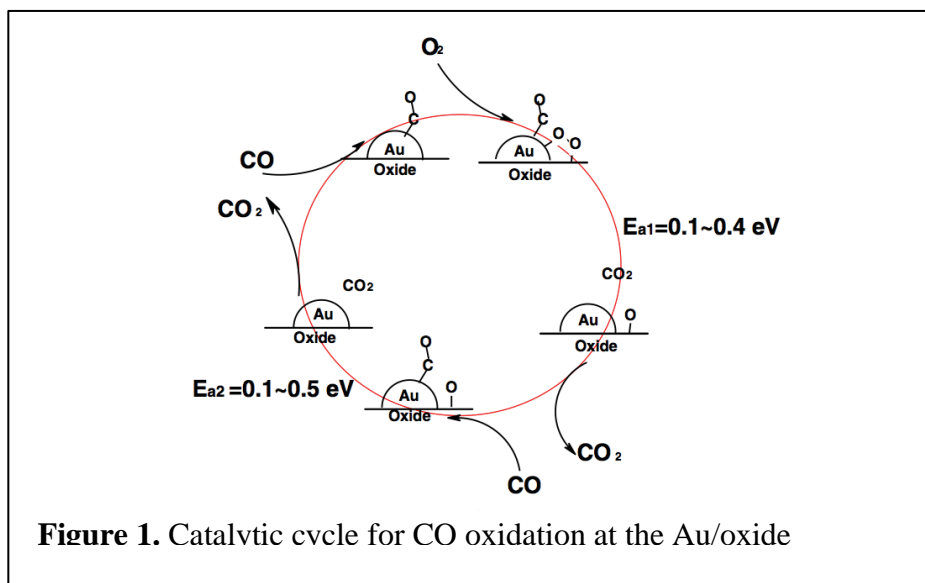
Introduction

Gold, which was once thought to have no catalytic activity due to its inertness, is now known to show high catalytic activity for certain oxidation reactions when it is in the

form of particles 2-5 nm in diameter.¹ Specifically, gold nanoparticles have been shown to effectively catalyze the oxidation of CO (Reaction 1) at ambient temperature, and its catalytic activity is greatly enhanced when deposited on a metal oxide support.^{2,3,4}



Since this discovery by Haruta *et al.*, there has been much debate over the mechanism by which CO is oxidized on Au-based catalysts.² More recently, CO oxidation over a Au/oxide catalyst has been generally understood to occur by the following mechanism: (i) CO adsorbs on dispersed gold clusters; (ii) O₂ adsorbs at the Au/oxide interface; (iii) CO reacts with O₂ to form CO₂, which then desorbs from the surface; (iv) the remaining O readily reacts with another adsorbed CO to complete the cycle.⁵ The catalytic cycle is shown in Figure 1, with activation energies determined for the CO + O₂ reaction by previous work.^{6,7,8}



Adsorption of molecules onto pure gold surfaces is rarely seen, except when gold is in the form of small clusters dispersed on an oxide support.⁹ It has been found that this is

largely due to the presence of a high concentration of low coordinated sites on the surface of very small particles (< 5 nm), especially at steps, edges, and corners of particles. Lower-coordinated gold atoms (coordination # < 8) decrease the adsorption energy, resulting in stronger bonding between CO and Au.^{10,11,8,11}

O₂ also prefers to bind at low-coordinated Au atoms; however, the binding energy of O₂ on Au clusters is weak relative to CO adsorption.⁶ It has been found that on reducible oxide supports, O₂ has a preference for binding at the Au/oxide interface.^{8,12,11} Stronger bonding of O₂ occurs here because the oxide support can induce a significant electron transfer from the Au atom to the 2- π antibonding states of O₂ that sit at the interface between the metals and the oxide.

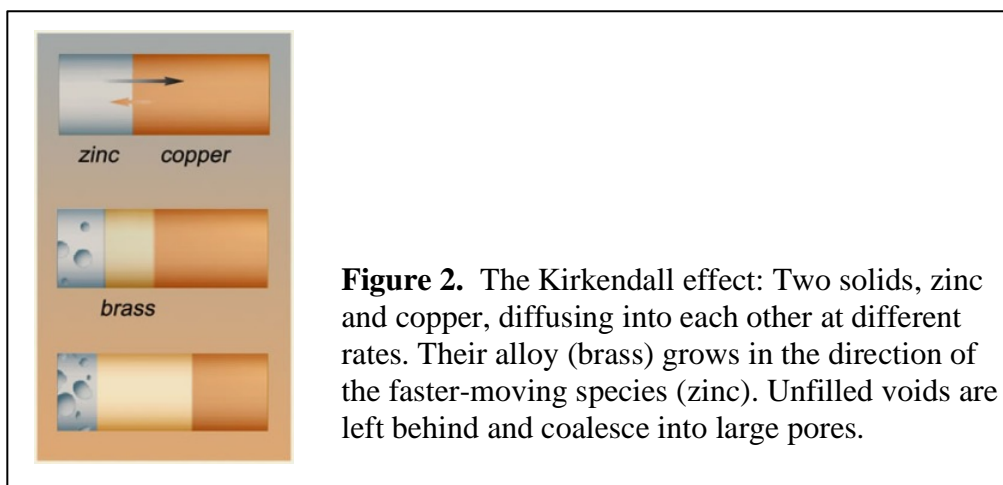
The electronic interactions between the support and Au also explain why Au supported on reducible oxides is more catalytically active than Au supported on irreducible oxides such as SiO₂ and MgO. Irreducible oxides are characterized by a large band gap that limits charge transfer to Au. Reducible oxides, characterized by small band gaps, promote charge transfer to Au so that deposited Au interacts more strongly with oxygen. This provides an ideal environment for O₂ activation and for oxidation reactions.¹³

As previously discussed, the catalytic properties of gold are affected not only by the type of oxide support used, but also depend greatly on the size of the particles.¹⁴ Au nanoparticles have a large surface energy and exhibit strong cohesion, making them highly likely to agglomerate, which would diminish their catalytic properties. In order to develop a superior catalyst for the oxidation of CO, it is therefore necessary that the size of the gold nanoparticles is controlled and stabilized, and that the possibility of

interaction between gold particles and their support is maximized. In order to satisfy both of these conditions, I am proposing the development of a nanoreactor for CO oxidation in which Au nanoparticles are isolated within hollow nanocrystals.

It is suggested here that isolating gold nanoparticles within hollow nanocrystals of reducible oxides will improve catalytic activity for the following reasons: 1) the size of the Au nanoparticles can be controlled and stabilized, 2) synergistic interactions between the gold and oxide support can be efficiently used, as each catalyst particle is in contact with a shell of the support material, and 3) any secondary reactions that degrade selectivity could be reduced.

Currently there are three ways in which hollow nanocrystals can be prepared. They can be synthesized with a surfactant present as a support, which is subsequently removed;¹⁵ or by sonochemical synthesis around a core, such as silica, which is then removed by acid etching.¹⁶ The method that will be employed here, however, is carried out by exploiting the Kirkendall Effect. This phenomenon occurs when the movement of the interface of a diffusion couple expands in the direction of the faster moving species, leaving behind voids that coalesce to form large cavities (Fig 2).¹⁷



The Kirkendall Effect can be initiated during synthesis to form uniform hollow nanocrystals, with cavity sizes that can be controlled by the proportions of the starting material. An important advantage to this synthetic method is its high yield, as it is a one pot process in which product is not lost through purification steps. It has been demonstrated that platinum catalyst particles can be isolated inside cobalt oxide nanocrystals and are able to effectively catalyze the reduction of ethylene to ethane with H₂, indicating that a route exists for small molecules to both enter and exit through a CoO shell.¹⁷

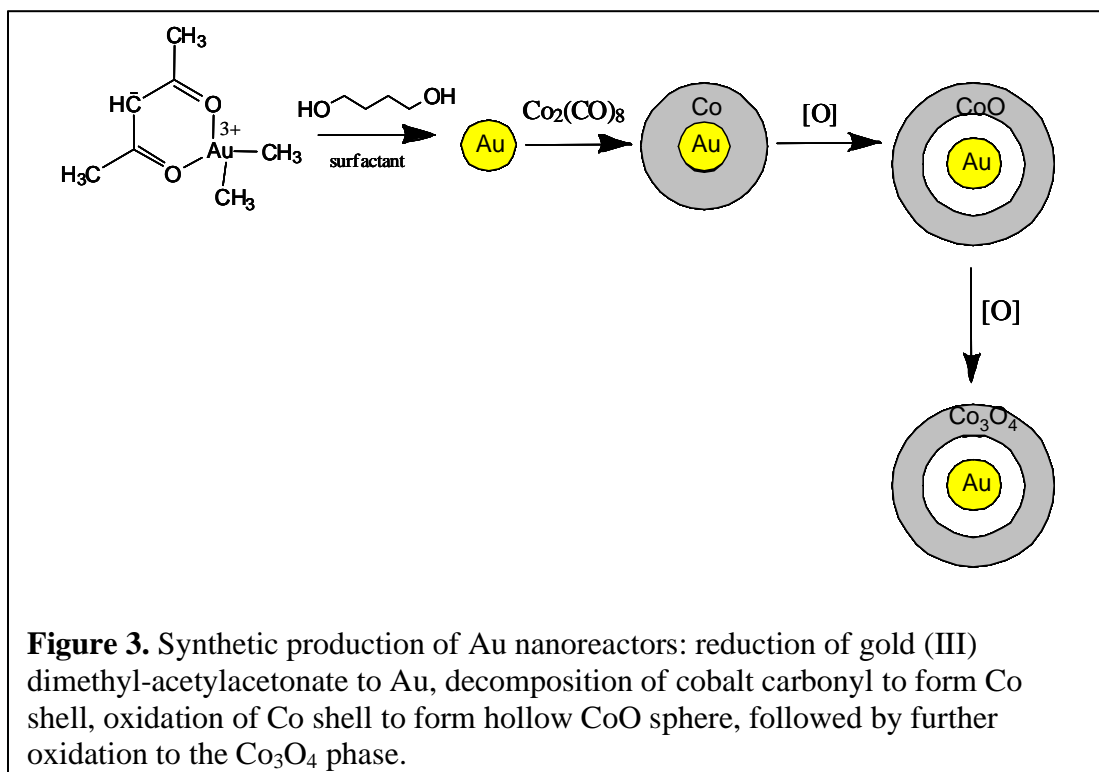
It is expected that gold particles isolated inside of Co₃O₄ shells would serve as nanoreactors that catalyze the oxidation of CO, and could be implemented in a variety of applications including CO removal in CO₂ lasers, CO gas sensors, air-purification devices for respiratory protection, and pollution control devices for removing CO from ambient air in submarines and space crafts on long duration missions.^{18,19,20,21,22}

Proposal

Synthesis of catalyst

Gold nanocrystals will be synthesized by a modified “polyol” process used by Sobal *et al.* to prepare platinum nanocrystals.²³ Briefly, gold (III) dimethyl-acetylacetonate is reduced with a long chain polyol to form a colloidal solution of uniform nanoparticles in the presence of surfactants such as oleic acid and oleylamine. The size of the gold particles can be tuned from 1-10 nm by varying the concentration of the surfactants. Cobalt carbonyl (Co₂(CO)₈) is then gradually added to the solution at 142 °C and decomposes to form a Co coating on the gold nanocrystals. The thickness of the coating

can be controlled by varying the amount of cobalt carbonyl. The Kirkendall Effect is then induced on the cobalt surface by blowing a stream of O_2/Ar through the colloidal solution of AuCo particles at $182\text{ }^\circ\text{C}$.² This synthetic process is demonstrated in the scheme shown in Figure 3.

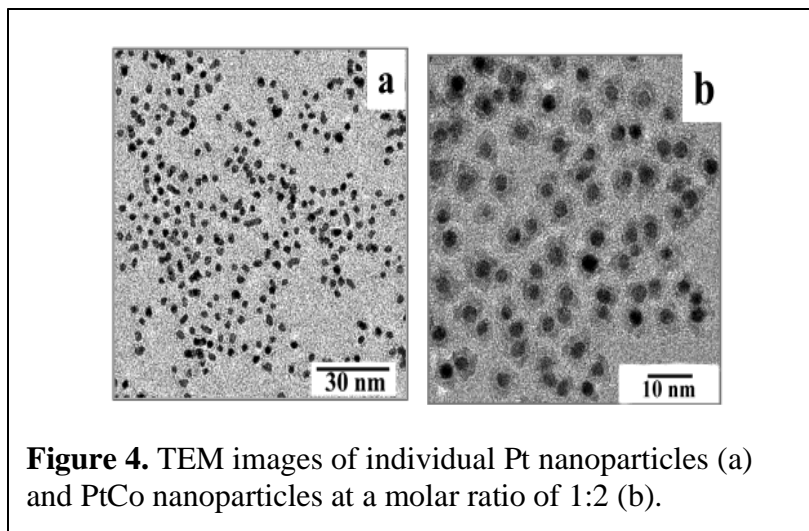


The CoO shell must be oxidized to obtain the desired Co_3O_4 , as this is the reducible cobalt oxide phase that yields enhanced catalytic activity. It was demonstrated by both Verelst *et al.* and Yeh *et al.* that oxidation to the spinel Co_3O_4 phase is favored over the CoO species as the temperature is raised. The temperature at which Co_3O_4 is favored is seen to increase with increasing size of particles, and may also be affected by the type of surfactant present in the colloidal solution during oxidation.^{4,24} It was also proven that this oxidation does not promote aggregation of the cobalt oxide nanoparticles, which is

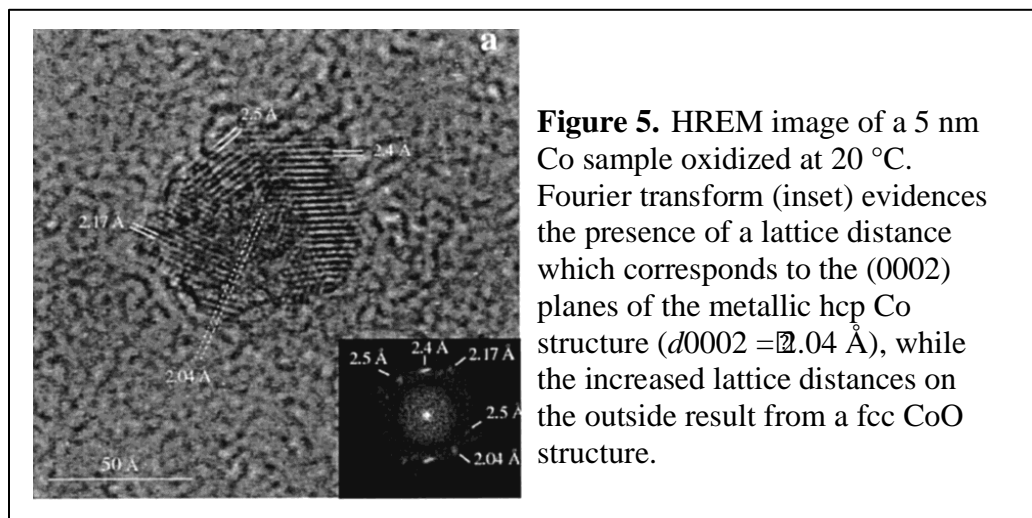
important to note as aggregation most likely would reduce catalytic efficiency. The effect of changing the ratio of reactants was demonstrated by the Alivisatos group when it was discovered that cobalt sulfide hollow nanocrystals exist in two phases (Co_9S_8 and Co_3S_4) depending on the ratio of sulfur to cobalt. In this case it was found that increasing the amount of sulfur relative to cobalt favors the Co_3S_4 phase. I am therefore suggesting that Co_3O_4 would be favored if the temperature was increased both during and after the oxidation from Co to CoO, and if the ratio of O_2 to Ar was increased during oxidation. The particles are then isolated from the colloidal solution by precipitation with methanol, and washed with non-polar solvents such as toluene.⁴

Characterization of nanoreactors

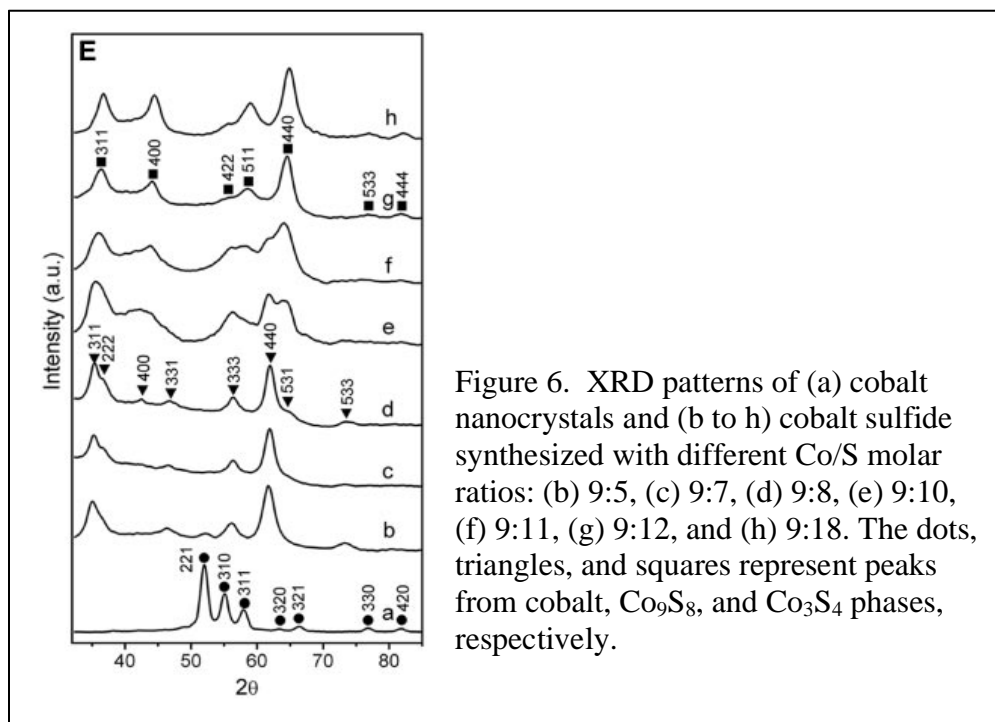
In order to confirm successful formation of the nanocrystals, the structure and material compositions of the particles can be assessed by a transmission electron microscope (TEM), and changes in crystal structure can be monitored by x-ray powder diffraction (XRD). Each step in the synthesis can be followed and success confirmed by TEM images, as was shown by Sobal et al (Figure 4) who carried out the synthesis of PtCo nanocrystals. Figure 4a shows individual Pt particles, while the image in Figure 4b shows PtCo nanoparticles at a molar ratio of 1:2. The shaded region formed around the platinum particles in Figure 4b clearly show that a Co coating is present.



High resolution TEM (HRTEM) allows you to observe the lattice structure, which confirms the material composition. This will be especially necessary in determining whether the oxidation of CoO to Co₃O₄ is successful, because while normal TEM images of these two oxides may look identical, HRTEM will indicate the transformation from the face centered cubic (fcc) lattice structure of the CoO to the spinel structure of Co₃O₄. As an example, a contrast of the different lattice structures of the hexagonal close packed (hcp) Co metal and its fcc CoO shell can be seen in the HRTEM images shown in Figure 5.²³



In addition to this, changes in crystal structure, determined by x-ray diffraction (XRD), will be monitored as an indication of successful formation of product at each step. An example of this was shown by Yin *et al.* when he synthesized hollow cobalt sulfide nanocrystals and demonstrated the effect of varying the S:Co ratio (Figure 6). Using XRD to monitor crystal structure, they were able to see which ratios yield predominately Co_9S_8 or Co_3S_4 . Regarding this proposal, this characterization technique will show the formation of the nanocrystals at each step as the crystal structure changes from that of Au nanoparticles to Au-CoO, and finally to the crystal structure of the Au- Co_3O_4 nanoreactors.



The catalytic activity of the product will be studied in a fixed bed flow reactor by passing a stream of reactant gas comprised of $\text{CO}/\text{O}_2/\text{He}$ in a ratio of 1:2:97 through the nanoreactors. The conversion of CO to CO_2 will be detected by gas chromatography

(GC). The synthetic conditions can then be tailored to vary the cavity size and outer shell thickness, and the effects of these changes on the catalytic activity can be examined. The goal is that efficient catalysis will be carried out at lower temperatures ($\sim 20\text{ }^{\circ}\text{C}$) as many applications that utilize the CO oxidation reaction require this. Because this is a novel way in which gold nanoparticles are cooperating with a support, the study of these nanoreactors for the oxidation of CO may also shed some light on the disputed mechanism of interaction between gold particles and a metal oxide.

References

- (1) Haruta, M.; Yamada, N.; Kobayashi, T.; Iijima, S., Gold catalysts prepared by coprecipitation for low-temperature oxidation of hydrogen and of carbon monoxide. *Journal of Catalysis* 1989, *115* (2), 301-309.
- (2) Haruta, M.; Tsubota, S.; Kobayashi, T.; Kageyama, H.; Genet, M. J.; Delmon, B., Low-Temperature Oxidation of CO over Gold Supported on TiO₂, [alpha]-Fe₂O₃, and Co₃O₄. *Journal of Catalysis* 1993, *144* (1), 175-192.
- (3) Thompson, D., An overview of gold-catalysed oxidation processes. *Topics in Catalysis* 2006, *38* (4), 231-240.
- (4) Chen, Y.-J. W., Dai-en; Yeh, Chuin-tih, Oxidation of Carbon Monoxide Over Nanoparticles of Cobalt Oxides. *Reviews on Advanced Materials Science* 2003, *5*, 41-46.
- (5) Chen, Y.; Crawford, P.; Hu, P., Recent Advances in Understanding CO Oxidation on Gold Nanoparticles Using Density Functional Theory. *Catalysis Letters* 2007, *119* (1), 21-28.
- (6) Molina, L. M.; Hammer, B., The activity of the tetrahedral Au₂₀ cluster: charging and impurity effects. *Journal of Catalysis* 2005, *233* (2), 399-404.
- (7) Lopez, N.; Norskov, J. K., Catalytic CO Oxidation by a Gold Nanoparticle: A Density Functional Study. *Journal of the American Chemical Society* 2002, *124* (38), 11262-11263.
- (8) Liu, Z.-P.; Gong, X.-Q.; Kohanoff, J.; Sanchez, C. n.; Hu, P., Catalytic Role of Metal Oxides in Gold-Based Catalysts: A First Principles Study of CO Oxidation on TiO₂ Supported Au. *Physical Review Letters* 2003, *91* (26), 266102.
- (9) Lopez, N.; Janssens, T. V. W.; Clausen, B. S.; Xu, Y.; Mavrikakis, M.; Bligaard, T.; Norskov, J. K., On the origin of the catalytic activity of gold nanoparticles for low-temperature CO oxidation. *Journal of Catalysis* 2004, *223* (1), 232-235.
- (10) Molina, L. M.; Hammer, B., Active Role of Oxide Support during CO Oxidation at Au/MgO. *Physical Review Letters* 2003, *90* (20), 206102.
- (11) Molina, L. M.; Rasmussen, M. D.; Hammer, B., Adsorption of O₂ and oxidation of CO at Au nanoparticles supported by TiO₂(110). *The Journal of Chemical Physics* 2004, *120* (16), 7673-7680.
- (12) Remediakis, I. N.; Lopez, N.; Nørskov, J. K., CO Oxidation on Rutile-Supported Au Nanoparticles. *Angewandte Chemie International Edition* 2005, *44* (12), 1824-1826.
- (13) Laursen, S.; Linic, S., Oxidation Catalysis by Oxide-Supported Au Nanostructures: The Role of Supports and the Effect of External Conditions. *Physical Review Letters* 2006, *97* (2), 026101.
- (14) Bond, G.; Thompson, D., Catalysis by Gold. *Catalysis Reviews: Science & Engineering* 1999, *41* (3/4), 319.
- (15) Wang, W. Z.; Poudel, B.; Wang, D. Z.; Ren, Z. F., Synthesis of PbTe Nanoboxes Using a Solvothermal Technique. *Advanced Materials* 2005, *17* (17), 2110-2114.
- (16) Dhas, N. A.; Suslick, K. S., Sonochemical Preparation of Hollow Nanospheres and Hollow Nanocrystals. *Journal of the American Chemical Society* 2005, *127* (8), 2368-2369.

- (17) Yin, Y.; Rioux, R. M.; Erdonmez, C. K.; Hughes, S.; Somorjai, G. A.; Alivisatos, A. P., Formation of Hollow Nanocrystals Through the Nanoscale Kirkendall Effect. *Science* 2004, *304* (5671), 711-714.
- (18) Hoflund, G. B.; Gardner, S. D.; Schryer, D. R.; Upchurch, B. T.; Kielin, E. J., Au/MnOx catalytic performance characteristics for low-temperature carbon monoxide oxidation. *Applied Catalysis B: Environmental* 1995, *6* (2), 117-126.
- (19) Bamwenda, G. R.; Tsubota, S.; Nakamura, T.; Haruta, M., The influence of the preparation methods on the catalytic activity of platinum and gold supported on TiO₂ for CO oxidation. *Catalysis Letters* 1997, *44* (1), 83-87.
- (20) Whyman, R., *J. Chem. Soc., Faraday Trans.* 1997, *93*, 187.
- (21) Kielin, E. J., *Applied Catalysis B* 1995, *6*, 117.
- (22) Bollinger, M. A. V., M. A., *Appl. Catal. B* 1996, *8*.
- (23) Sobal, N. S.; Ebels, U.; M $\sqrt{\partial}$ hwald, H.; Giersig, M., Synthesis of Core, àShell PtCo Nanocrystals, Ä † . *The Journal of Physical Chemistry B* 2003, *107* (30), 7351-7354.
- (24) Verelst, M.; Ely, T. O.; Amiens, C.; Snoeck, E.; Lecante, P.; Mosset, A.; Respaud, M.; Broto, J. M.; Chaudret, B., Synthesis and Characterization of CoO, Co₃O₄, and Mixed Co/CoO Nanoparticules. *Chemistry of Materials* 1999, *11* (10), 2702-2708.